International Journal of Engineering Technologies (IJET)

International Journal of Engineering Technologies (IJET) is included in:

International Journal of Engineering Technologies (IJET) is

harvested by the following service:

Organization	URL	Starting Date	Feature
The OpenAIRE2020 Project	https://www.openaire.eu/	2015	Open Access

From the Editor

Dear Colleagues,

On behalf of the editorial board of International Journal of Engineering Technologies (IJET), I would like to share our happiness to publish the sixth issue of IJET. My special thanks are for members of editorial board, editorial team, referees, authors and other technical staff.

Please find the sixth issue of International Journal of Engineering Technologies at http://dergipark.ulakbim.gov.tr/ijet. We invite you to review the Table of Contents by visiting our web site and review articles and items of interest. IJET will continue to publish high level scientific research papers in the field of Engineering Technologies as an international peer-reviewed scientific and academic journal of Istanbul Gelisim University.

Thanks for your continuing interest in our work,

International Journal of
Engineering Technologies

IJET

Table of Contents

International Journal of Engineering Technologies, IJET

On Load Single Phase Solid State Tap Changer

Mohammad H. Taha

Electrical and Computer Engineering Department, Rafik Hariri University, Lebanon

(TahaMH@rhu.edu.lb)

Corresponding Author; Mohammad H. Taha, Electrical and Computer Engineering Department, Rafik Hariri University, Lebanon, Tel: +9615603090, Fax: +9615601380, TahaMH@rhu.edu.lb

Abstract-In electric energy transmission and distribution system, voltage control is an essential part to maintain proper voltage limit at the consumer's terminal. On-load tap-changers are indispensable in regulating power transformers used in electrical energy networks and industrial applications. General switching principles and application for the On-load tap-changers are discussed and presented. A single phase Tap-Changer using a GTO with antiparallel thyristor to perform switching of one upward or downward transition is described in this paper. The logic of operation, simulation and experimental results for resistive, inductive loads are presented.

Keywords: Voltage control, thyristors, tap-changer, loads.

1. Introduction

For more than 100 years on load tap changer was the essential part in general electrical power installation. The main task of on load tap changer is the ability to regulate output voltage without any interruption on any electric network. This can be done by monitoring the output voltage and changing the turns ration between the primary and secondary winding in order to change the level of the secondary voltage. [1-3].

On-load Tap-Changers are used when load disconnection is not acceptable, so its main task is to transfer the transformer load current from one regulating winding tapping to another without any interruption of the current from the transformer to the load. However, on load tap changer design has not radically changed in the past two decades [4-6], mainly because the performance has always matched the system requirement. In general, reliability has been the main criterion for a good design to fulfil the relatively slow automatic voltage control characteristics. Hence the conventional mechanical arrangement using oil breaks contactors has been adequate [2, 3],

The more recent innovations in Tap-Changer design have been orientated towards eliminating contact wear and oil pollution to improve reliability and reduce maintenance. Various methods have been employed to reduce the arcing which is accompanied at the contacts, however some contact erosion and oil contamination still take place [2,3].

Conventional transformer Tap-Changers inserts resistance or reactance during the switching operation, and

the three or four transition stages often required many cycles of the supply frequency. Solid-state Tap-Changers eliminate the need for switching resistors or reactors and operate in less than one cycle eliminate the maintenance and minimize the arcing associated with switching transition [6-8].

There are several conditions which are very important for the design of the Tap-Changers [1,2]:

1- Transformer rating.

2- Number of taps.

3- Tap voltage.

Furthermore, current should not be interrupted during the operation of the on load tap changer.

2. Tapping Winding Arrangement

To select the tapping range from the tap changer few comment arrangements are used. Usually the leads from the winding can be taken off to get required range of the tapping [2,3]. Three methods are in common use for providing tapping at neutral end of a high voltage winding.

2.1. Tapping by Coarse/fine

Figure 1 shows the general arrangement of the Coarse/fine tapping. As can be seen from the figure a winding extension (coarse part) set on the main winding and controlled by changeover selector. The fine section is set on the main tapping winding. The lead from the fine section is brought out by a special rotary (one for odd and one for even

tapping).In this arrangement to cover the range for the required tap , the gauged selectors operates in a sequential operation manner and this would make two revolutions, one revolution with the coarse section out of service and the other after the operation of the range over sector.
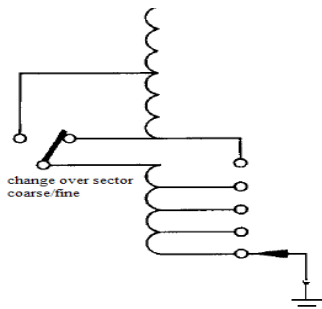
Fig.1. Coarse/ fine tapping arrangement

2.2. Arrangement by reverse tapping winding

Figure 2 shows the reverse tapping method. In this arrangement main winding could be boosted or bucked by using a main winding tapping separator. (This can be done by either increasing or decreasing the number of the main winding section in order to change the voltage ratio).

General reverse tapping winding arrangement can be done by tapping ten sections and using two selectors (one for odd and one for even tapping)
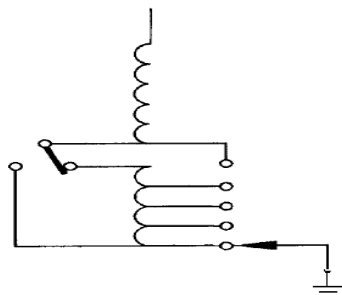
Fig. 2. Reverse tapping winding

2.3. Linear arrangement

Figure 3 shows a linear tapping arrangement, it acts like a linear potentiometer which changes the output voltage linearly with the number of tapping. Two type selectors are used for even and odd taps. This arrangement has the advantage of the mechanical design simplicity.
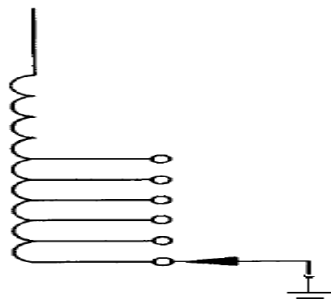
Fig. 3. Linear tapping winding

3. Thyristors Tap Changer

To illustrate the principle of operation consider a single phase, using two antiparallel thyristors for each tap as shown in Figure 4 The sequence of events for switching up or down when the load current and voltage are in phase or out of phase is presented below. Switching up will be achieved when operation of thyristors TH3 and TH4 (normal operation) are transferred to thyristors TH1 and TH2, the voltage will increase from VB to VA. Switching down will be achieved when thyristors TH5 and TH6 are turned-on and the other thyristors are turned-off, the voltage will decrease to VC. In practice many operational requirements have to be considered and appropriate strategies developed[7-9].

1-At least one pair of inverse parallel connected thyristors must be gated prior to transformer energization.

2- Transient on the load current durring transformer energization or a sudden changing of load.

3- A sudden change of load current in either magnitude and/or phase immediately prior to a tap change instruction.

4- Transformer currents on over load

5- Systems faults. [10-12]
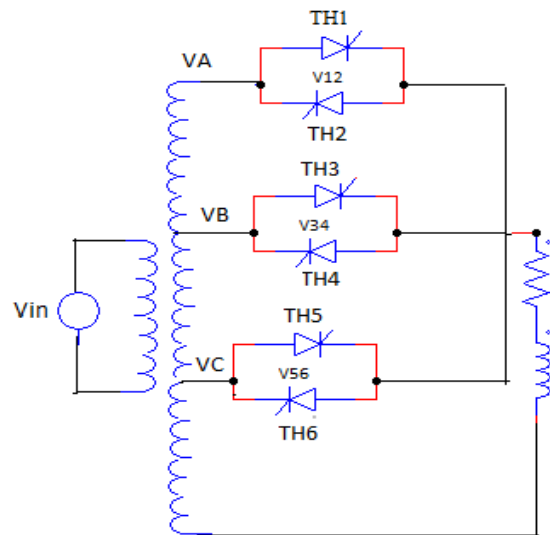
Fig. 4. Thyristors tap changer

First consider the load as a purely resistive (voltage and current are in phase)and the circuit is initialized by gating thyristors TH3 and TH4. Then the load current is:

$$i_L = \frac{VB}{R} \sin(\omega t) \tag{1}$$

To switch up, let TH1 be turned on at any time over a positive half cycle. Then:

Kirchoff's voltage law for the circuit mesh including TH1 and TH2 gives:

$$V12 - V34 - VAB = 0 \tag{2}$$

But V12 =0, therefore:

$$V34 = -VAB \tag{3}$$

TH3 has a reverse voltage which is ready to commutate. When TH2 is turned-on to conduct over the negative half cycle, again V12 =0, for the circuit mesh including TH2 and TH4 equation (2) and(3) apply. Because VAB < 0, and therefore V34 > 0, TH4 will commutate and the upward transition will take place.

For switching down, let again TH3 and TH4 be turned on throughout alternate half cycles. Let TH5 be turned on at any time over a positive half cycle, therefore:

Kirchoff's voltage law for the circuit mesh including TH5 and TH6 gives:

$$V34 - V56 - VBC = 0 \tag{4}$$

But V56 =0, therefore:

$$V34 = VBC \tag{5}$$

Note that: V12, V34 and V56 are the voltage drop across the devices for each tap.

Thus, TH3 will still has a forward voltage and does not turn-off, a short circuit will occur which may damage the system. To avoid the short circuit, TH5 and TH6 must be gated at the instant when the voltage on tap B and tap C is about to change their polarities. Furthermore another important factor is the device turn-off time which affects the phenomena of the switching. If TH3 has not yet deionized completely, it can be forced into conduction if a forward voltage exists across it. If the device can get its forward blocking capability as soon as the current ceases, switching down transition is accomplished by transferring the conduction from TH3 to TH6 or TH4 to TH5.

The operation with inductive load is not as the same as the resistive load, the current keeps flowing through the device when a reverse voltage exists across it. There is a limit time to switch up or down as illustrated below.

Let TH3 and TH4 again be turned-on through alternate half cycles, then the load current is:

$$i_L = \frac{VB}{Z} \sin(\omega t - \phi) \tag{6}$$

$$z = \sqrt{R^2 + (\omega L)^2} \tag{7}$$

$$\phi = \tan^{-1} \frac{\omega L}{R} \tag{8}$$

Now let TH1 be turned on at time less than the impedance angle φ because TH4 is still conducting (the load current still negative) then V34 = 0, therefore the upper half of the transformer secondary winding will be short circuited through TH1 and TH4. TH1 may not be turned-on until the load current becomes positive, similarly TH2 may not be turned-on until the load current becomes negative. Thus an upward transition can only takes place when the voltage and current have the same polarities. Downward transition can only take place when the voltage and the current have opposite polarities.

4. GTOs/Thyristors Tap-Changer

The use of two antiparallel thyristors as an element switch for a Tap-Changer associated with certain problems as mentioned before mainly with switch down transition. To tackle these problems a GTO with antiparallel thyristor for each tap could be used. This allows switching up or down could be happen at any time when the current flows through the GTO. The block diagram for the circuit configuration is shown in Figure 5, the GTO conducts over a positive half cycle and the thyristor over a negative half cycle. Under normal operation GTO2 and TH2 are gated, for switching up transition let GTO1 be turned on by injecting a positive current into its gate and let GTO2 be turned-off by applying a negative voltage between its gate and cathode. At the same time the driving pulses will be removed from the gate of TH2 and transferred to the gate of TH1, this will have a reverse voltage which will turned it off. For switching down , first GTO3 will turn-on and GTO2 will turn-off, TH3 will conduct over the negative half cycle while TH2 will have a reverse voltage which turned it off.
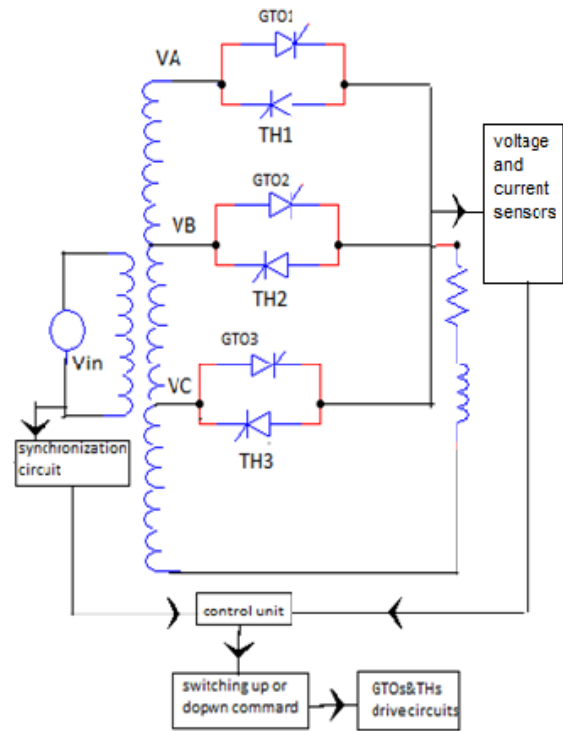
Fig. 5. GTOs/ Thyristors tap changer

A control circuit is designed to ensure that only one tap operates at a time, switching up or down depends on the level of the output voltage and current. These are sensed by voltage and current transformer and feed back to the control circuit via a switching logic circuit which in turn selects the right pulses for the required tap.

Since the three GTOs have the same common point for their cathodes, a single unit power supply is enough for their driving circuits. Referring to Figure 5 witching up or down could be achieved by two different way:

1- If the input voltage changes, the voltage and current sensors produce signals which are the necessary condition for switching transition. This type of control is very useful, the load voltage could be set to a fixed value. Any variation in

the input voltage causes the switching logic circuit to choose the right tap to keep the output constant, when the output voltage increases, the normal operation is overridden and a different mode of operation takes place. A voltage transformer is used to sense the output voltage, when this voltage is higher or lower than a reference voltage . the controller automatically choose the switching condition and upward or down ward command will be achieved.

2- Manual switching by choosing the required tap in the transformer. For switching up or down three position slide switches. When the selected switch is closed, its output connects to the control circuit unit which in turn choose the required tap. This type of control is very useful at low voltage for an induction motor starting and can be switched to a rated voltage by a touch of a switch.

5. Simulation and Experimental Results

A single-phase GTO / thyristor switched Tap-Changer as shown in Figure 5, was simulated designed and built.

The circuit was designed with power flows in one direction and for switching up or down one step at a time (45V), the primary of the transformer is connected to 210V RMS input voltage, the. The secondary of the transformer is tapped from 0 to 115% of the primary voltage. Referring to Figure 5, tap (B) is the normal operation which connected to a point gives 100% the input, tap (A) is the upward transition which connected to a point gives 115% the input voltage, and finally tap (C) downward transition is connected to a point which gives 85% of the input voltage. The circuit was tested under various load conditions, Simulation results for the waveforms of the load voltages and currents for resistive and inductive loads are shown in Figures 6 to 9. Experimental results are shown in figures 10 to 15.
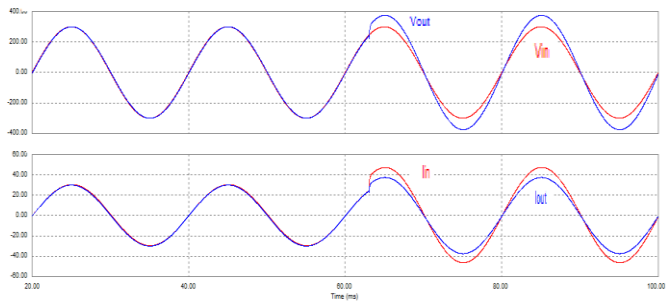
Fig. 6. Switching up simulation, for input and output voltage and current for resistive load
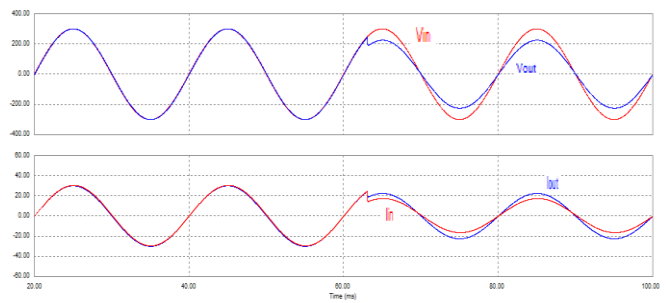
Fig. 7. Switching down simulation, for input and output voltage and current for resistive load
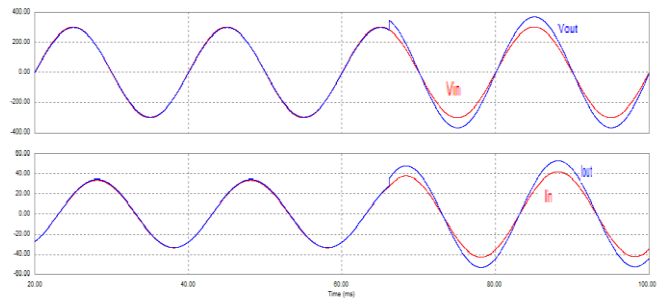
Fig. 8. Switching up simulation, for input and output voltage and current for inductive load
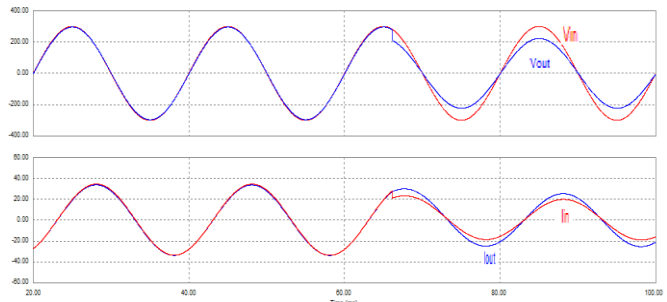
Fig. 9. Switching down simulation, for input and output voltage and current for inductive load
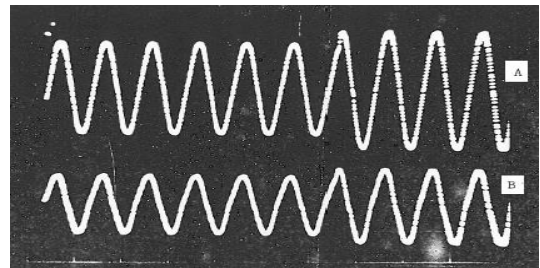
Fig. 10. Load voltage (A) and current (B) for resistive load (switching up)
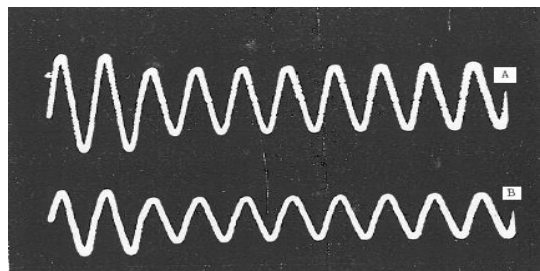
Fig. 11. Load voltage (A) and current (B) for resistive load (switching down)
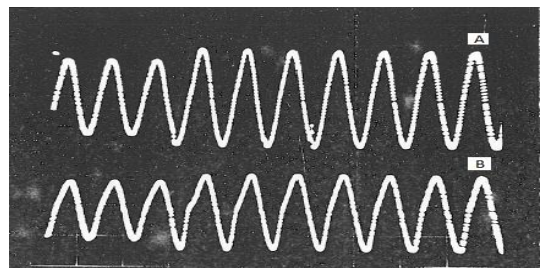
Fig. 12. Load voltage (A) and current (B) for inductive load (switching up)

32
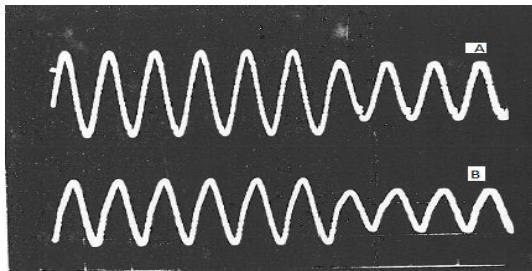
Fig. 13. Load voltage (A) and current (B) for inductive load (switching down)
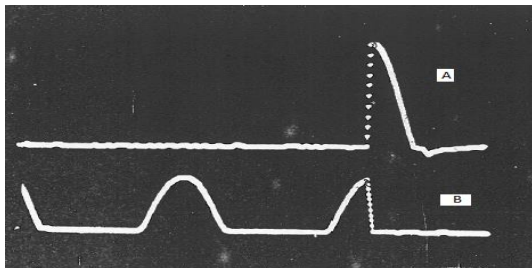
Fig. 14. GTO currents with resistive load (switching up)
A- Current through GTO1. B- Current through GTO2
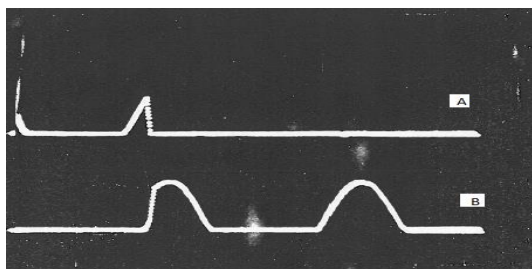
Fig. 15. GTO currents with resistive load (switching down)
A- Current through GTO2, B- Current through GTO

6. Conclusion

The paper describes the operation of both GTO and thyristor tap changers. For thyristors tap changer it was illustrated that, switching up should be done when voltage and current has the same direction and switching up when they are in opposite direction otherwise a short circuit could occur and damage the system. For GTO tape changer switching up or down could be occurred at any time when the GTO is conducting.

The circuit was responding satisfactorily to the switching transition and this took place with a very low voltage transient across the devices. It is possible to have multi-tap transformers with power flows in either direction or switching up or down to any required voltage within the transformer rating. A microprocessor control could be engaged for deciding the switching and could be used in the electrical distribution networks which would replace the conventional on load Tap-Changes which are extremely expensive and require frequent maintenance.

PSIM software tools used to simulate the proposed tap changer, this verified the performance of the controller of the tap changer. Experimental results showed the system behaviour against any change of the input voltage.

References

[1] R. Feinberg, "Modern Power Transformer Practice", Macmillan Press Ltd, 1979.

[2] D. O'kelly and G. Musgrave, "An Appraisal of Transformer Tap-Changing Technique", IEEE Conference Publication, no. 137, pp. 105-109, Jan. 1973.

[3] A.F. Plessis, "Microprocessor Based Power Transformer Voltage Control Scheme", IFAC Symp, Pretoria, South Africa, pp. 165-172, September 1980.

[4] H. Jiang, R. Shuttleworth, B.A.T. Al Zahawi, X. Tian, and A. Power, "Fast response GTO assisted novel tap-changer", IEEE Trans. Power Del., vol. 16, no. 1, pp. 111–115, Jan. 2001.

[5] R. Shuttleworth, X. Tian, C. Fan, and A. Power, "New tap changing scheme", Inst. Elect. Eng., Electic Power Applications, vol. 143, no. 1, pp. 108–112, Jan. 1996.

[6] J. Harlow, "Discussion of Fast response GTO assisted novel tap changer", IEEE Trans. Power Del., vol. 16, no. 4, pp. 826–827, Oct. 2001.

[7] G.H. Cooke and K.T. Williams, "Thyristor assisted on-load tap-changers for transformers", Power Electronics and Variable-Speed Drives, pp. 127–131, Jul. 1990.

[8] G. H. Cooke and K. T. Williams "New thyristor assisted diverter switch for on-load transformer tap-changers", Inst. Elect. Eng., Electric Power Applications, vol.139, no. 6, pp. 507–511, Nov. 1992.

[9] T. Larsson, R. Innanen, and G. Norstrom, "Static electronic tap-changer for electric machines and voltage control", IEEE Fast Phase and Drives Conf., May 1997, pp. TC3/4.1–TC3/4.3.

[10] V. Sanchez, R. Echavarria, M. Cotoragea and A. Claudio, "Design and implementation of a fast on-load tap-changing regulator using soft-switching commutation techniques", PESC, pp. 488–493, Jun. 2000.

[11] R. Echavarria, V. Sanchez, M. Ponce, M. Cotorogea, and A. Claudio, "Analysis and design of a quasiresonant fast on-load tap changing regulator", J. Circuit, Syst, Comput., vol. 13, no. 4, Aug. 2004.

[12] R. Echavarria, V. Sanchez, M. Ponce, A. Claudio and M. Cotorogea, "Parametric analysis of a quasiresonant fast on-load tap-changing regulator", PESC, 2002, pp. 1809–1814.

Review on Natural Dye-Sensitized Solar Cells (DSSCs)

Oluwaseun Adedokun‡, Kamil Titilope, Ayodeji Oladiran Awodugba

Department of Pure and Applied Physics, Ladoke Akintola University of Technology, P.M.B. 4000, Ogbomoso, Nigeria

(oadedokun@lautech.edu.ng, katitilope@student.lautech.edu.ng, aoawodugba@lautech.edu.ng)

‡Corresponding Author: Oluwaseun Adedokun, Department of Pure and Applied Physics, Ladoke Akintola University of Technology, P.M.B. 4000, Ogbomoso, Nigeria, Tel: +2347031195750, oadedokun@lautech.edu.ng

Abstract-In a conversion system of pure and non-convectional solar energy to electricity, dye sensitized solar cells (DSSCs) encourage the fabrication of photovoltaic devices providing high conversion efficiency at low cost. The dye as a sensitizer plays a vital role in performance evaluation of DSSCs. Natural dyes (organic dyes) has come to be a worth-while substitute to the rare and expensive inorganic sensitizers because of its cost effective, extreme availability and biodegradable. Different parts of a plant like fruits, leaves, flowers petals and bark have been tested over the years as sensitizers. The properties, together with some other parameters of these pigments give rise to improve in the operation standard of DSSCs. This review hash-out the history of DSSC with a focus on the recent developments of the natural dyes applications in this specific area with their overall appearance, the various components and the working principle of DSSCs as well as the work done over the years on natural dye based DSSCs.

Keywords: Natural dye, DSSCs, photovoltaic device, Photo-electrode, photo-sensitizer.

1. Introduction

Solar energy provides a clean, renewable and cheaper energy source for human race, while serving as a primary energy source for another type of energy sources, namely; wind energy, water, bio-energy and fossil fuel. The solar cells used in harvesting the solar power are commonly categorized into different types in respect to the composition of their material e.g organic dye solar cells, non-crystal, multiple crystal, and single crystal silicon solar cells. A solar cell usually signifies the cell that is made from silicon crystal material. Nevertheless, the production cost of the solar cells based on silicon crystal material compared to the dye-sensitized solar cells (DSSCs) is high. DSSCs have triggered a great attention and they are of powerful interest due to the advantages of its lower cost of manufacturing.

DSSCs are devices that convert solar to electric energy by light sensitization established on wide energy band semiconductor [1]. DSSC shows a very promising future in the field of photovoltaic cells [2, 3]. DSSC also known as Grätzel cell is a new type of solar cell [4], and have attracted a great interest due to their minimal production cost, and environmental friendliness. DSSC comprises of a counter electrode, an electrolyte containing iodide and triiodide ions, and a nano-crystalline porous semiconductor electrode-absorbed dye. The dye which acts as sensitizers in DSSCs plays an important task in absorption and conversion of incident light ray to electricity.

Dyes are classified into organic (natural dye) and inorganic dye. Inorganic dyes such as Ruthenium (Ru) dyes are presently known to be the most significant dye for the fabrication of DSSCs with great efficiency. However, they are quite expensive and difficult in their purification. Therefore, in finding alternative to the expensive and rare inorganic sensitizers, natural dyes are considered as the best viable alternative. The main advantages of using natural pigment as sensitizer in DSSCs are low fabrication cost, easy achievability, low time of energy payback, flexibility, availability supply of raw materials, non-environmental risk, and great performance at diffuse light and multicolor options. Different parts of plant e.g leaves, flowers petal and barks have been examined as sensitizers [5]. The nature and some other parameters of these pigments gave rise to varying performance in their efficiency [5].

The operations of DSSCs are based on the photo-sensitization created by the dyes on wide band-gap mesoporous metal oxide semiconductors; this sensitization is

due to the dye absorption of part of the visible light spectrum [6, 7]. The use of natural pigments as sensitizing dye for the transformation of solar to electric energy is remarkable because, it enhances the economical aspect and in addition, it has important advantages from the environmental perspective [8, 9]. DSSCs became more interesting since large collections of dye including natural dye can be used as light harvesting elements to provide the charge carriers. This review hash-out the history of DSSC with a focus on the recent developments of the natural dyes applications in this specific area with their overall appearance, the various components and the working principle of DSSCs as well as the work done over the years on natural dye based DSSCs.

2. Structure and Operation of DSSCs

2.1. Structure of DSSC

DSSC differs from other solar cell devices both by its basic construction and the physical processes behind its operation. In contrast to the first and second generation, PV devices based on solid-state semiconductor materials, the typical DSSC arrangement combines liquid and solid phases. DSSC comprises of a transparent conducting glass electrode (anode) that allows the passage light through the cell [11, 12]. Transparent glasses are used as electrode substrates due of their availability, affordable cost, and great transparency in the visible spectrum. The fluorine tin dioxide $F:SnO_2$ coating has a transparent conductive face. The mesh titanium nanoparticle TiO_2 acts as a dye container, and provides electron passage through the cell. The TiO_2 particles are coated with dye molecules (light sensitizer) that convert photons into excited electrons and cause current to flow. The dye is surrounded by the electrolyte layer (usually iodide) that acts as a source to compensate the lost electron. The counter electrodes (cathode) on the other side of the cell are typically coated with platinum or graphite.

2.2. Operation of DSSCs

Operation in DSSC is similar to photosynthesis with dye replacing chlorophyll as light harvesting element for the production of excited electrons, carbon dioxide being replaced TiO_2 as the electron acceptor; oxygen as the electron donor and oxidation product; electrolyte substitutes water; and a multilayer structure to improve both absorption of light and efficiency in collection of electron. The light driven electro-chemical process in DSSC is regenerative as shown in Figure 1 and the working voltage produced by the device is the difference between the chemical potential of the TiO_2 (Fermi level) and the redox potential of the mediator [13]. The transferred of electron to the electrolyte is made at the cathode. The electrolytes containing I^-/I_3^- are used as brokers between the cathode (carbon plated counter electrode) and the TiO_2 photo electrode. Thus, the oxidized dye receives electron from I^- ion redox to replace the lost electron [14–16], and the iodide molecules are then oxidized into tri-iodide ions (I_3^-). This process is described by Equation 4. Hence, the DSSCs efficiency sensitized by Ru compound, adsorbed on the semiconductor nano-crystalline TiO_2 has reached 11–12% [17, 18].
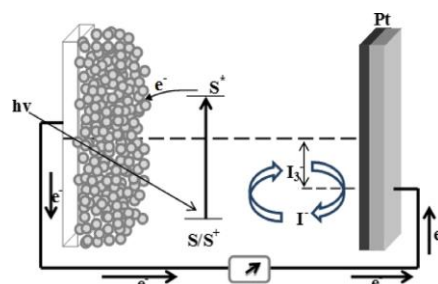
Fig. 1. A Schematic diagram and operational principle of DSSC [10]

The operation cycle is summarized in chemical reaction as [19]:

Anode:

$$S + hv \rightarrow S* \qquad \text{Absorption} \qquad (1)$$
$$S* \rightarrow S^+ + (TiO_2) \qquad \text{Electron injection} \qquad (2)$$
$$2S^+ + 3I^- \rightarrow 2S + I^3 \qquad \text{Regeneration} \qquad (3)$$

Cathode:

$$I_3^- - 2e^-(Pt) \rightarrow 3I^- \qquad (4)$$

Cells:

$$e^-(Pt) + hv \rightarrow 3I^- \qquad (5)$$
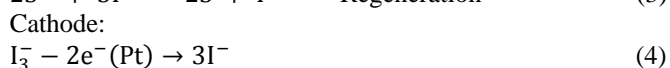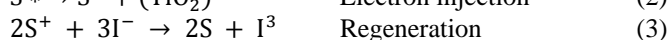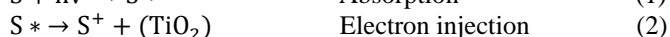
where S is the dye molecule and hv is the photon energy.

There are no consumption or production of any chemical substances during the operational cycle, thus the operation of the cell is regenerative in nature, as shown in Equation 5.

3. Components of DSSCs

The conversion of light energy in-to electricity done by DSSC is based on sensitization of wide band gap semiconductors and mainly consists of dye, photo electrode, electrolyte, counter electrodes and substrates glass with the transparent conductive oxide (TCO) layer. The optimization of each of them is highly significant to improve the overall efficiency.

3.1. Photosensitizer

An efficient photosensitizer has several basic fabrication requirements including:

- Strong dye adsorption particles onto the semiconductor surface;
- Large visible light harvesting capacity;
- Injection of electron efficiently into the semiconductors conduction band;
- Lastly, ─O or ─OH groups with anchoring capability on TiO_2 surface, ensuring high rates in transfer of electron.

Dye has essential roles in absorbing and converting solar to electric energy. Numerous researches focused on molecular engineering of several inorganic metal complexes and organic dyes. Transition coordination complexes are used as charge transfer sensitizers, harvesting around 11% solar to electric energy in standard global air mass AM 1.5 of sunlight [20]. These complexes are also one of the most effective sensitizers because of their greater efficiency, chemical stability, favorable photo-electrochemical properties etc. [21, 22]. Nonetheless, Ru complexes contained heavy metals which are hazardous

environmentally, aside from their complicated and expensive synthesis. Moreover, Ru complexes have the tendency to degrade in the presence of water [4, 23-24].

Grätzel and his group developed many Ru complex photosensitizers [22] which represent the most efficient sensitizers (~ 11%) because of their intense range of absorption from the visible to the near-infrared region [25, 26]. Regardless of their chemical stability and the possible exchange of charging with semiconducting solids, Ru complexes have large visible light-harvesting capacity which makes them a wise choice for the manufacture of solar energy conversion devices [27, 28].

3.2. Electrolytes

The electrolyte plays a very essential role in the DSSC by enabling the transport of charge between the photo-electrode and counter electrode. The ideal electrolyte solvent is one that has small vapor pressure, very low viscosity, high dielectric properties and high boiling point. From industrial point view, factor like easy processing, robustness (chemical inertness), and environmental sustainability are also important. Presently, the most successful redox mediator used in DSSC includes a liquid electrolyte containing the redox couple iodide/triiodide. The redox electrolyte comprises of iodine, iodides and often additional additives. Ionic liquids are promising alternative electrolytes which provide advantages like high thermal and chemical stability, non-volatility, and excellent ionic conductivity. Finding a superior redox couple is one of the main challenges for future DSSCs research.

3.3. Conductive Glass or Substrates

Clear conductive glasses are usually employed as substrate due to their relatively minimal cost, abundant in supply, high optical. Conductive coating is made by deposition of one side of the substrate in form of thin transparent conductive oxide (TCO). This layer is crucial because it enables the penetration of sunlight into the cell while conducting electron carriers to outer circuit. The conductive film ascertain a very low electrical resistance of about 10-20 Ω per square at room temperature. The nanostructure wide band gap oxide semiconductor (electron acceptor) is applied on the conductive side.

3.4. Photo-Electrode

The photo-electrode in a DSSC comprises of a nanostructure semiconductor materials, clipped to a transparent conducting substrate. The most widely used semiconductor material is TiO_2 because TiO_2 is an inexpensive, nontoxic and abundant material. The electrode comprises of interconnected nanoparticles, with size ranging between 15-30 nm. They appear as a transparent porous electrode, with an average thickness of 10-15 μm. The deposition techniques mainly employed for the film preparation are screen printing and doctor blading. Both methods involve the deposition of viscous colloidal TiO_2 onto a substrate before sintering process. Sintering is commonly carried out at temperatures of 450-500 ℃. The high temperature results in electrical interconnection among the nanoparticles, and eventually forms the nanostructure porous electrode. The sensitization of dye is performed by dipping the electrode into a dye solution for some time.

3.5. Counter Electrode

The counter electrode is an essential component in DSSC where the reduction of mediator takes place. It comprises of fluorine-doped tin oxide (FTO), glass coated with platinum to ensure more reversible transfer of electron. The counter electrode enables electrons transfer coming from the external circuit back to the redox electrolyte. Furthermore, it serves to carry the photo-current over the width of each solar cell. Therefore, the counter electrode must be conducting efficiently and show a low over-voltage for redox couple reduction. Until now, platinum (Pt) has been the desired material for the counter electrode because of its excellent performance in reduction of I_3^- [29].

4. Reviews of Dyes Used in DSSCs

The dyes applied in DSSCs are categorized into two types which are organic and inorganic dyes. Inorganic dyes comprises of metal complex, e.g polypyridyl complexes of Ruthenium and Osmium, metal porphyrin, phthalocyanine and inorganic quantum dots, while organic dye comprises of natural and synthetic dyes.

4.1. Natural Dye Sensitizers

Another type of dye sensitizers used is the organic or natural dye. Natural dyes offers a suitable alternative to high cost inorganic based DSSCs. Naturally, the fruits, flowers and leafs of plant shows different colors from red to purple and include different natural dyes which can be extracted using simple procedure and used for DSSC fabrication [30]. Consideration have been made on natural pigments as a promising alternative sensitizer dyes for DSSC because of their simple production technique, affordable cost, complete biodegradation, easy availability, purity grade, environmental friendly, high reduction of noble metal, and chemical synthesis cost [31–33]. Plant pigmentation results from the electronic structure of pigments reacting with sunlight to change the wavelengths as may be perceived by the viewer. The pigment can be described by the maximum absorption wavelength (λ_{max}) [34]. The performance of natural dye sensitizer in DSSC has been estimated using fill factor (FF), energy conversion efficiency (η) (J_{sc}), open circuit voltage (V_{oc}), and short circuit current. Many parts of a plant have been tested by Researchers (see Table 1) and various useful dyes have been highlighted as photo-sensitizers for DSSC from natural products [35-42].

Common pigments are (a) Betalains (b) Carotenoids (c) Chlorophyll and (d) Flavonoids as Anthocyanins etc. Structures of some natural dyes employed in DSSCs are shown in Figure 2, 3 and 4.

4.1.1. Flavonoids

➢ Flavonoids are widely distributed plant pigments. The word "flavonoid" is commonly employed to define a large group of natural products including C6 - C3 - C6 carbon structure or more specifically phenylbenzopyran functionality.

Table 1. Photovoltaic parameters of natural dye based DSSCs

Natural dyes	Jsc (mAcm^{-2})	Voc (V)	FF	Efficiency (%)	References
Bougainvillea	2.10	0.30	0.57	0.36	35
Sicilian Indian	2.70	0.38	0.54	0.50	
Perilla	1.36	0.522	0.69	0.50	36
Tangerine peel	0.74	0.592	0.63	0.28	
Petunia	0.85	0.616	0.60	0.32	
Yellow rose	0.74	0.609	0.57	0.26	
Violet	1.02	0.498	0.64	0.33	
Begonia	0.63	0.537	0.72	0.24	
Flowery knotweed	0.60	0.554	0.62	0.21	
Lily	0.51	0.498	0.67	0.17	
Fructus lycii	0.53	0.689	0.46	0.17	
Mangosteen pericap	2.69	0.686	0.63	1.17	
Bauhinia tree	0.96	0.572	0.66	0.36	
Rhododendron	1.61	0.585	0.61	0.57	
Chinese rose	0.90	0.483	0.62	0.27	
Cofee	0.85	0.559	0.68	0.33	
Marigold	0.51	0.542	0.83	0.23	
Lithospermum	0.14	0.337	0.58	0.03	
Rose	0.97	0.595	0.66	0.38	
Mixed rosella blue pea	0.82	0.38	0.47	0.15	37
Kelp	0.43	0.44	0.62		38
Capsicum	0.23	0.41	0.63		
Black rice	1.14	0.55	0.52		
Rosa xanthina	0.64	0.49	0.52		
Erythrina variegate	0.78	0.48	0.55		
Annatto	0.53	0.56	0.66	0.19	39
Bixin	1.10	0.57	0.59	0.37	
Norbixin	0.38	0.53	0.64	0.13	
Crocin	0.45	0.58	0.60	0.16	40
Crocetin	2.84	0.43	0.46	0.56	
Syrup of Calafate	1.50	0.38	0.2		41
Fruit of Calafate	6.20	0.47	0.36		
Skin of Jaboticaba	7.20	0.59	0.54		
Nerium olender	2.46	0.41	0.59	0.59	42
Hibiscus rosasinesis	4.04	0.40	0.63	1.02	
Hibiscus surattensis	5.45	0.39	0.54	1.14	
Ixora macrothyrsa	1.31	0.40	0.57	0.30	
Sesbania grandiflora	4.40	0.41	0.57	1.02	

Over 5000 naturally occurring flavonoids have been extracted from various plants, and divided according to their chemical structure as follows: flavonols, flavones, flavanones, isoflavones, catechins, anthocyanin, and chalcones. There are three classes of flavonols which are: flavonoids (2-phenylbenzopyrans), isoflavonoids (3-benzopyrans), and neoflavanoids (4-bezopyrans). Flavonoids contain 15-carbon (C15) based structure with two phenyl-rings joined by three carbon bridges, forming a third ring. The phenyl ring oxidation degree (C-ring) identifies the different colors of flavonoids. However, not all flavonoids have the capability of absorbing visible light, although they have similar structures. Flavonoid molecules are characterized by loose electrons; thus, the energy required for electron excitation to LUMO is lowered, allowing visible light to energize the pigment molecules. Flavonoids regularly occur in fruits, where animals that feed and diffuse the seeds of fruits are attracted, as well as in flowers where insect pollinators are attracted. Many flavones and flavonols absorb radiations most concentrated in ultraviolet (UV) region forming special UV patterns on flowers which are visible to bees. They are also present in the leaves of many species, where they protect plants by screening out harmful ultraviolet radiation from the Sun. Flavonols, Anthocyanins, and proanthocyanidins are three major subcategories of flavonoid compounds.

4.1.2. Carotenoids

Carotenoids are organic pigments found in both chloroplasts and chromoplasts of plants and some other photosynthetic organisms, including some fungi and bacteria. Carotenoids play two important roles in plants and algae: absorption of light energy for use in photosynthesis, and protection of chlorophyll from photo-damage [43]. Carotenoid pigments do make provisions for many flowers and fruits with typically red, yellow and orange colors, and numbers of carotenoid derived aromas. There are over 600 carotenoids known and are divided into two categories; carotenes (pure hydrocarbons) and xanthophylls (which contain oxygen). All carotenoids are tetraterpenoids, meaning that they are produced from 8 isoprene molecules and contain 40 carbon atoms. Generally, carotenoids absorb wavelengths ranging from 400-550 nanometers (violet to green light).
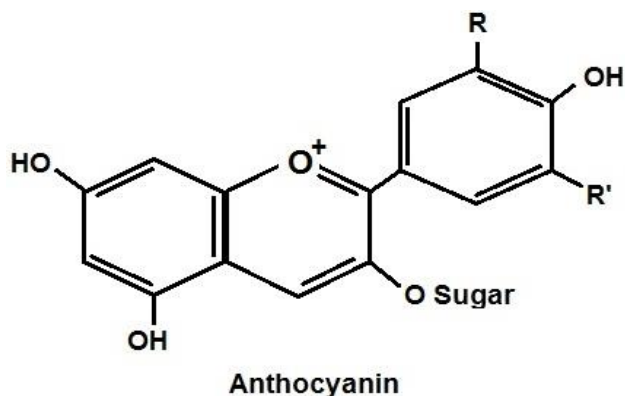
Fig. 2. Structure of Flavonoid (Anthocyanin)
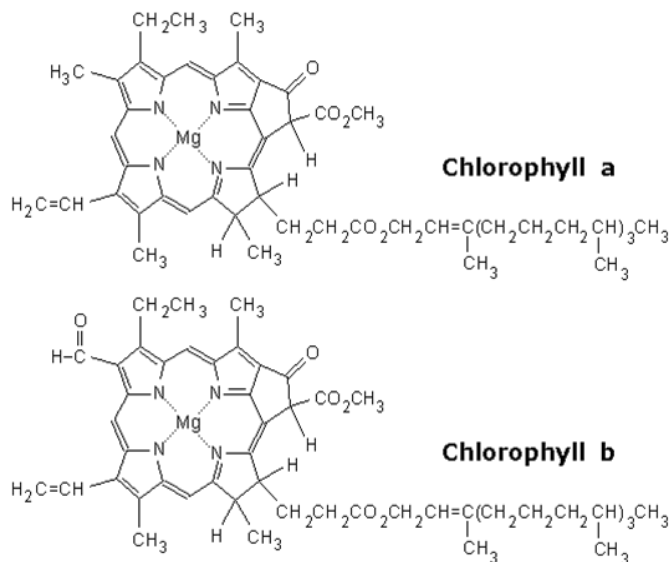
Fig. 3. Structure of Chlorophyll a and b
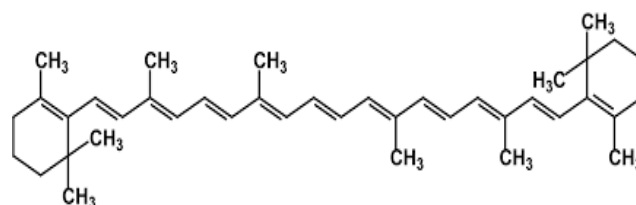
Fig. 4. Structure of carotenoids

4.1.3. Chlorophyll

Chlorophyll (Chl) is a green pigment found in the leaves of most green plants, cyanobacteria, and algae. There are six types of chlorophyll pigment, and the most occurring type is Chl a. Chlorophyll is a compound known as a chelate which is composed of hydrogen, carbon, a central metal ion joined to a large organic molecule, and some other elements like oxygen and nitrogen. In photosynthesis, absorption of energy is done by chlorophyll for the transformation of carbon dioxide to carbohydrates and water to oxygen. This process converts solar energy to a form that can be utilized by plants. The molecular structure contains chlorine ring with Mg center, together with various side chains and a hydrocarbon trail, depending on the Chl type (Fig. 3). Chls are the most important pigments in natural photosynthetic systems [44, 45]. Their functions consist harvesting sunlight, converting solar to chemical energy, and electrons transfer. Chls include a group of more than 50 tetrapyrrolic pigments [46]. Chls and their derivatives are inserted into DSSC as dye sensitizers because of their beneficial light absorption tendency modes; the most efficient of which is Chl α (chlorine 2) derivative-methyl trans-3^2-carboxy-pyropheophorbide α. Xiao et al., reported that chlorine 2 has an ability to lead 4semiconductors TiO_2 and ZnO surfaces through different modes [47]. Maximum absorption is achieved by Chlorophyll at 670 nm because of an interesting compound that acts as a photosensitizer in the visible light range.

Chlorophyll-a is the primary pigment for photosynthesis in plants with the composition $C_{55}H_{72}O_5N_4Mg$ (Fig. 3). It

exhibits a grass-green visual color and absorption peaks at 430nm and 662nm.

Chlorophyll-b has the composition $C_{55}H_{70}O_6N_4Mg$, the difference from chlorophyll-a being the replacement of a methyl group with a CHO (Fig. 3). It exhibits a blue-green visual color and absorption peaks at 453nm and 642nm.

5. Performance Evaluation of DSSCs

After the fabrication of a DSSC, it is now important to evaluate its performance. The two main criteria to consider are: Overall Energy Conversion Efficiency and the Photo-chemical stability. Other required parameters are IPCE (Incident Photon to Current Efficiency also known as Quantum efficiency), I_{sc} (short-circuit-current), V_{oc} (open-circuit-voltage), FF (fill-factor). The short circuit-current is the current across the solar cell when the voltage passing through the solar cell is zero (i.e., when the solar cell is short circuited). Open Voltage Current is the maximum voltage available from a solar cell and this occurs at zero current. Fill factor is described as the rate of the maximum power from the actual solar cell per maximum power from an ideal solar cell. Efficiency is described as the ratio of energy output from the solar cell to input energy from the sun. Any photovoltaic device should have a serviceable life of about 20 years without significant loss of performance. Efficient dyes like N3 sustained 108 cycles after long time illumination. Regeneration is an important factor here, and it should occur fast to maintain the long term stability of the cell. Common tests are based on1000h stability tests at 80oC for evaluating the photochemical stability of the DSSC.

The absorption spectra of dye solutions and dyes adsorbed on TiO_2 surface were recorded using a VIS Spectrophotometer (Spectrum lab 23A GHM Great Medical England).

The fill factor (FF) is defined as:

$$FF = \frac{(I_{max} \times V_{max})}{(I_{sc} \times V_{oc})} \qquad (6)$$

where I_{max} is photo-current and V_{max} is photovoltage.

I_{sc} is short-circuit photo-current and V_{oc} open-circuit photo-voltage, respectively.

Energy conversion efficiency (η) is defined as:

$$\eta = \frac{(I_{sc} \times V_{oc} \times FF)}{P_{in}} \qquad (7)$$

where, P_{in} is incident light power.

6. Challenges

Despite the fact that the cost DSSCs compared to the silicon solar cells is predicted to be at least five times lower which then encourage the use of DSSCs, they also have their limitations regardless of their low cost and easy procedure in fabrication. The main limitation of DSSCs can be recapped as low scalability, low efficiency, and low stability. The efficiency depends on many factors, like V_{oc} (open circuit voltage), I_{sc} (short circuit current), internal resistances and FF (fill factor). DSSCs make use of an organic dye to absorb incidence light ray to give off excited electrons and produce an energy which is then transferred to a material, like titanium dioxide (TiO_2). The energy is therefore collected through a transparent conducting medium. This task presents experimental challenges due to the various basic components found in these cells and their several likely combinations. The obtained photo-conversion efficiencies till date are still low, despite the substantial experimental struggle on their enhancement. At present, its conversion efficiency ranges between 8% and 11% which is below the standard of most current solar technology. The conversion efficiency could be improved through the reduction of some internal resistances. Several ways for the reduction of the cell internal resistances are: adjusting the thickness of the electrode conducting layer, adjust the roughness factor and minimizing the gaps between electrodes. Stability study shows that DSSCs are not yet reliable to predict their efficiency and performance for a long time. The DSSC system in respect to the sealing procedure and material needs to be further studied.

7. Conclusions

Ruthenium (Ru) dyes as part of the inorganic dyes are presently taken as the best dye for the fabrication of efficient DSSC having efficiency of 10-11%. Meanwhile, the noble metal Ruthenium is not abundant and very expensive. Therefore, to achieve a cheaper dyes for DSSC, the use of natural dyes (organic dye) extracted from different easily available fruits and flowers as sensitizers in DSSCs are the suitable alternative for possible application as sensitizers to inorganic dyes because of their low cost, metal-free, eco-friendliness, availability, simple preparation technique and wide availability. Recent developments on different kinds of sensitizers for DSSC devices have led to the use of natural dyes that absorb sunlight within the visible spectrum with higher efficiencies. The nature of the dye used as sensitizers is the main factor affecting the DSSC efficiency. The betalain pigment in red turnip extract recorded the highest efficiency of 1.70%. Although the results obtained on the efficiencies of DSSC with natural dyes are lower than the expectations required for large-scale fabrication, the efficiency are still encouraging and can enhance further researches on the study of new natural sensitizers and to improve the standard of compatible solar cell components for such dyes. This study encourages further research on the use of new natural dye sensitizers to increase the efficiency and stability of DSSC for future satisfactory photoelectric conversion efficiency. Moreover, the new sensitizers should have the following characteristics:

- Higher redox cycles without undergoing decomposition;
- Ability to carry attachment groups, such as phosphonate or carboxylate, to absorb TiO_2; and
- Capability to take-in all the sunlight under the threshold wavelength of 920 nm.

References

[1] M. Gratzel, (2003) Dye-sensitized solar cells, J. Photochem. Photobiol. C, 4: 145-153.

[2] B. O'Regan, M. Gratzel, (1991) A Low-cost high-efficiency solar cell based on dye-sensitized colloidal TiO2 films, Nature, 353: 737-740.

[3] J. O. Ozuomba, A. J. Ekpunobi, P. I. Ekwo, (2011) The viability of prophyrin local dye in the fabrication of dye-sensitized solar cells, Digest J. Nanomaterials and Biostructures, 6(3): 1043 – 1051.

[4] M. Gratzel, (1991) Review article photo-electrochemical Cells, Nature 414, 338–344.

[5] M.R. Narayan, (2012) Review: Dye sensitized Solar Cells based on natural photosensitizers, Renewable and Sustainable Energy Reviews 16:208– 215.

[6] M. Grätzel, (2005) Solar Energy Conversion by Dye-Sensitized Photovoltaic Cells, Inorg. Chem. 44: 6841-6851.

[7] N.M. Gómez-Ortíz, I.A. Vázquez-Maldonado, A.R. Pérez-Espadas, G.J. Mena-Rejón, J.A. Azamar-Barrios, G. Oskam, (2009) Dye-sensitized solar cells with natural dyes extracted from a chiote seeds. Sol. Energy Mater. Sol. Cells, 94: 40-44.

[8] A. Kay and M. Gratzel, (1993) Natural Pigment-Based Dye-Sensitized Solar Cells, J. Phys. Chem., 97 (23): 6272–6277.

[9] M. K. Nazeeruddin, A. Kay, I. Rodicio, (1993) Conversion of light to electricity by cis-X2bis(2,2'-bipyridyl-4,4'-dicarboxylate) ruthenium(II) charge-transfer sensitizers (X = Cl-, Br-, I-, CN-, and SCN-) on nanocrystalline titanium dioxide electrodes, J. Amer. Chem. Soc., 115 (14): 6382-6390.

[10] I. Jinchu, C.O Sreekala, K.S. Sreelatha, (2014) Dye sensitized solar cells using Natural dyes as chromophores – Review, Material Science Forum 741: 39-51.

[11] C. Bauer, G. Boschloo, E. Mukhtar, A. Hagfeldt, (2002) Interfacial electron-transfer dynamics in Ru(tcterpy)(NCS)3-sensitized TiO_2 nanocrystalline solar cells. J PhysChem B, 106:12693–704.

[12] L. Antonio, S. Hegedus, (2003) Handbook of photovoltaic science and engineering. 1st ed.. UK: John Wiley & Sons Ltd Publishers

[13] N.J. Cherepy, G.P. Smestad, M. Grätzel, J.Z. Zhang, (1997) Ultrafast electron injection: implications for a photo-electrochemical cell utilizing an anthocyanin dye-sensitized TiO_2 nano-crystalline electrode. Journal of Physical Chemistry; 101: 9342–51.

[14] G.P. Smestad, (1998) Education and solar conversion: demonstrating electron transfer, Sol Energy Mater Sol Cells; 55:157–78.

[15] G. Calogero, G.D. Marco, (2008) Red Sicilian orange and purple eggplant fruite as natural sensitizers for dye-sensitized solar cells, Sol Energy Mater Sol Cells; 92:1341–6.

[16] C. Bauer, G. Boschloo, E. Mukhtar, A. Hagfeldt (2002) Ultrafast studies of electron injection in Ru dye sensitized SnO_2 nanocrystalline thin film, Int. J Photo- energy; 4:17–20.

[17] Y. Chiba, A. Islam, Y. Watanabe, R. Komiya, N. Koide, L.Y. Han, (2006) Dye sensitized solar cells with conversion efficiency of 11.1%. Jpn J Appl Phys, 45: L638–L640.

[18] R. Buscaino, C. Baiocchi, C. Barolo, C. Medana, M. Gratzel, M.D.K. Nazeeruddin, (2008) A mass spectrometric analysis of sensitizer solution used for dye sensitized solar cell. Inorg Chim Acta, 361:798–805.

[19] D. Matthews, P. Infelta, M. Grätzel, (1996) Calculation of the photocurrent-potential characteristic for regenerative, sensitized semiconductor electrodes. Solar Energy Materials and Solar Cells, 44:119–55.

[20] N.A. Ludin, A.M. Al-Alwani Mahmoud, A. Mohamad, A.H. Kadhum, K. Sopian, N. S. Abdul Karim, (2014) Review on the development of natural dye photosensitizer for dye-sensitized solar cells, Renewable and Sustainable Energy Reviews 31: 386–396.

[21] Hao S, Wu J, Huang Y, Lin J. (2006). Natural dyes as photosensitizers for dye-sensitized solar cell. Sol. Energy 80: 209–214.

[22] Hernandez-Martinez A.R., Estevez M, Vargas S, Quintanilla F, Radriguez R. (2012) Natural pigment based dye-sensitized solar cells. J Appl Res Technol., 10: 38–47.

[23] Zhang D, Lanier S.M., Downing J.A., Avent J.L., Lum J., Mc Hale J.L. (2008) Betalain pigments for dye-sensitized solar cells. J Photo chem Photo bio l A: Chem, 195:72–80.

[24] P.S. Greg, M. Grätzel (1998) Demonstrating electron transfer and nanotechnology: a natural dye sensitized nanocrystalline energy converter. J Chem Educ., 75:752–6.

[25] Monari A, Assfeld X, Beley M, Gros P.C. (2011) Theoretical study of new ruthenium based dyes for dye-sensitized solar cells. J Phys Chem A, 115:3596–603.

[26] M.K. Nazeeruddin, P. Péchy, T. Renouard, (2001) Engineering of efficient panchromatic sensitizers for nanocrystalline TiO_2 based solar cells. J Am Chem Soc., 123:1613–24.

[27] A.O. Adeloye, P.A. Ajibade, (2011) A high molar extinction coefficient mono- anthracenyl bipyridyl heteroleptic Ruthenium(II) complex: synthesis, photo-physical and electrochemical properties. Molecules, 16:4615–31.

[28] Yuancheng Q, Peng Q. (2012) Review articles: Ruthenium sensitizers and their application in dye sensitized solar cells. Int. J Photoenergy, 2012: 21 (Article ID291579).

[29] Luque A, Hegedus S. (2003) Handbook of photovoltaic science and engineering. The Netherlands: Elsevier.

[30] Chang H, Lo Y.J. (2010) Pomegranate leaves and mulberry fruit as natural sensitizers for dye sensitized solar cells. Sol Energy, 84:1833–7.

[31] Kishiomoto S, Maoka T, Sumitomo K, Ohmya A. (2005) Analysis of carotenoid composition in petals of calendula (Calendula of ficinalis L).Biosci Biotechnol Biochem., 69:2122–8.

[32] Keka S, Saha P.D., Datta S. (2012) Extraction of natural dye from etals Flam of forest (Buteamonosperma) flower: process optimization using response surface methodology (RSM). J Dyes Pigment, 94: 212–6.

[33] Nishantha M.R., Yapa YPYP, Perera VPS. (2012) Sensitization of photoelectrochemical solar cells with a natural dye extracted from Kopsia flavida fruit. Proceed Tech Sess., 28:54–8.

[34] Davies KM. (2004) Plant pigments and their manipulation, USA: Blackwell Publishing Ltd. Annual Plant Reviews; 342.

[35] Calogero G, Marco G.D., Cazzanti S., Caramori S., Argazzi R., Carlo A.D., (2010) Efficient dye-sensitized solar cells using red turnip and purple wild Sicilian prickly pear fruits. International Journal of Molecular Sciences 11: 254–267.

[36] Zhou H., Wu L., Gao Y., Ma T. (2011) 'Dye-sensitized solar cells using 20 natural dyes as sensitizers'. J. Photochem. Photobiol. A: Chem. 219: 188–194.

[37] Wongcharee K., Meeyoo V., Chavadej S. (2007) Dye-sensitized solar cell using natural dyes extracted from rosella and blue pea flowers. Sol. Energy Mater. Sol. Cells, 91: 566–571.

[38] Hao S, Wu J, Huang Y, Lin J. (2006) Natural dyes as photosensitizers for dye-sensitized solar cell. Sol. Energy 80: 209–214.

[39] Gòmez-Ortíz N.M., Vázquez-Maldonado I.A., Pérez-Espadas A.R., Mena-Rejón G.J., Azamar-Barrios J.A., Oskam G. (2009) Dye-sensitized solar cells with natural dyes extracted from achiote seeds. Sol. Energy Mater. Sol. Cells, 94: 40-44.

[40] Yamazaki E, Murayama M, Nishikawa N, Hashimoto N, Shoyama M, Kurita O. (2007) Utilization ofnatural carotenoids as photosensitizers for dye-sensitized solar cells. Sol. Energy 81: 512–516.

[41] Polo AS, Iha NYM. (2006) Blue sensitizers for solar cells: natural dyes from Calafate and Jaboticaba. Sol. Energy Mater. Sol. Cells, 90: 1936–1944.

[42] Hernández-Martínez AR, Vargas S, Estevez M, Rodríguez R. (2010) Dye-sensitized solar cells from extracted bracts bougainvillea betalain pigments. In: 1st International Congress on Instrumentation and Applied Sciences, 1–15.

[43] G.A. Armstrong, J.E. Hearst (1996) Carotenoids 2: Genetics and molecular biology of carotenoid pigment biosynthesis. FASEB J. **10** (2): 228–37. PMID 8641556.

[44] X.F. Wang, J. Xiang, P. Wang, Y. Koyama (2005) Dye sensitized solar cells using chlorophyll a derivate as the sensitizer and carotenoids having different conjugation lengths as redox spacers. Chem Phys Lett., 408: 409–14.

[45] H. Chang, M.J. Kao, T.L. Chen, H.G. Kuo, K.C. Choand, X.-P. Lin, (2011) Natural sensitizer for dye-sensitized solar cells using three layers of photoelectrode thin films with a Schottky barrier. Am J Eng Appl Sci., 4: 214–22.

[46] H.I. Scheer In: B.R. Green, W.W. Parson, Editors. (2003) Light-harvesting antennas in photosynthesis. Dordrecht: Kluwer Academic Publishers; p. 513.

[47] X.F. Wang, K. Osomu, H. Eiji, Z. Haoshen, S. Shin ichi, T. Hitoshi, (2010). TiO$_2$ and ZnO based solar cells using a chlorophyll a derivative sensitizer for light-harvesting and energy conversion. J Photochem Photobiol A: Chem, 210: 145–52.

Artificial Neural Networks Study on Prediction of Dielectric Permittivity of Basalt/PANI Composites

Onder Eyecioglu*‡, Mehmet Kilic**, Yasar Karabul **, Umit Alkan***, Orhan Icelli**

*Department of Mechatronics Engineering, Faculty of Engineering and Architecture, Istanbul Gelişim University, 34215, Istanbul, Turkey.

**Department of Physics, Faculty of Science and Letters, Yildiz Technical University, 34220 Istanbul, Turkey.

***Department of Computer Engineering, Faculty of Engineering and Architecture, Istanbul Gelişim University, 34215, Istanbul, Turkey.

(oeyecioglu@gelisim.edu.tr, mekilic@yildiz.edu.tr, karabul@yildiz.edu.tr, ualkan@gelisim.edu.tr, oicelli@yildiz.edu.tr)

‡ Corresponding Author: Onder Eyecioglu, Department of Mechatronics Engineering, Faculty of Engineering and Architecture, Istanbul Gelisim University, 34215, Istanbul, Turkey, Tel: +90 212 422 7020/288, oeyecioglu@gelisim.edu.tr

Abstract-In the present study, the dielectric permittivity change of basalt (two type basalt; CM-1, KYZ-13) reinforced PANI composites were studied to determine the effects of PANI additivities (10.0, 25.0, 50.0 wt.%) at several frequencies from 100 Hz to 17.5 MHz by a dielectric spectroscopy method at the room temperature and artificial neural networks (ANNs) simulation. Also, the dielectric permittivity at 30.0 wt.% of PANI additivity was obtained by ANNs without experimental process. That process, a significant predictive instrument was produced which allows optimization of dielectric properties for numerous composites without substantial experimentation. It has been observed that PANI additivities decreased to dielectric constant of composites at low frequencies. Furthermore, the ANNs method have satisfactory accuracy for prediction of dielectric parameters.

Keywords: Artificial neural networks, dielectric permittivity, basalt, PANI, composite.

1. Introduction

There is growing interest in reinforcing polymer matrix composites with basalt reinforced polymers because of their moderate cost, high stiffness and strength, excellent corrosion and oxidation resistance, and heat resistance and thermal stability. Basalt is a very common volcanic rock, dark colored and comparatively rich in iron and magnesium, which is located at almost every country in the world. Basalt is used for a wide variety of purposes. It has been used in the rock industry to create industrial construction, highway engineering and building tiles for other purposes [1]. Polyaniline (PANI) is one of the most promising conductive polymers for technological applications due to its easy synthesis, high environmental stability, huge electrical conductivity, as well as a comparatively low cost [2, 3]. PANI is synthesized for specific applications like organic electronics [3], circuit component (such as varistors [4], super capacitors [3, 5]), electrochemical catalysis [5, 6], corrosion protection [7, 8] and sensors [9].

Artificial neural networks (ANNs) are becoming well-known because of their achievement where complicated nonlinear relationships occur amongst data. ANNs are biologically influenced computer programs created to simulate the way in which the human brain processes knowledge. ANNs collect this information through detecting the relationships and patterns in learned via experience and data. The broad use of ANNs is a result of their ability and versatility to model nonlinear systems without earlier information of an empirical model. They do not require a specific formulation of the physical or mathematical relationships of the undertaking issue. These give ANNs an advantage over traditional fitting methods for numerous application. [10].

In this work, the dielectric permittivity values of basalt reinforced PANI were determined at several frequencies from 100 Hz to 17.5 MHz by using experimental Impedance spectroscopy technique, and this data was used to develop an artificial neural networks model for next prediction of dielectric permittivity. The data samples were produced three different composite (10.0, 25.0, 50.0 wt.%). Then, we

calculated the dielectric permittivity for 30.0 wt.% PANI additivity as a sample application of developed ANNs model.

2. Materials and Method

2.1. Materials

Basalt samples (two type basalt samples and coded CM-1, KYZ-13) obtained from different regions of Van in Turkey. Chemical analyses of the basalt samples are taken by X-ray fluorescence (XRF) instrument. Operating conditions of the XRF device of Philips PW-2400 were fixed at 50 mA and 60 kV. The results of chemical analysis of basalt samples are given in Table 1.

Table 1. Chemical composition of basalt samples [1].

Sample Comp.	CM-1	KYZ-13
SiO_2	41.668	47.790
TiO_2	2.0800	1.3950
Al_2O_3	13.106	16.918
Fe_2O_3	13.823	10.878
MnO	0.1920	0.1630
MgO	9.7540	7.6190
CaO	10.602	11.357
Na_2O	5.2610	3.1370
K_2O	1.7370	0.5190
P_2O_5	1.7770	0.2240

Polyaniline (emeraldine base, average Mw ~5000) was purchased from Sigma-Aldrich. To investigate effects of PANI additive percentages (10.0, 25.0, 50.0 wt.%) on the dielectric properties of basalt mechanically modified by PANI. These composites were prepared by mixing of basalt samples with PANI and were molded by compression in a cold press at room temperature. Each one of these mixtures prepared as a pellet having 13±0.02 mm diameter, 0.500±0.050 g weight and 1.9-2.2 mm thickness.

2.2. Dielectric Measurements

The dielectric measurements were carried out with a two-point probe arrangement. Dielectric measurements have been performed by using an HP 4194A Impedance Analyzer in the frequency range from 100 Hz–15 MHz at room temperature with a high accuracy (0.17% typ.) In this work, the overall errors the dielectric measurements are 2.5% and the RMS amplitude of the instruments is ~500mV.

2.3. Artificial Neural Networks (ANNs)

ANNs are a mathematical model that can be defined as an interconnected set of nodes their connections. Also neural network is a network of neurons. The neurons are the pre-defined computational units that are grouped in sets of layers. Basically, there are three types of layers, input, output and hidden layer as seen in Fig. 1. The input layer receives data from the outside and transfers them to sub layers. The data comes from input layer is processed in the hidden layer by performing interconnection of neurons and sending the results to the neuron in the output layer.
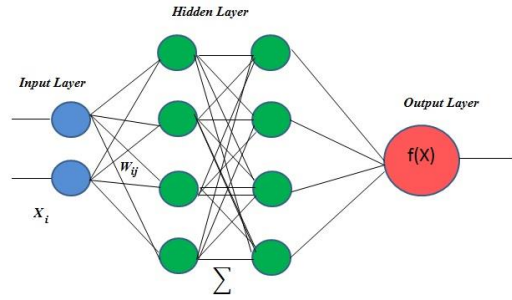
Fig. 1. The architecture of the ANNs algorithm.

The output layer submits the output data. The neurons perform weighted summation of the inputs that are applied to the networks calculated as [11];

$$Net_i = \sum_{j=1}^{N} X_{ij}.W_{ij} + n_i \tag{1}$$

Where W_{ij} is the weight between the i th neuron in the previous layer to the j th neuron. X_{ij} is the output of i th neuron and n_i is the bias value of previous layer.

The output of the i th neuron is calculated using a sigmoidal activation function as follows.

$$out_i = f\left(Net_i\right) = \frac{1}{1+e^{(-aNet_i)}} \tag{2}$$

Here, a is a constant used for controlling the slope of the semi-linear region [11].

There are two stages to process the network for an ANNs model. First of them is training and the other is testing. In the training stage, the network is training to predict an output based on the input. After that the training stage, the predicted output is compared with given output. This testing decides whether to stop or continue training of the network.

For the training of the network, a back propagation algorithm (BP) has been used. The Levenberg - Marquard (LM) algorithm [12, 13] is used to update the weights (W_{ij}) for minimizing the error function that defined as absolute difference between predicted output value and given actual value. In the LM algorithm, the Hessian matrix can be approximated as;

$$H = J^T J \tag{3}$$

and this approximation is used for the iteration of the weights;

$$x_{k+1} = x_k - \left[J^T J - \mu I\right]^{-1} J^T e \tag{4}$$

Where J is the Jacobian matrix, e is a vector of network errors, μ is the scalar learning rate and I is the identity matrix. When μ is large, this becomes gradient descent method. This method used as adaption function in this study.

The prediction accuracy performance of the networks was calculated using coefficient of determination (R) and relative error (RE);

$$R = \left(\frac{\sum_{i=1}^{N}(y_i - \overline{y}_i)(x_i - \overline{x}_i)}{\sqrt{\sum_{i=1}^{N}\left(y_i - \overline{y}_i\right)^2 \sum_{i=1}^{N}\left(x - \overline{x}_i\right)^2}} \right) \tag{5}$$

$$RE\left(\%\right) = \frac{|x_i - y_i|}{x_i} \times 100 \tag{6}$$

where y_i and x_i are predicted and actual values respectively.

3. Results

Dielectric spectroscopy is most reliable and powerful experimental technique which has been effectively used for the characterization of electrical properties of the polar materials [14]. The DS technique is based on analyzing the alternative current (a.c.) response of a materials to a sinusoidal perturbation, and subsequent calculation of dielectric parameters as a function of frequency and temperature [15].

The dielectric analysis gives the permittivity and conductivity of material as a complex permittivity $\varepsilon^*(\omega)$ parameter. Dielectric permittivity is a principal parameter that determines the coupling and distribution of electromagnetic energy during microwave and radiofrequency processing [15, 16]. The frequency dependence complex dielectric permittivity $\varepsilon^*(\omega)$ is given by

$$\varepsilon^*(\omega) = \varepsilon'(\omega) + i\varepsilon''(\omega) \tag{7}$$

Here, ω, $\varepsilon'(\omega)$ and $\varepsilon''(\omega)$ are the angular frequency, the real part of complex permittivity (or called dielectric constant) and the imaginary part of the complex dielectric permittivity (or called loss factor), respectively. In dielectric material $\varepsilon'(\omega)$ represents the alignment of dipoles, which is the energy storage component and $\varepsilon''(\omega)$ represents the ionic conduction component [15].

In this study, experimental results of $\varepsilon'(\omega)$ and $\varepsilon''(\omega)$ for samples have been shown in Fig. 2-5. The increase of the doping percentage of PANI decreases the dielectric constant for both composites in low-frequencies. Moreover, the $\varepsilon'(\omega)$ and $\varepsilon''(\omega)$ have large values in the low-frequency region and decreases rapidly in 10.0 wt.% PANI composites.

Furthermore, the ANNs model is developed to predict the dielectric parameters ($\varepsilon'(\omega)$ and $\varepsilon''(\omega)$) of these composites. The experimental measurements are used to obtain the 200 data samples of dielectric parameters ($\varepsilon'(\omega)$, $\varepsilon''(\omega)$) for various concentration (wt.%) and frequency (ω). Concentration and frequency of 200 data samples are used as input and, dielectric parameters of corresponding them are used as output (target). 80% percent of the data are used as training data and the other 20% are the testing data. The training and testing data are selected us randomly.
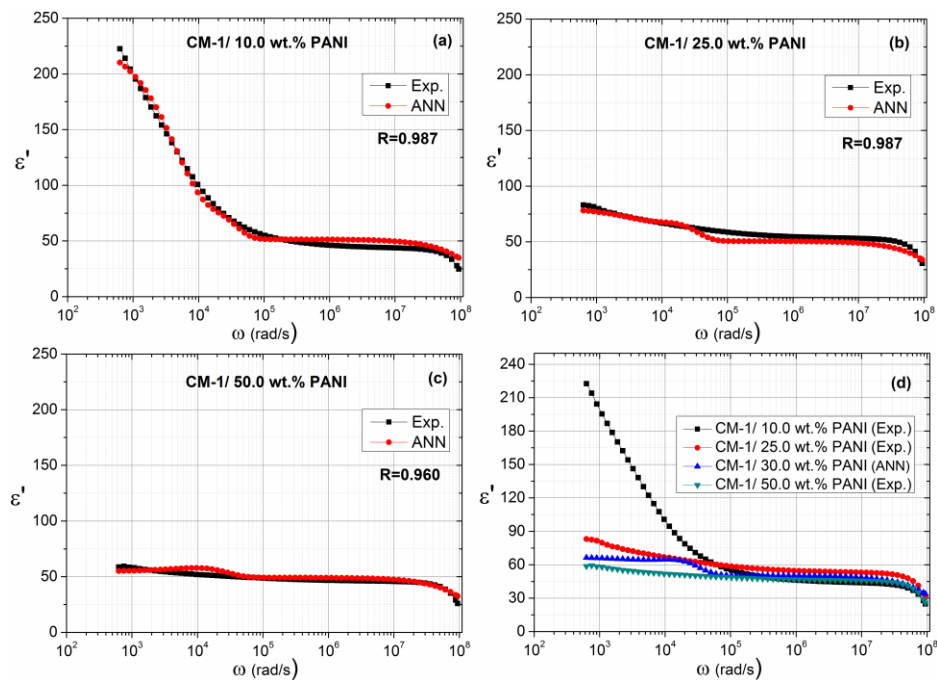
Fig. 2. Comparison of desired experimental results and predicted values of $\varepsilon'(\omega)$ for samples of **(a)** CM-1/ 10.0 wt.% PANI **(b)** CM-1/ 25.0 wt.% PANI **(c)** CM-1/ 50.0 wt.% PANI composites and **(d)** $\varepsilon'(\omega)$ prediction of CM-1/ 50.0 wt.% PANI composite
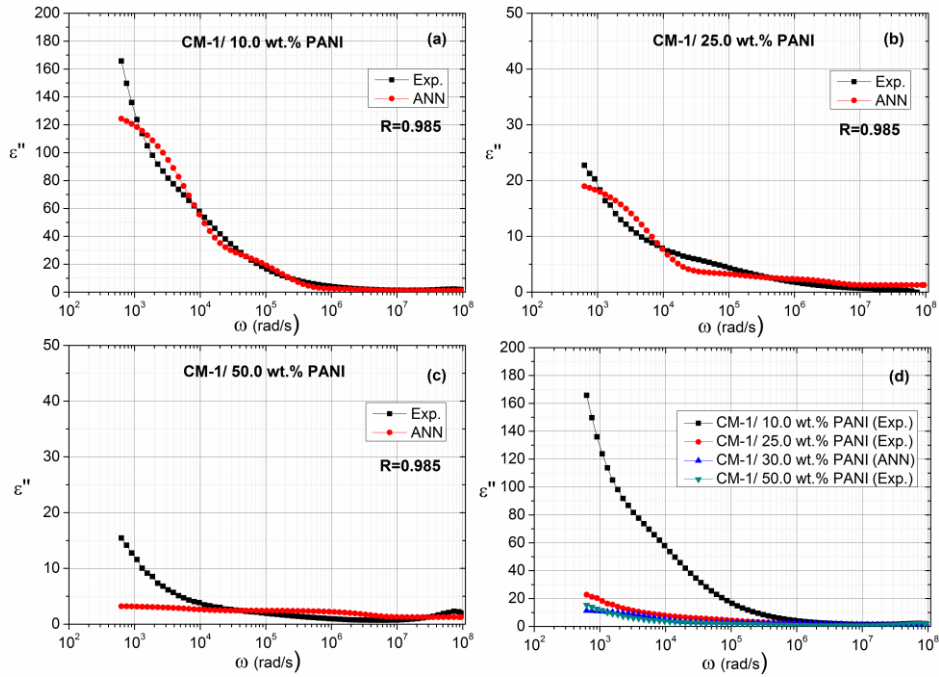
Fig. 3. Comparison of desired experimental results and predicted values of $\varepsilon''(\omega)$ for samples of **(a)** CM-1/ 10.0 wt.% PANI **(b)** CM-1/ 25.0 wt.% PANI **(c)** CM-1/ 50.0 wt.% PANI composites and **(d)** $\varepsilon''(\omega)$ prediction of CM-1/ 30.0 wt.% PANI composite

The comparisons of experimental results and output values predicted by ANNs of CM-1 are illustrated in Fig. 2-3. The figures show the variation of $\varepsilon'(\omega)$ and $\varepsilon''(\omega)$ with the frequency for various concentration (10.0 wt.%, 25.0 wt.% and 50.0 wt.%,). From these figures, it is seen that the high accuracy between experimental and simulated data.

Therefore, it can be concluded easily that the outputs efficiently modeled by the ANNs model.

Also, it can be concluded from Fig. 4 and Fig. 5, that the KYZ-13 values can be efficiently modeled by the ANNs model similar to the CM-1.
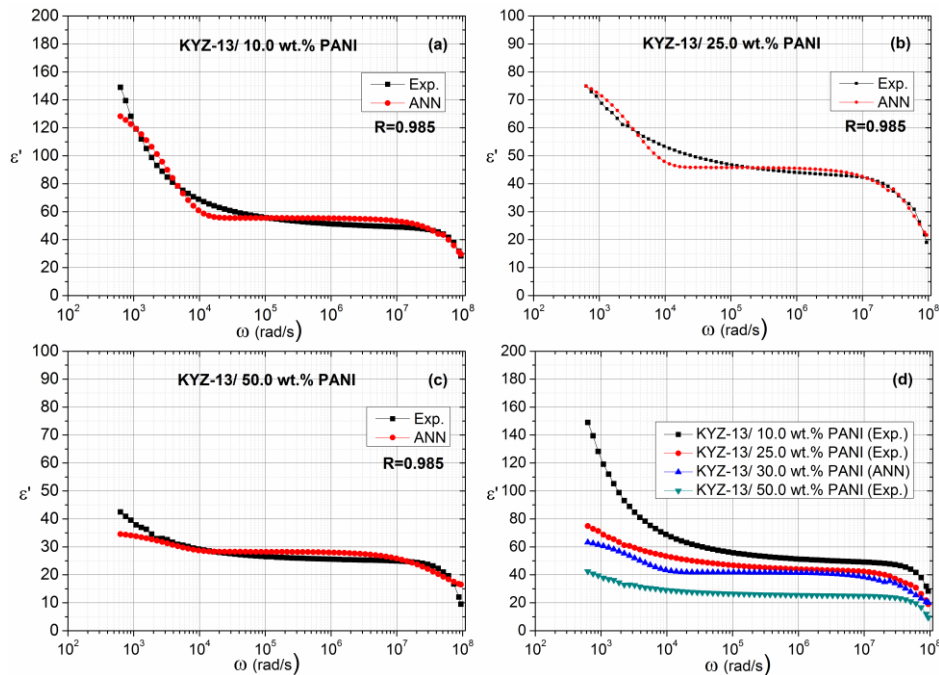
Fig. 4. Comparison of desired experimental results and predicted values of $\varepsilon'(\omega)$ for samples of **(a)** KYZ-13/ 10.0 wt.% PANI **(b)** KYZ-13/ 25.0 wt.% PANI **(c)** KYZ-13/ 50.0 wt.% PANI composites and **(d)** $\varepsilon'(\omega)$ prediction of KYZ-13/ 50.0 wt.% PANI composite
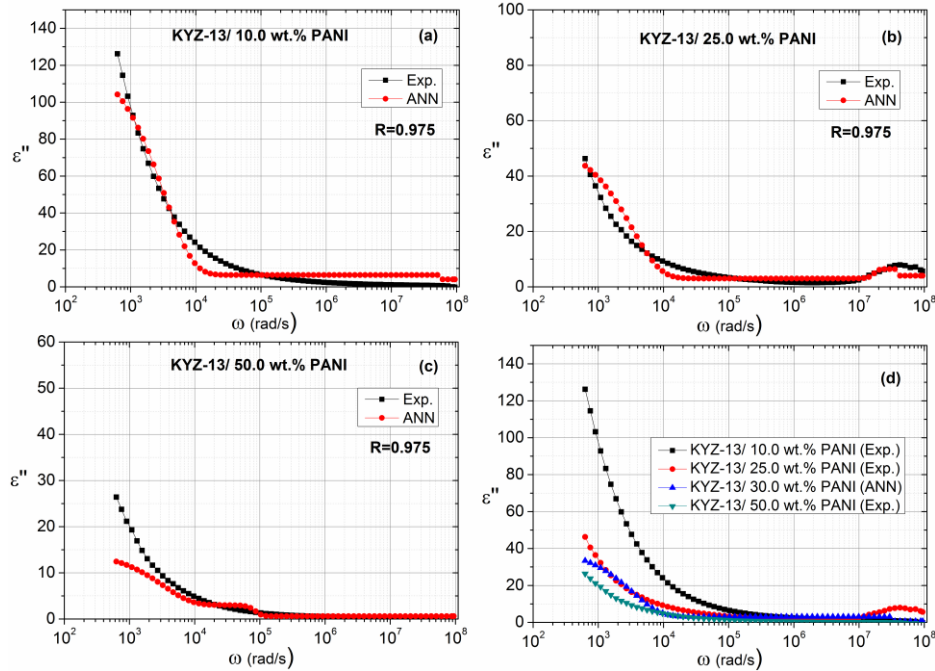
Fig. 5. Comparison of desired experimental results and predicted values of $\varepsilon''(\omega)$ for samples of **(a)** KYZ-13/ 10.0 wt.% PANI **(b)** KYZ-13/ 25.0 wt.% PANI **(c)** KYZ-13/ 50.0 wt.% PANI composites and **(d)** $\varepsilon''(\omega)$ prediction of KYZ-13/ 30.0 wt.% PANI composite

By using efficient training algorithm, the output values of $\varepsilon'(\omega)$ and $\varepsilon''(\omega)$ has been predicted for CM-1/ 30.0 wt. % PANI samples that were not measured in our experiments. The variation of predicted $\varepsilon'(\omega)$ and $\varepsilon''(\omega)$ values are figured in Fig. 2-d, Fig. 3-d, Fig. 4-d and Fig. 5-d. It can be seen that suitable output values can be obtained from ANN model for $\varepsilon'(\omega)$ and $\varepsilon''(\omega)$.

The performance of the model on training and testing stages in terms of R is presented in Fig. 6 and Fig. 7.
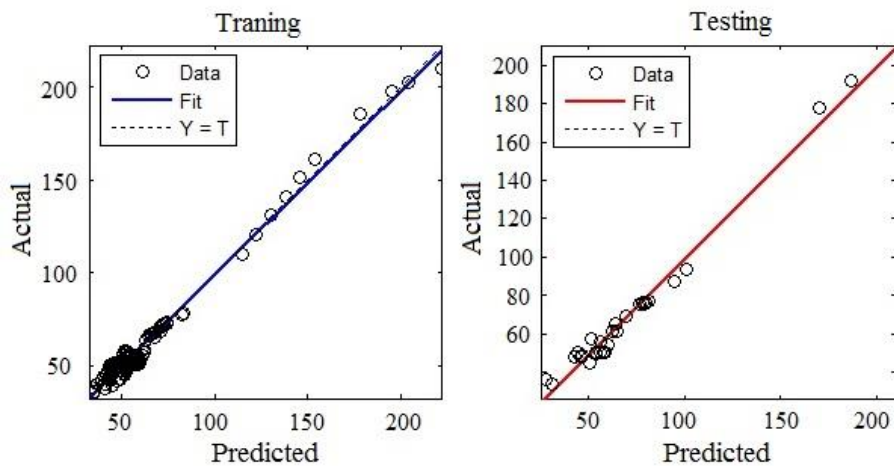
Fig. 6. Fit of ANNs model on **(a)** training data and **(b)** testing data of CM-1/PANI composites
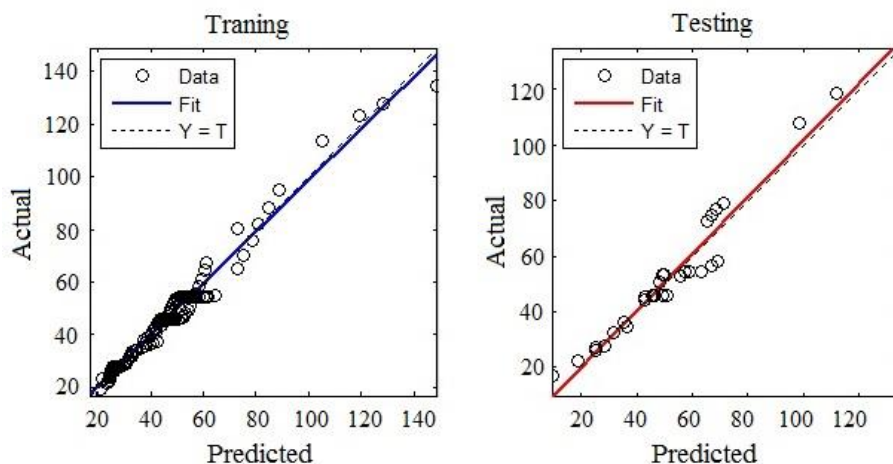
Fig. 7. Fit of ANNs model on **(a)** training data and **(b)** testing data of KYZ-13/PANI composites

The graphs show that the training algorithm worked well, and learned the non-linear relation between concentration, frequency and dielectric constant with high R value for both CM-1 and KYZ-13 samples. The R values of both training and testing are given in Table 2.

Table 2. Coefficient of determination (R) parameters of ANN for CM-1 and KYZ-13 composites

Sample R	CM-1	KYZ-13
R (Training)	0.991	0.987
R (Testing)	0.989	0.972

4. Conclusion

This study represents the results of our investigation on the dielectric properties of two type Basalt/PANI composite using dielectric spectroscopy and an application of the ANNs method in the prediction of dielectric properties of basalt materials depend on additive percentage (%) and frequency (ω).

The results given in this paper prove that the ANN method has satisfactory accuracy for prediction of desired properties ($\varepsilon'(\omega)$ and $\varepsilon''(\omega)$). So the ANNs model can be used as an appropriate and practical method to compute dielectric properties of materials under various experimental conditions such as, concentration, frequency or temperature.

References

[1] Y. Karabul, L.A. Susam, O. İçelli and Ö. Eyecioğlu, "Computation of EABF and EBF for basalt rock samples", Nucl. Instrum. Methods. Phys. Res. A, vol. 797, pp. 29–36, 2015.

[2] H.S. Nalwa, Handbook of Organic Conductive Molecules and Polymers, New York: Wiley, 1997.

[3] Z.A. Boeva and V.G. Sergeyev, "Polyaniline: Synthesis, Properties, and Application", Polymer Science Series C vol. 56, pp. 144–153, 2014.

[4] H. Bidadi, A. Olad, M. Parhizkar, S.M. Aref and M. Ghafouri, "Nonlinear Properties of ZnO-Polymer Composites Prepared by Solution-casting Method", Vacuum, vol. 87, pp. 50–54, 2013.

[5] H. Tang, Y. Ding, C. Zang, J. Gu, Q. Shen and J. Kan, "Effect of Temperature on Electrochemical Degradation of Polyaniline", Int. J. Electrochem. Sci., vol. 9, pp. 7252–7239, 2014.

[6] Z. Wen-Zhi, K. Xian-Wen, J. Shou-Feng, S. Jin-Gao, Y. Dong-Sheng and F. Bin, "Electrochemical characteristics and catalytic activity of polyaniline doped with ferrocene perchlorate", Journal of Applied Polymer Science, vol. 102, pp. 5633–5639, 2006.

[7] E. Akbarinezhad, M. Ebrahimia, F. Sharif, M.M. Attar and H. R. Faridi, "Synthesis and evaluating corrosion protection effects of emeraldine base Pani/clay nanocomposite as a barrier pigment in zinc-rich ethyl silicate primer", Progress in Organic Coatings, vol. 70, pp. 39–44, 2011.

[8] A.B. Samui, A.S. Patankar, J. Rangarajan and P.C. Deb, "Study of polyaniline containing paint for corrosion prevention", Progress in Organic Coatings, vol. 47, pp. 1–7, 2003.

[9] M. Ates, "A review study of (bio) sensor systems based on conducting polymers", Materials Science and Engineering C, vol. 33, pp. 1853–1859, 2013.

[10] A. Habibi-Yangjeh, "Prediction dielectric constant of different ternary liquid mixtures at various temperatures and compositions using artificial neural networks",

Physics and Chemistry of Liquids, vol.45, pp. 471–478, 2007.

[11] H. Kurt and M. Kayfeci, "Prediction of thermal conductivity of ethylene glycol–water solutions by using artificial neural networks", Applied Energy, vol. 86, pp. 2244–2248, 2009.

[12] K. Levenberg, "A Method for the Solution of Certain Non-Linear Problems in Least Squares" Quarterly of Applied Mathematics, vol. 2, pp. 164–168, 1944.

[13] D. Marquardt, "An Algorithm for Least-Squares Estimation of Nonlinear Parameters", SIAM Journal on Applied Mathematics, vol. 11, pp. 431–441, 1963.

[14] A.S. Nowick, A.V. Vaysleyb and I. Kuskovsky, "Universal dielectric response of variously doped CeO_2 ionically conducting ceramics", Phys Rev B, vol. 58, pp. 8398–8406, 1998.

[15] V.F. Lvovich, Impedance Spectroscopy Applications to Electrochemical and Dielectric Phenomena, New Jersey: Wiley, 2012, ch. 4.

[16] J. Suchanicz, "The low-frequency dielectric relaxation $Na_{0.5}$ $Bi_{0.5}$ TiO_3 ceramics" Mater Sci Eng B-Adv, vol. 55, pp. 114–118, 1998.

Determination of Some Physical Properties of Rapeseed

Mehmet Firat Baran*‡, Mehmet Recai Durgut**, Turkan Aktas**,

Poyraz Ulger**, Birol Kayisoglu**

*University of Adıyaman, Faculty of Technology, Energy Systems Engineering, 02040 Adıyaman, Turkey.

**University of Namık Kemal, Faculty of Agriculture, Biosystems Engineering, 59100 Tekirdağ, Turkey.

(mbaran@adiyaman.edu.tr, mrdurgut@hotmail.com, taktas@nku.edu.tr , pulger@nku.edu.tr, bkayisoglu@nku.edu.tr)

‡ Corresponding author: Mehmet Firat Baran, University of Adıyaman, Faculty of Technology, Energy Systems Engineering, 02040 Adıyaman, Turkey, Tel: +90 416 223 38 00, Fax: +90 416 223 17 74, mbaran@adiyaman.edu.tr

Abstract-Rapeseeds (*Brassica napus oleifera* L.) were analyzed for some physical properties production in Kırklareli province. Also some physical properties of rapeseed such as seed moisture content, length, diameter, mass of single seed, thousand seed mass, geometric mean diameter, sphericity, seed volume, density, accumulation angle and friction coefficient have been determined. Kernel moisture, thousand kernel mass, plant length, plant stem diameter, yield of the harvested crop were determined as 8.34 %, 4.74 g, 158.2 cm, 8.10 mm, 3204 kg/ha, respectively. Length, diameter, mass of single kernel, geometric mean diameter, sphericity, bulk density, accumulation angle and friction coefficient were found as 2.35 mm, 1.93 mm, 0.0047g, 2.07 mm, 0.88, 5.07 mm^3, 617 kg/m^3, 29^0, 0.318 (on galvanized sheet), 0.288 (stainless steel), 0.305 (aluminium), respectively.

Keywords: Rapeseed, physical properties, plant properties, seed properties

1. Introduction

As a of source vegetable oil, canola is a valuable oil crop plant, in fact the second highest produced in the world, following soya. In 2008, 57.86 million tons of canola seeds have been produced in the world in a total area of 30.30 million ha, while out of the approximate 392 million tons of the global vegetable oil production, 57.86 million tonnes have been met from canola [1]. China, Germany, India, Poland, England, France and Canada, in particular, are the most prominent canola oil producers and consumers in the world. In Turkey, canola farming started after World War II by the Bulgarian and Romanian immigrants in Thrace Region and over time it spread to other regions and by 1979 it reached an area of 27 thousand ha. However, after that date use of rapeseed varieties have been prohibited on the grounds that they contain high levels of fatty erucic acid and by 1985, it's farming was reduced to 100 ha. However, after the introduction of 00-type rapeseed varieties (canola) not containing fatty erucic acid and glucosinolate, it has become to be reproduced, particularly in Cukurova and Thrace regions [2].

In Turkey, the amount of successfully planted oil crop plants in winter conditions, such as canola, is highly limited. Canola farming displays significant similarities with wheat growing techniques, and they are being planted and harvested almost within the same time period (September-July). Therefore, particularly in dry farming areas with heavy cereal production, it becomes crucial as an alternative to cereals. When rosette leaves have already blossomed before winter months, certain aspects of canola, such as being highly durable against colds, not requiring any additional irrigation other than natural precipitation, reaching harvest maturity by July at the latest, being easily harvestable by a combined harvester and yielding more products, on average 30.1 kg/ha, than grains in dry farming conditions [3] makes canola indispensable. Oils containing high levels of erucic acid are harmful for human health, and similarly, cossets containing high levels of glucosinolate are harmful for animal health [4,5]. Therefore, rapeseed varieties which do not contain erucic acid in their oil, and those not containing glucosinolate in their cossets have been improved [6,7]. In modern times, 00 type rapeseed varieties containing low levels of (>2%) erucic acid (C22.1) in oil and low levels of (>30 μmol/g) glucosinolate in cossets are called canola [7,8].

Canola oil contains 65% oleic, %20 linoleic, 9% linolenic, 4% palmitic and 2% stearic acids on average [7,9]. Thus, containing over 60% oleic acid, canola oil differs from other vegetable oils (such as sunflower, soya, corn oils) while displaying similarities with olive oil [7].

It is possible to examine the physical characteristics of agricultural products by taking the single unit of each product variety or bulk stocking type as a basis. The important thing here is to correctly define and present the engineering parameters such as the product's shape, size, volume density and surface area. [10].

Physical characteristics are highly important in terms of sowing equipment, harvesting, handling, stocking and processing of the canola seed [11]. For the designation of granaries, silos and agricultural machinery, the friction coefficients of the agricultural products on various surfaces are needed. When designing granaries and silos, friction coefficient is used to calculate the vertical load on the membranes. In pneumatic transmission, particularly in high product concentrations, product-membrane friction creates an important resistance force. Flowing characteristics of granulated products are related to friction coefficients. Friction contributes to cutting, meshing and pressing of agricultural products. The movement of a granulated product on a rotating disc is affected by friction.

All these examples indicate that friction is present in almost all agricultural acts and is not to be ignored [10].

There have been a number of studies performed with the purpose of determining the productivity and physical characteristics of canola seed.

Çalışır et al[11] reported that, 2005, have analysed certain physical characteristics (size, length, diameter, geometric average diameter, roundness, mass of single seed, 1000 seed mass, volume density, final velocity, surface area and porosity) of canola seeds at three different moisture content levels (4.7%, 13.14%, 23.96%). The results have been listed as; 2.07-2.29mm, 1,84-1.99mm, 1.91-2.08 mm, 0,93-0.91, 0,0040-0,0065 g, 5,10-6,36g, 3,96-5,15 mm^3, 612,1-585,1 kg/m^3, 3,16-3,74m/s, 3,71-4,67mm^2, 48,2%-60,6% respectively. The study has concluded that all the dimensions of the canola seed has increased with an increase in porosity, surface area, 1000 seed mass and final velocity, moisture content; volume density and roundness has been reduced with an increase in moisture content; while static and dynamic friction coefficient characteristics have increased when moisture content was increased.

İzli et al.[12] reported that, 2009, have analysed some physical and mechanic characteristics such as size, length, diameter, geometric average diameter, sphericity, 1000 seed mass, surface area, volume density, porosity, final velocity and friction coefficient of three different canola seeds in two different moisture content levels (8,3%-25,9%, 7,7%-27,4%, 7,3%-26,4%) for each seed. The results acquired were as follows; size 2,26-2,54mm, diameter 1,85-2,08mm, geometric diameter 1,96-2,23 mm, sphericity 86,1%-89,8%, surface area 12,1-15,7 mm^2, volume value i 4,56-6,60 mm^3, accumulation angle 18,22-26,81^0, final velocity value 3,44-3,77 m/s and friction

coefficient (0,244-0,358 in galvanized surface, 0,233-0,331 in stainless steel surface, and 0,237-0,335 in aluminium surface). In their study, they have determined that the all the porosity, surface area, 1000 seed mass, final velocity and friction coefficient values of canola seed as increased when moisture content was increased, while volume density and roundness values decreased upon a decrease in moisture content.

Hazbavi and Minaei[13] reported that 2009, have used standard methods to determine certain physical characteristics such as size, length, diameter, geometric average diameter, sphericity, surface area, volume values and porosity of 7 different canola seeds (Option, Orient, Talaye, Global, Hyola 401, Hyola 308 and Colvert), based on freshness, in 6 different moisture levels (5,49, 4,55, 5,41, 4,74, 5,53 and 5,32). Conclusion of the study has revealed; 1,84-2,30mm, 1,76-2,15mm, 1,59-1,90mm, 1,76-2,09mm, 0,91-0,96, 9,74-13,86 mm^2, 2,67-6,44 mm^3, 928,01-1370 kg/m^3, 675,61-741,6 kg/m^3, 25,3%-45,9% respectively. They have noticed that certain physical characteristics produce significantly different values based on the canola variety and canola moisture content.

In this study, the object was to determine the agricultural characteristics (plant size, number of side branch and number of carob in the plant, number of grain in carob) of canola plant which has reached harvest moisture, seed yield, as well as the harvest related physical characteristics (moisture content, 1000 seed mass size characteristics, sphericity, mass of single seed, volume mass, accumulation angle and friction coefficient on 3 different surfaces) of the harvested seed. The distinguishing aspect of the study is that not only the seed characteristics of harvest period Elvis variety canola plant have been determined but also the herbal component characteristics have been defined.

2. Material and Method

2.1. Material

The plant material in the study was Elvis variety winter canola of *Brassica Napus L.* species. Elvis variety is a fast growing winter canola variety with a strong root and stalk structure, durable against cold, high levels of fat (40-45%) high hectolitre weight and 00 erucic acid level.

Trials took place at a farmer's land in Ürünlü village of Kırklareli city. The 5*20m trail zone has been divided into three parcels and samples of canola plant have been taken.

The trial zone has been made ready for planning by early September. During the seedbed preparations stage, 20 kg/da 20-20-0 composed fertilizer has been broadcasted to the whole trial zone. Planting norm has been applied at a rate of 450 gr/da. No herbicide has been applied but weeds have been removed by the use of a hand hoe. Once the plants have reached the 6 leaf stage, they have been thinned at an interval of 10 cm rows. During the month of March, 26% ammonium nitrate fertilizer has been applied at a rate of 25 kg/da. No irrigation took place. Pesticide has been applied twice in May and June against leaf beetle. Harvesting took place in June.

In addition to the plant material used in the study, a tape line has been used for plant size measurements, a calliper for plant stalk thickness measurement, a micrometre with a precision of 0.01 mm for the measurement of seed lengths, humectant containers to measure the product moisture content, precision balance and microprocessor controlled thermostat and a timer and dryer (drying oven) with a temperature precision of +5 ^{0}C - 250 ^{0}C, as well as 3 friction surfaces, galvanized metal, stainless steel and aluminium, to determine the friction characteristics of the material on different surfaces.

2.2. Method

2.2.1. Determining the Harvest Related Characteristics of Canola Plant

Depending on the warm or rainy weather conditions and early rising of the variety, canola plant reaches harvest maturity between 40 to 50 days after blossoming. When canola reaches harvest maturity, the stalks, leaves and capsules of the plant completely dry up and turn pale, and a yellow colour occurs. If the seed has turned brown and seed moisture content drops below 10%, it means that it is time to harvest the plant. Maturing in canola plants occurs from bottom to top. Waiting for full maturity in harvesting may lead to cracks and shedding may occur in lower capsules [2].

2.2.1.1. Stalk (Trunk) Diameter

25 samples have been taken from the relevant trial parcel for calculating the plant stalk (trunk) diameter. The samples have been measured by the use of a calliper to define the average stalk (trunk) diameter value.

2.2.1.2. Measuring the plant length

25 samples have been taken from the parcels at the trial zone to measure the plant length. Samples have been cut by scissors right above the soil, and measured by a tape line to define the average plant length values.

2.2.1.3. Counting the amount of side branches

25 sample plants have been taken from all parcels to count the number of side branches and the figures have been divided to the number of samples to define the average number of side branches.

2.2.1.4. Counting the number of carob (capsule) in the plant:

Once the canola flowers are inseminated, the ovarium develops, and fruits in the shape of capsule or carob with approximately 10-26 seeds occur inside, the fruits consist of two sections, divided by a placenta (membrane) [2]. 25 samples have been taken from the parcels at the canola trial zone and the number of carobs per plant has been counted before dividing the total figure to the number of samples to define the average values.

2.2.1.5. Counting the number of grains in the carob

25 samples have been taken from the parcels at the canola trial zone and the number of grains per carob has

been calculated, before dividing the total figure to the number of samples to define the average values.

2.2.1.6. Defining the field product yields

In order to define the field yield, samples have been taken from three different parts of the field within a 1 square meter area before harvesting the measured parcels, the samples in this section have been manually harvested, the product has been weighed and average values have been calculated, which have been related to the yield per decare [14].

$$Q_T = \frac{qt}{n} \qquad (1)$$

In this equation;

Q_T : Field grain yield (kg/da)

qt : Grain yield total of the samples (gr/m^2),

n : Number of samples taken from the fields.

2.2.2. Defining the Harvest Related Characteristics of Canola Seed

2.2.2.1. Defining the seed moisture content

Harvesting of canola plant takes place when the moisture of the seed is below 8-10% [15]. In order to confirm whether the product has reached harvest moisture, samples have been taken at certain intervals during the harvest period, and the moisture content of the seed has been defined in conformity to the standards [16]. Seed moisture content has been calculated by using the following equation on the basis of freshness.

$$N_{yb} = \frac{W_s}{W_s + W_m} \qquad (2)$$

In this equation,

N_{yb} : Seed moisture content (%),

W_s : Wet weight of product (g),

W_m : Dry weight of product (g).

2.2.2.2. Defining the thousand grain mass

Certain amounts of samples have been taken from the harvested product to define the thousand grain mass and divided into groups of 100, and these groups of 100 samples have been weighed 4 times. Scale averages of the 100's groups have been taken and this average has been multiplied by 10 to find out the 1000 seed mass of the product [17].

2.2.2.3. Defining the seed lengths

In order to calculate the seed lengths, 10 sample groups containing 100 seeds have been randomly selected and then their related length, width and diameter values have been measured.

2.2.2.4. Defining the sphericity and geometric average diameter values:

Sphericity value is a scale of the disfigurement of the seed too [18]. Based on the seed length, the sphericity and geometric diameter values of the canola seed have been calculated by using the below equations [19,20].

$$\o = (L.D^2)^{1/3} / L \qquad (3)$$

$$D_g = (L.D^2)^{1/3} \qquad (4)$$

In these equations,

$\o$: Sphericity (%),

D_g : Geometric average diameter (mm),

D   : Diameter (mm),

L   : Length (mm).

2.2.2.5. Defining the grain volume

Grain volume has been calculated in accordance with the weight of the fluid replaced by the grains placed into the liquid (toluene) [21,22]. With this purpose, 50 canola seed grains have been used in 3 repetitions and the average bulk density has been calculated.

2.2.2.6. Defining the accumulation angle

Cleaned seeds have been carefully placed inside a vertical cylinder and then slowly poured. The height and base diameter of the resulting cone shaped seed pile have been measured to calculate the accumulation angle by using the below relation. This has been repeated 24 times to determine the average accumulation angle [23,24].

$$\o = \tan^{-1}(2H /d) \qquad (5)$$

In this equation;

H: height (mm),

d: diameter value (mm).

2.2.2.7. Defining the friction coefficient:

In order to determine the friction characteristics of the material on different surfaces, 3 different friction surfaces, galvanized metal, stainless steel and aluminium, have been used. Before conducting the friction test, the product should be skid sufficient times (50 times) on the friction surface, hence preparing the friction surface to the product [10].

For the purposes of defining the friction coefficient (μ_s) of the piled product, a dipping plated measurement device has been used. The dipping plated measurement device has a plate with an adjustable angle. In this mechanism, friction plate's inclination is increased until the moment the product starts to slide. The (Θ) tangent of the angle between the bed and the dipping plate has been taken as the friction coefficient. This procedure has been repeated 10 times to measure the required sliding heights for then to be able to move in 3 different friction plates. By using the sliding heights the friction coefficients in different friction materials have been found [25,26].

$$\mu_s = \tan\Theta \qquad (6)$$

3. Result and Discussion

3.1. Results Related to the Characteristics of Canola Plant

As well as the harvesting method, canola harvesting is also affected by various generative characteristics such as stalk thickness of the plant, plant length, number of side branches, number of carobs etc. Therefore, the plant characteristics of the Elvis variety canola and field product yield have been defined after harvest at the trial field. The results related to these characteristics have been presented in Table 1.

Table 1. Value related to the plant characteristics of canola plant that has reached harvest maturity

Properties	Average Values
Plant Stalk Diameter (mm)	8.10 ±0,3
Plant Length (cm)	158.2 ± 1,0
Number of Side Branches (pcs)	8.9 ±0,0
Number of Grain (pcs) in Carob (capsule)	27.1± 2,0
Number of Carob (capsule) (pcs)	358.3 ± 4,0
Yield (kg/ha)	3204 ±10.

Reviewing some of the previous studies indicate that seed yield values have been calculated as 2593 kg/ha [27], 2777 kg/ha [28], 3097 kg/ha [29], 2357 kg/ha [30], 2466 kg/ha [31] and 2180 kg/ha [32]. Looking at these values, our yield value (3204 kg/ha) seems to be very high. It is assumed that the reason for this seed yield value to be higher than those reported by other researchers is due to the variety characteristic of the seed and early planting period.

Plant stalk (trunk) thickness has been defined as 8.10 mm, plant length as 158.2 cm, number of side branch as 8,9, number of carob per plant as 358.3 and number of grains per carob has been defined as 27.1. According to some studies related to winter canola; plant length values have been defined as 178.2 cm [33], 152.0 cm [34], 156.9 cm [32]. Number of side branches have been defined as 8.5 pcs. [35], 8.1 pcs [32] ; while number of grain in the carob have been defined as 28.0 pcs/carob [28] , 26.35 pcs /carob [36], 30 pcs /carob [32] and 25.3 pcs /carob [37]. Number of carobs in plant, on the other hand, have been defined as 336.0 pcs [38] and 338.7 pcs [32].When we compare the values defined for plant in this study conducted under Kırklareli conditions, with the results of other studies, it can be said that the plant characteristics defined in other previous researches are in parallel to our data.

3.2. Conclusions Related to Canola Seed's Harvest Related Features

Moisture content related average of the canola seeds acquired from the trial zone during harvesting has been defined as 8.34% and product harvesting has been started on the assumption that sufficient moisture level required for harvesting has been reached. Some physical characteristics of the seed observed at 8.34% moisture content have been presented in Table 2. Looking at Table

2; the average length of the seed is 2.35 mm, average diameter is 1.93 mm, geometric average diameter 2.07 mm, sphericity value 0.88, single seed weight 0.0047 g, thousand grain weight 4.74 g, seed mass 5.07 mm^3, volumetric weight 617 kg/m^3, accumulation angle is 29°, friction coefficient on galvanized metal surface is 0.318, on stainless steel surface it is 0.288, and on aluminium surface it is 0.305.

Table 2. Some physical characteristics of canola seed measured at 8,4% moisture value

Properties	Average Values
Length (mm)	2.35±0,20
Width (diameter) (mm)	1.93±0,13
Geometric Average Diameter (mm)	2.07±0,15
Mass of single seed (g)	0.0047±0,0001
1000 grain weight (g)	4.74± 0,15
Sphericity (%)	0.88±3,29
Seed bulk density (mm^3)	5.07± 1,02
Volumetric weight (kg/m^3)	617±2,2
Accumulation angle (^{0})	29±1,02
Friction coefficient (Galvanized metal surface)	0.318±0,024
Friction coefficient (Stainless steel surface)	0.288±0,018
Friction coefficient (Aluminium surface)	0.305±0,012

The average sphericity value, calculated by using the length, width and thickness values of the canola seeds with an average moisture content of 8.34%, is 0.88. reviewing the results of similar studies conducted on canola seed, Razavi *et al.* [20] reported that (2009), 4 different varieties of canola seed (Hyola, Okapi, Orient and SLM) in two different moisture level (5.27%-23.69%), depending on the variety, length values vary between 1.925-2.262 mm, diameter values between 1.475-1.911 mm, geometric average diameter values between 1.625-2.02 mm, while sphericity values vary between 0,82-0,93. *Çalışır et al* [11] reported that, 2005 under different moisture levels (4.7%, 13.14%, 23.96%), length values of canola seeds varied between 2.07-2.29 mm, diameter values between 1.84-1.99 mm, geometric average diameter values between 1.91-2.08 mm, and sphericity values varied between 0.93-091. *İzli et al* [12] reported that (2009) performed similar measurements for 3 canola seed varieties (Capitol, Samurai and Jetneuf) under two different moisture content levels (8.3%- 25.9%, 7.7%-27.4%, 7.3%-26.4%) and for Capitol variety, length values varied between 2.46-2.57 mm, diameter values between 1.96-2.08 mm, geometric average diameter values between 2.11-2.23 mm, and sphericity values varied between 86.1%-86.8%; while for Jetneuf variety; length values varied between 2.26-2.36 mm, diameter values varied between 1.85-2.00 mm, geometric average diameter values varied between 1.98-2.12 mm, and sphericity values varied between 87,4%-89,8%. Following the study conducted on the Samurai variety, they have reported that the geometric characteristics have varied, even if very little; while the length values varied between 2.25-2.31 mm, diameter values varied between 1.82-1.98 mm, geometric average diameter values varied between 1.96-2.09 mm, and sphericity values varied between 86.8%-89.6%.

Looking at the results given in Table 2, we can say that the average 1000 seed mass of the canola seeds used in the study was 4.74 gr, while mass of single seed was 0.0047 gr. Similarly, Razavi et al[20] reported that (2009) 1000 seed mass of the canola seed they have used in their study was 3.06-4.84 g; while Çalışır et al[11] reported that (2005) the mass of single seed value as 0.0040-0.0065 gr.

According to Table 2, the seed volume is 5.07 mm^3, while the volumetric mass has been calculated as 617 kg/m^3. Similarly, [20] reported that the volumetric mass of canola to be between 666,6-738,8 kg/m^3, [11] calculated it to be between 612.1-585.1 kg/m^3. [12] reported that depending on the variety, have reported the seed volume in capitol variety to be between 4.45-6.60 mm^3, [13] have reported the seed volume to vary between 2.66 mm^3-6.44 mm^3.

Based on the results of the study, accumulation angle of the canola seed has been calculated as 29°. A similar result was reported by [20], where the accumulation angle value has been reported to vary between 25.37-28.54°.

Analysing the results related to friction coefficient, which is an important parameter in almost every post-harvest works, it has been observed that Elvis variety canola seed displays different friction behaviours on different friction surfaces. The study has concluded that the lowest friction coefficient was on stainless steel surface by 0.288. This value has been calculated as 0.305 on aluminium surface, while on galvanized metal surface, it has reached maximum value and was reported to be 0.318. Similar findings have been reported by [20]. Researchers have calculated the friction coefficient as 0.301- 0.419 on galvanized metal, 0.260-0.414 on fiberglass surface, and 0,358-0,450 on carton surface. Based on the measurements conducted by [12] on galvanized metal surface, albeit depending on variety, they have reported that the friction coefficient values range between 0.244-0.358. The closest value to the friction coefficient value of Elvis variety canola seed, used in our study, on galvanized metal has been observed in Capitol variety (0.314-0.358). On the other hand, friction coefficient values of Jetneuf (0.251-0.274) and Samurai (0.244-0.272) varieties have proved to be very low.

4. Conclusion

In conclusion, when we compare the conclusions of this study with the data acquired in other studies, we see similarities in general, while the tiny differences between them are assumed to be related to the use of different canola seed varieties and the difference in moisture content of the seeds. The outcomes of this study, related to the plant and seed characteristics acquired during harvesting, shall be useful for the selection and designing of harvest machineries and the equipment to be used for post-harvest purposes for canola plant, which is being widely planted in Turkey.

References

[1] FAO, 2008. Production, Yield, Harvested Area Values of Rapeseed. Avaliable from FAOSTAT (April, 2010). www.fao.org.

[2] Süzer, S., 2008. Kanola Tarımı Kitabı. Hasad Yayıncılık.

[3] TUİK, 2008. Plant Production Techniques, (April 2010). www.tuik.gov.tr.

[4] Adolphe, D., 1987. Canola: The Universal Oilseed. 7th International Rapeseed Congress, 11-14 May, Poznan-Poland.

[5] Mailer, R.J., and Wratten, N., 1987. Glucosinolate Variability in Rapeseed in Australia. 7th International Rapeseed Congress, 11-14 May, Poznan-Poland.

[6] Zukalova, H., Vasak, J., Fabry, A., 1985. Changes in the Quality Characteristics of Winter Rape Cultivars Free from Erucic and Glucosinolates. Rostlinna-Vyroba. 31 :685-692.

[7] Baydar, H.,2005. Yield and Quality Characteristics of Canola Varieties in Isparta Conditions. S.D.Ü. Fen Bilimleri Enst. Dergisi,9-3(2005), Isparta.

[8] Röbbelen, G., Downey, R.K. and Ashri, A., 1989. Oilcrops of the World. McGraw Hill, USA.

[9] Weiss, E.A., 2000. Rapeseed. In: Oilseed Crops. Blackwell Sci. Ltd., Victoria, Australia.

[10] Kara, Turgut, N. ve M., 1999. Agricultural productsin Physical characteristic. Atatürk Üniversitesi Ziraat Fakültesi Ders Notları No: 212, Erzurum.

[11] Çalışır, S., Marakoğlu, T., Öğüt, H., and Öztürk, Ö., 2005. Physical Properties of Rapeseed. Journal of Food Engineering. 69:61-66.

[12] İzli, N., Ünal, H., and Sincik, M., 2009. Physical and Mechanical Properties of Rapeseed at Different Moisture Content. Institute of Agrophysics, Polish Academy of Sciences, .23:137-145.

[13] Hazbavi, I. and Minaei, S., 2009. Determination and Investigation of Some Physical Properties of Seven Variety Rapeseed. Iranıan Journal of Food Scıence and Technology Wınter. 5(4):21-28.

[14] Ülger, P., 1982. Buğday Hasat Harmanında Uygulanan Degişik Mekanizasyon Sistemlerinin Tane Ürün Kayıplarına Etkileri. Hasat Öncesi ve Hasat Sonrası Ürün Kayıpları Seminer Bildirileri, 13–17 Aralık p.: 195-243, Ankara

[15] Anonymous, 2009. Swathing, Combining "Harvest Management" http://www.canola.org/ chapter 11.aspx (26.01.2009)

[16] ASAE, 1997. ASAE S358.2, Moisture Measurement Unground Grain and Seed. In: ASAE 398 Standards, ASAE Press, St. Joseph. MI, USA.

[17] Şehirali, S., 1989. Seed Technology. Ders Kitabı, Ankara

[18] Önal, İ., 1995. Ekim Bakım Gübreleme Makinaları, E.Ü. Ziraat Fakültesi Yayınları No: 490, Bornova, İzmir.

[19] Mohsenin, N. N., 1970. Physical Properties of Plant and Animal Material. New York: Gordon and Breach Science Publishers.

[20] Razavi, S.M.A., Yeganehzad, S. and Sadeghi A., 2009. Moisture Dependent Physical Properties of Canola Seeds. J. Agric. Sci. Technol. 11:3009-322 .

[21] Lewis, M.J., 1996. Physical Properties of Foods and Food Processing Systems. Woodhead Publishing Limited, Cambridge, England

[22] Kayişoğlu, B. ve Esen, M., 2007. Ayçiçeği Tanesinin Nem Absorbsiyon Özelliklerinin Saptanması. Tekirdağ Ziraat Fakültesi Dergisi. 4 (2).

[23] Irtwange S.V., 2000. The Effect of Accession on Some Physical and Engineering Properties of African Yam Bean. Unpublished PhD Thesis, Department of Agricultural Engineering, University of Ibadan, Nigeria.

[24] Akaaimo D.I. and Raji A.O., 2006. Some Physical and Engineering Properties of Prosopis Africana seed. Bio systems Eng., 95(2):197-205.

[25] Kocabıyık, H., 1997. Ayçiçeğinin Hasada Yönelik Bazı Fiziksel ve Mekaniksel Özelliklerinin Saptanması Üzerine Bir Araştırma. Yüksek Lisans Tezi, T.Ü.Fen Bilimleri Enst. Tarım Makinaları Anabilim Dalı, 1997,Tekirdağ.

[26] Aktas T.; Celen, I. and Durgut, R., 2006. Some Physical and Mechanical Properties of Sunflower Seed (Carthamus tinctorius L.). Journal of Agronomy, 5 (4):613-616.

[27] Şaman, S., 1983. II. Ürün Tarımı Araştırma Yayım Projesi Rapeseed Dilimi, 1982-1983 Yılı Gelişme Raporu. T.C.T.O.K.B. Proje ve Uygulama Genel Müd., Antalya.

[28] Kolsarıcı, Ö. ve Er, C., 1988. Amasya İlinde Rapeseed Tarımında En Uygun Ekim Zamanı, Çeşit ve Bitki Sıklığı Tesbiti Üzerinde Araştırmalar. 2:163-177.

[29] Başalma, D., 1999. The Effects of Different Planting Norms on Plant Characteristics and Yield and Quality of Winter Rapeseed Varieties. 3rd Field Crops Congress, Turkey, 5-18 November, 317-322, Adana.

[30] Sağlam, C., Arslanoğlu, F. ve Kaba, S., 1999. Kışlık Rapeseed Çeşitlerinin Tekirdağ Koşullarına Adaptasyonu. 3rd Field Crops Congress, Turkey, 5-18 November, p:344-347, Adana.

[31] Karaaslan, D., 1999. Diyarbakır Koşullarında Yetiştirilebilecek Rapeseed Çeşitlerinin Saptanması Üzerine Bir Araştırma. 3rd Field Crops Congress, Turkey, 5-18 November, 328-333, Adana.

[32] Öz, M., 2002. Bursa Mustafakemalpaşa Koşullarında Different Ekim Zamanlarının Kışlık Rapeseed Çeşitlerinde Verim ve Bazı Verim Unsurları Üzerine Olan Etkileri. Uludağ Üniv. Zir. Fak. Dergisi. 16: 1-13.

[33] Kolsarıcı, Ö. ve Başoğlu, F., 1984. Yağ Kalitesi ve Yağ Oranı Yüksek Kışlık Rapeseed Çeşit ve Hatlarının Verim Komponentleri Yönünden Karşılaştırılması. A.Ü. Ziraat Fakültesi Yıllığı, s.66-76.

[34] Raymer, P.L., Bullock, D.G. and Thomas, D.L., 1990. Potential of Winter and Spring Rapeseed Cultivars for Oilseed Production in the Southern United States, s:223-225, Timber Press.

[35] Karacaoğlu, N., Kaya, Ç. ve Çiçek, N., 1998. Canola Araştırmaları. T. O. K. B. Ege Agricultural Araştırma Enstitüsü, İzmir.

[36] Kolsarıcı, Ö. ve Er, C., Tarman, D., 1985. Islah Edilmiş Kışlık Rapeseed Çeşitlerinde Verim Komponentlerinin Karşılaştırılması. A.Ü. Ziraat Fakültesi Yıllığı, 61-74.

[37] Göksoy, A.T. ve Turan, Z.M., 1986. Studies on Yield and Quality Characteristics of Certain Rapeseed Varieties. U. Ü. Ziraat Fakültesi Dergisi. 5: 75-83.

[38] İlisulu, K., 1970. Adaptation, Seed Yields and Other Characteristics of Rapeseed Varieties, Brought from France and Germany, under Ankara Climate and Soil Conditions. A.Ü. Z.F. Yıllığı, s.132-157.

Steering Wheel Tie Rod Fatigue Life Determination According to Turkish Mission Profiles

Arif Senol Sener[‡]

Department of Mechanical Engineering, Faculty of Architecture and Engineering, Istanbul Gelisim University, Avcılar, Istanbul, Turkey.

(assener@gelisim.edu.tr)

[‡] Corresponding Author; Arif Senol Sener, Department of Mechanical Engineering, Faculty of Architecture and Engineering, Istanbul Gelisim University, Avcılar, Istanbul, Turkey, Tel: +90 212 422 7000, Fax: +90 212 422 7401, ssener@gelisim.edu.tr

Abstract-In this study, Turkish customer automobile usage was determined by a questionnaire in order to form the Turkish Mission profile for a LCV (light commercial vehicle). A comparison between Turkish customer usage and a of the European County's mission profile was done. Referencing sale percentage of this vehicle and the region of the failures come out on other model vehicles were produced before and also Turkey's geographic and climate condition, a new test road was formed for this kind of vehicle. İn order to determine Turkey's rods fatigue characteristics a road test executed. About 50 road routes and some rough road's fatigue characteristics were acquitted with a LCV (Light Commercial vehicle) equipped with sensors. Collected data were elaborated with a software program such as; spike analysis, frequency analysis, artihmethic manipulation etc.. After that the general load spectrum of Turkey's roads belong to the steering wheel tie rod is formed. Rain-flow statistical counting method was applied steering wheel tie rod's signals in order to make fatigue comparisons meaningfully and other application. Then Fatigue analysis of the steering wheel tie rod according to MP (Turkish mission profiles) were calculated by using FEA (Finite Element Analysis) and verified by the Palsmgren-Miner rule.

Keywords: Customer usage, steering wheel tie rod, finite element analysis, fatigue analysis, Palmgren-Miner rule.

1. Introduction

Due to typical vehicle development time getting shorter, automobile firms look for advanced techniques to facilitate more rapid progress service load data acquisition and analysis method [1]. One of the most parameters of the vehicle performance is the fatigue life that is difficult verify in a normal process in a short time because fatigue problem arises in the long-mileage as well [2-3]**.** Hence, automobile companies uses new techniques in order to eliminate fatigue failures come out on prototype vehicles during is very important in terms of customer expectation and guarantee cost within the vehicle development time. The major parameters that effects the durability of a component are material, geometry and load spectrum [2,4,5]. The prediction of service life, reliability and safety are essential for the design process of road vehicle structures [6]. Fig. 1 shows the basic parameters necessary to complete the fatigue analysis based on finite element theory. These parameters are linear analysis results, dynamic load data, and the material specifications [2, 5].
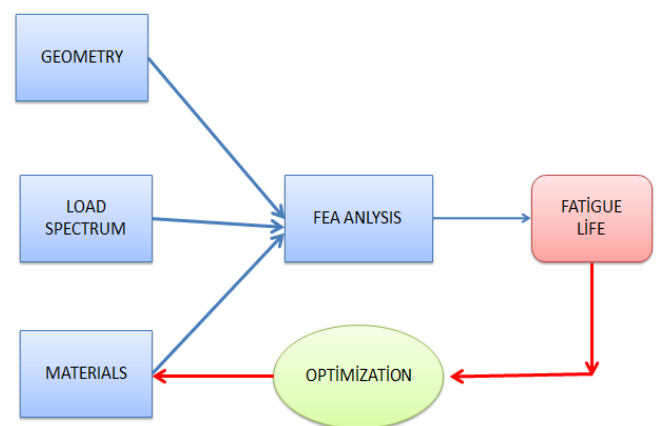

Fig. 1. Fatigue calculation based on the FEA [5]

For the service life of a product operational loading conditions are main importance [4]. The requirements on the strength, however, strongly depend on the loads in actual customer usage. Without appropriate knowledge of these loads one needs large safety factors, restrictive weight or cost

reduction potentials [7]. By executing real test and computer analysis fatigue life prediction and the undamaged time of a vehicle component, which is affected by load spectrum, must determine referencing customer usage in which market component run [4].
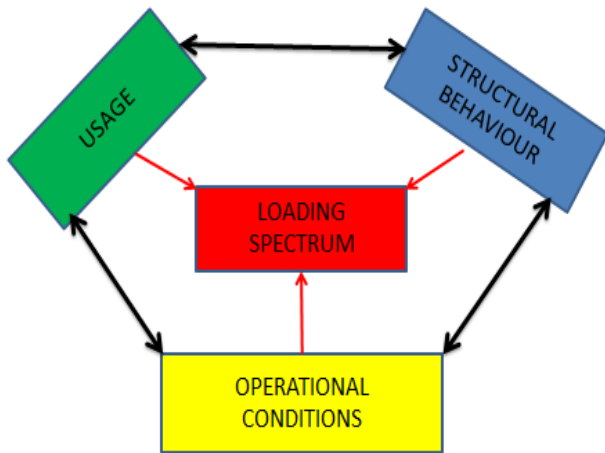

Fig. 2. Load spectrum parameters [2]

Essentially, automotive companies use four durability test methods: fatigue analysis based on Finite Element Analysis (FEA), test rigs, test benches (one particular actuator test), and accelerated test track. Rates of them in the four methods have advantages and disadvantage [6, 7]. As a result, during design and verification process automobile companies use one or several methods together on automobile parts [3]. Durability test of a car, it encounter throughout their entire lifetime loads, type of usage, environmental and operational conditions will represent the entire load spectrum is provided by the determination [3, 4, 6]. Such a study on the most important and difficult is that how the representative load spectrum is determined. For the reason that all the methods used to date are either too weak or too extremely heavy [3].

The most popular method used for the determination of load spectrum for the whole life of vehicle is a customer usage based method [3-8].

One example of a customer usage study which includes dry and wet ground usage of tractor and agriculture as well as non-agriculture tractor usage and also regional tractor usage examination is a study on a tractor usage in India, which was performed by ETEC (Eicher Tractors Engineering Centre) and ARIA (Automotive Research Association of India **[9]**. Another example is a customer usage study performed by FIAT Co. for Brazilian and Italian markets. As we know that Brazil and Turkey have not special proving ground in order to make tests on standard fatigue road for development of new car models, FIAT Co. compared proving ground profile effects of public roads of Italy and Brazil in addition to customer usage effects on the vehicles by using frequency based fatigue life [10]. Another example is of a customer usage study was done by FIAT Co. AMOA (automobile mode of operation systems) on Ritmo 60 and Tipo1372 DGT [11]. And one of the other example is of customer usage study was performed by FIAT Co. for defining Turkish customer vehicle usage on a B segment vehicle Punto [12]. And one of the other example is of

customer usage study was performed by TOFAS A.Ş. for defining Turkish customer vehicle usage profile and fatigue characteristic effect of Turkey's road profiles on a light commercial vehicles [13,14,15]**.**

The first important difference of the study compared to other studies is that the Turkish customer automotive usage profile was determined by a questionaries' method. Holiday time and the distance from the home which is one of the parameter of the questionnaire which has been monitored by FIAT Co. in 1993 [8]. FIAT had accepted the holiday concept as the interval of holiday more than three days and if the distance is far away more than 300 km from the residence area. In our study the holiday concept is restudied and holiday interval was decreased from one week to three days and the holiday distance was accepted as 300 km from the residence area. These parameters were applied on the Turkish customer in 2001 as a questionnaire [13]. The second important difference of the study compared to other studies is that those considered road roughness fatigue characteristic effects on the vehicle which were acquired from public roads (city roads, intercity, mountain and highway) were also mixed with some special proving ground data. Because Turkey no has not standard proving ground very heavy village roads including mostly potholes and sharp curves as well as bad rocked road profiles were defined quantity into the public roads [2, 13]. The third important difference of this study compared to other studies is that road roughness fatigue data were mostly acquired from about 20 km of the sample roads, i.e., road fatigue characteristic data were not acquired from one city to another city totally. For example, Iveco and nCode Co. realized one study in 1999 in Australia [3, 13]. During this study they acquired 28 load measurements, 12 micro-strains, 2 weight conditions, 16 test track surfaces revealing 1280 signals with approx. 1.5 gigabytes and 26 road route surfaces revealing 280 signals with approx. 4 gigabytes. But in this study on 50 roads, approx. 45 gigabytes raw data were acquired and after processing the raw data, the total data file size was enlarged from 45 gigabytes to approx. 200 gigabytes [13].

In this study, the road fatigue characteristics were totally measured from one city to another city to find out the effect of different roads and to form new reliability roads that are necessary during the process and pre-series production around the interested factory. The design of test roads is extremely important for accurately simulating vehicle life. In the following sections, to determine a test track for a light commercial vehicle that benefited a lot from sensor data that one of driving shaft strain-gauge sensor, on test methodology is described

In the previous studies about the steering wheel tie rod, in 2006, a SUV's tie rod breaking problems were investigated [16]. In 2013 Static stress and natural frequency calculations of a steering wheel tie rod and steering wheel arm at an angle was done by Patil.M.A [17,18]. All equipment is made in the static structural analysis results for the model geometry as a single piece, it was determined that equipment is safe. A tool rod linkage parts of a minivan in 2014, was made separately by the modeling. The computer analysis performed and analytical improvements have been made according to 2000 Newton axial loads concerning in

the specification of the FIR and the warranty is based on the application documents [19,20].

In terms of time and cost, although all of them largely by the superior, as in the test rig, also the CEA in terms of weather and road conditions, process failures, driver errors, etc. are not expected to face assimilation a hundred percentages [14,15].

In this article, the measured steering wheel tie rod raw data were collected, processed in order to find out MP (mission profile road characteristic) for a light commercial vehicle that benefited a lot from sensor data that one of steering wheel tie rod sensor, on test methodology is described.

2. Methods and Analysis

This method implements a large telephone survey designed to acquire information about the distribution of route types (city, extra urban, mountain, highway) the distribution of loads (driver without loads, driver and half load, driver and full load) customer education level, and the purpose of vehicle usage etc. [3, 13]. After acquiring the questionnaire results, a road test simulation is performed to collect data with an equipped vehicle or several equipped vehicles on public roads and special proving ground, during various maneuvers (braking, curving, accelerating), during power generation (engine and transmission components, in various location, on various type of roads (city, intercity, mountainous, rural), and by a test driver or multiple test drivers[6,13].Then the collected row data are elaborated like spike, filtering, manipulation etc. Then each road signal is subjected to statistically counting method 3D matrix or 2D range. So it is possible to make comparison of each road signal for each sensor. By multiplying the questionnaire with road type and target km to form the target mission profile which consists of road excitation signals taking into account 90th percentile distribution of customer automotive usage, load, and the target MP is obtained for each sensor [3, 13].

The methodology is based on the following principle, if the same inputs are reproduced, then same damage will occur [3]. After forming MP, it is then possible to find mixes of tracks or rig drivers that match to the inputs for accelerated test including track or test rig that are corresponding to the same damage effect of MP. If the same inputs are maintained, matrix calculation of various forms will provide a scheme for assessing the mixture of road excitation signals, and for optimizing the test length or test time.

A [X1] + B[X2] + C[X3] +……………..+Z[Xn] = [Y]

Where

A, B, C ….Z: Multipliers of test data,

[X1], [X2]……….. [Xn]: matrix of test measurements,

[Y]: matrix of customer target measurements.

This can be interpreted quite easily as: A times track X1, followed by times track X2, and so on, so that it gives the same effect as y of the target [3].

3. Implementation

In this study for road test acquisitions, FIAT Doblo Passenger car is selected as LCV. In Fig. 3 the algorithm of the study is presented.
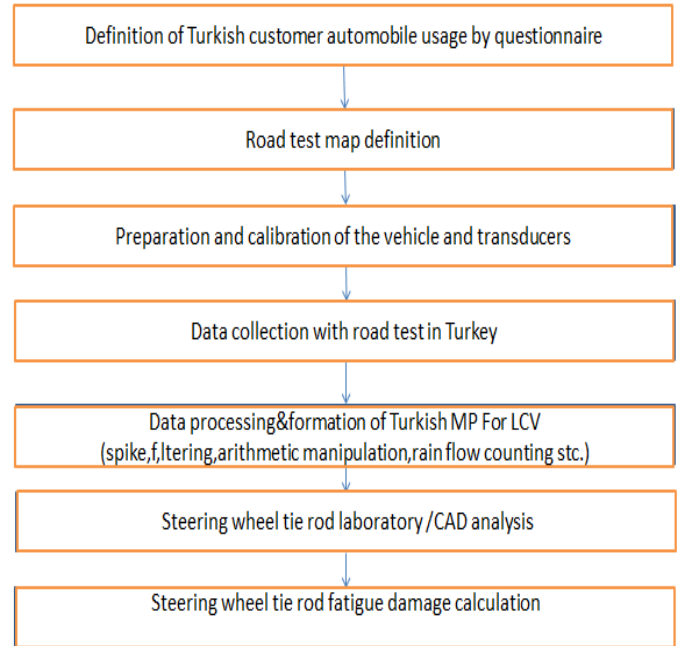
Fig. 3. Algorithm of the study

3.1. Definition of the Turkish Profile –Questionnaire Application.

As the questionnaire method allows a faster data collection, provides flexibility on data elaboration and reduces cost compared to the black box method as such, it was the method of choice in this study. The Turkish customer usage profile of a LCV that is used for transporting both goods and passengers was developed based on a questionnaire administered to Turkish customer with my support and also with the support of automotive dealers representing the LCV manufacturer[13].

3.2. Definition of the Turkish Profile-Definition of Road Map.

The defined test road map represents 90 % of customer usage in Turkey. Those test roads in the road test map was designed taking reference of the sale percentages of LCVs according to region, customer complaints, previous model experiences, climatic conditions, and geography [3,12,13]. Roads were allocated in four groups: city road usage was found to be more common around the Istanbul district; Mountain roads were more common in the Black Sea region. Intercity roads, which include hot climatic and curved road condition, were found around the Mediterranean Sea. Roads in Central Anatolia were characterized by high altitudes, hot temperatures, and long distances between cities. For the highway road characteristics Istanbul-Ankara and Adana – Gaziantep roads were subjected to data acquisitions.

3.3. Definition of the Turkish Profile-Data Acquisition to Define the Mission Profile Target.

In this study, data acquisitions from the roads in Turkey were carried out with a vehicle equipped with sensors and driven over customers on chosen roads by an expert test driver and an engineer at full loads. Test vehicle was equipped with load transducers, two strain-gauges on the leaf spring, one strain-gauge on front left driving shaft, and one strain-gauge on the steering wheel tie rod. In Fig.4 and 5 subsequently demonstrate that the steering wheel tie rod with strain-gauge applied before and after fixing on the test vehicle. All sensor, transducers and strain gauges were calibrated and analyzed in the laboratory before being assembled on the test vehicle. Vertical acceleration caused by different maneuvers and road roughness were measured by accelerometers that were fixed at the bottom of shock absorber. Lateral and longitudinal body accelerations of the test vehicle were measured using two accelerometers positioned at the center of mass of the vehicle. Breaking maneuvers was measured by recording pressure in the hydraulic circuit. Two displacement sensors were used to define body movements. Ultimately the test vehicle speed, engine crank shaft rpm and temperatures (12 thermocouples) were digitally recorded [13]. The strain gauge application on the steering wheel tie rod and its assembly on the test vehicle are subsequently presented in Fig.4 and Fig.5.

Fig. 4. Steering wheel tie rod with strain-gauge applied

Fig. 5. Steering wheel tie rod with strain-gauge assembled on the vehicle

3.4. Data Processing

For fatigue data collection at time domain, we could not measure external loads directly. Instead of that we measured their reactions at certain points of vehicle part [21].The collected signals were processed by spike analysis, frequency analysis, filtering, arithmetic manipulation and statistical counting operation [8].

Spike Analysis: During data acquisition some ''spikes'' which were occurred due to environmental and physical factors, were eliminated by visual and statistical methods [22].

Filtering: As it is known that vehicle suspension parts frequency range of interest for fatigue analyses is between 40 Hz and 60 Hz. For road simulation, it is generally accepted that excitation over 100 Hz can be neglected [13]. In Fig.6, low amplitude signals with frequencies above 100 Hz are not significant for fatigue analyses were removed from the original data by means of a low-pass filter [12, 13, 14, 15, 22].
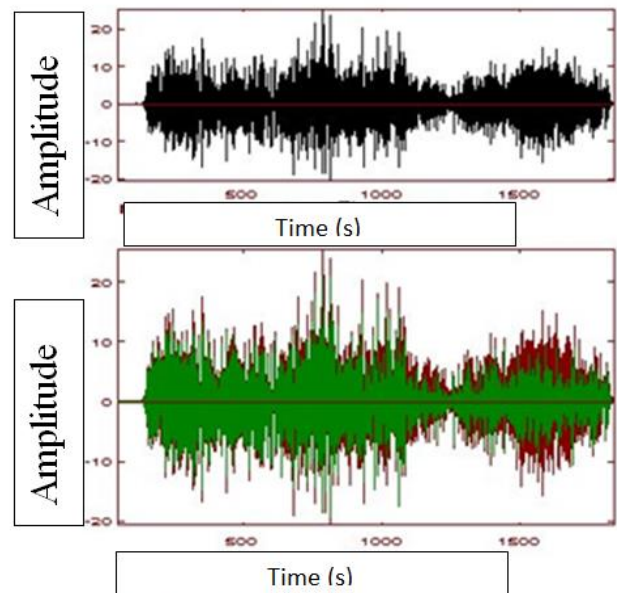
Fig. 6. Data filtering above 100 Hz [13]

Arithmetic Manipulations: In this study, acquired each test data which is not useful for fatigue life calculation is extracted before the vehicle movement is presented in Fig.7 [13,22]

Statistical Road Excitation Signal Counting: It is known that the road signal is formed by random and stationary signals that are time-varying. Time –varying signals should be converted to an equivalent value independent of time for comparison. The rain flow statistical counting method was applied to succeed in this conversion [23].The steering wheel tie rod strain-gauge axial data were reduced to foreseen 200000 km MP values taking into account mean amplitude [12,13,14,15, 24].

Forming Mission Profile Target: As the each acquired data had different lengths, the each measured data was normalized to convenient distance in kilometers (i.e., 1 km or 1000 km) in order to compare and extrapolate for MP

[12,13,14,15]. Each normalized measurement was classified according to road type (city, intercity, mountain, and highway); each road type was averaged within its class. Then each classified measurement was extrapolated to the estimated target km of MP and then multiplied by the percent Turkish customer usage distribution which the given road type based on the questionnaire. Fig. 7 illustrates that the histogram of steering wheel tie rod axial data MP (Turkish customer automobile usage fatigue characteristic of steering wheel tie rod for 200000 km).
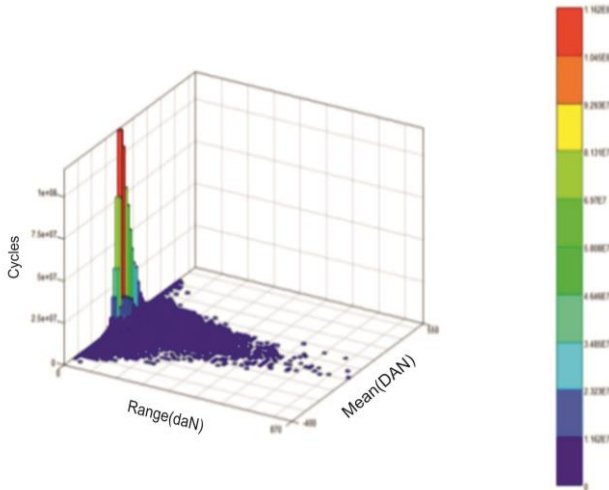
Fig. 7. Steering wheel tie rod Mission Profile rain-flow histogram (200 000 km)

4. Simulation of Experimental Data by Finite Element Analysis

4.1. Steering wheel tie rod CAD model

Fig. 8 shows the CAD model of the steering wheel ties rod was designed in Solidworks software program [25]. Tetra hydrogen solid elements were used for the steering wheel tie rod in order to precise modelling due to having a complex structure especially on the neck of the rod surface [26]. Then 3D CAD model of the steering wheel rod was exported to ANSYS program to perform FEA analysis. 3D CAD model of driving shaft was formed from 72233 tetra hexagon elements and 124827 nodes is presented in Fig.9 [26].
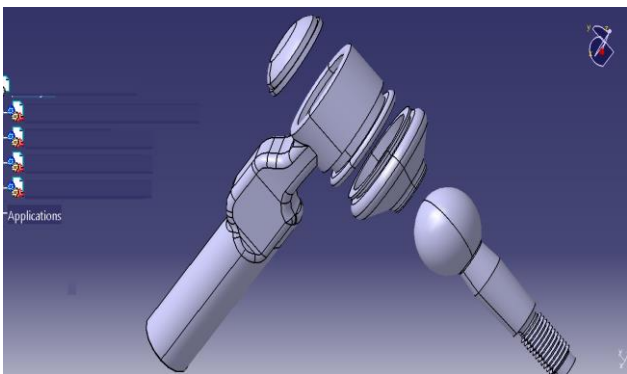
Fig. 8. CAD model of steering wheel tie rod
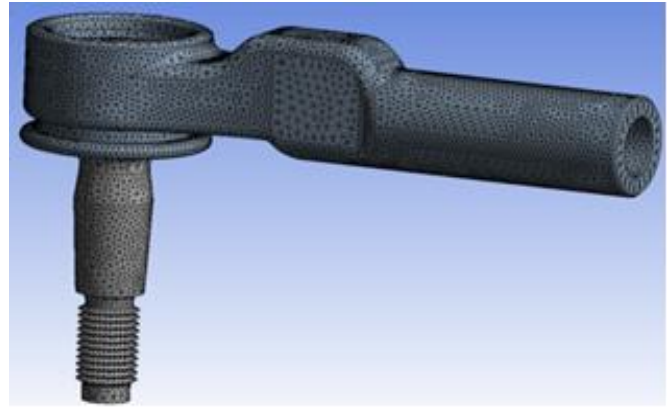
Fig. 9. FE Model of the steering wheel tie rod

4.2. Boundary Condition

The steering wheel tie rod's boundary condition of is illustrated in Fig.10. As it can be seen from illustration, the red arrow at the right surface of tie rod demonstrates the applied axial pulling load direction, which is allowed free only extension axis while the other balling rod side that is demonstrated with blue arrow that is connected to knuckle with a bold, is demonstrated and the fixed point is not allowed freely both rotation and shift every three axis [26, 27].
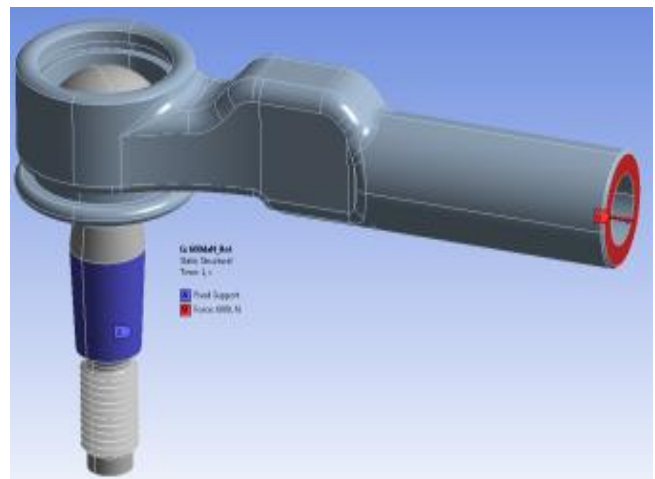
Fig. 10. Boundary conditions

The ball joint connection between the surface and the spherical guide surface around 3 degrees of freedom (DOF) has been defined links. Because the steering wheel tie rod is fixed from the each side both steering wheel cramayer shaft and the rack at the knuckle freedom is allowed to return are depicted. Here, in three axes of translational freedom (x, y, z) of linear movement, the freedom of rotation in three axes (Rx, Rz, Rz) represents rotation.

4.3. Static and Fatigue Analysis

Fig.11. shows the most critical load signal, which was acquired during road test in Turkey, of the steering wheel tie rod used for the linear static analysis of part.
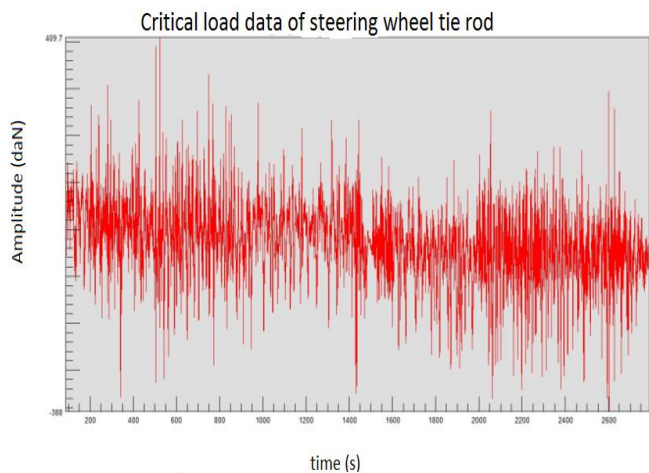
Fig. 11. Critical road data axial force -time signal of steering wheel tie rod

The linear static analysis of the steering wheel tie rod was performed using the most critical load that was picked up during road tests in Turkey is displayed in Fig.12. For the statistical analysis of steering wheel tie rod, the maximum load data, measured during the road test, horizontally 900 daN axial pulling forces was applied from the side of steering wheel tie rod connection by using the FE model. In Fig.12, it can be seen that after applying 900 daN axial pulling force on the spherical joint branches 0.0061938 με strain was derived. Simultaneously, the maximum nominal stress was found 1397 Mpa at node 5796 according to the von-Misses method by means of the most critical load condition in the linear static analysis [13, 27].
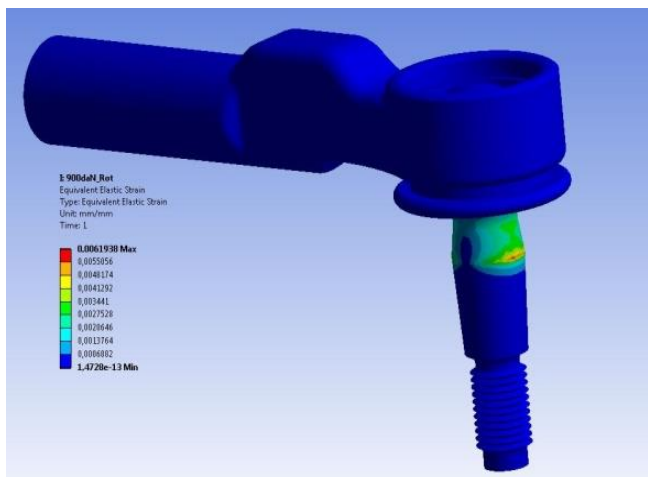
Fig. 12. Static strain analysis of steering wheel tie rod according to 900 daN axial force

Fig.13 shows the comparison of the steering wheel tie rod real bench test and CAD static analysis strain values. As it can be seen from the graphics, the vertical axis demonstrates physically applied axial force loads whereas the axial axis demonstrates derived unit normal strain on the driving shaft in laboratory and CAD during calibration test. Blue square symbol demonstrate us physically applied axial real force load on the steering wheel tie rod in lab while red triangle symbol shows us the CAD static analysis result after applying same loads on the FE model of steering wheel tie rod. When 100 daN is applied 0.0009427 με by the physical

test, 0.0006882 με by the computer analysis test were measured.
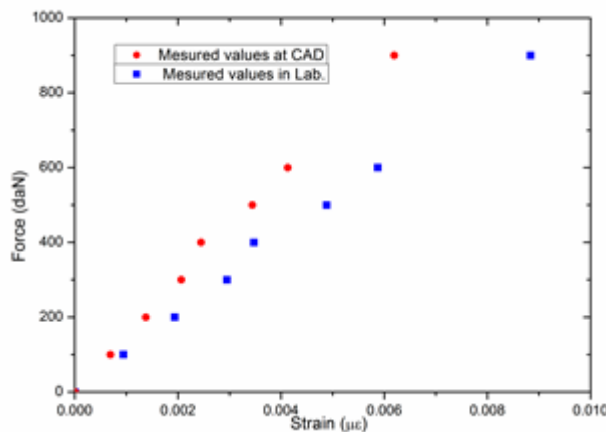
Fig. 13. Steering wheel tie rod real bench test and CAD static analysis strain values comparison

It is determined that the maximum stress is much lower than the actual yield stress of the steering wheel tie rod material yield stress. For these reason the S-N method was chosen [13, 27]. Fig.14 illustrates the Wohler line S (stress) - N (number of cycles) of the material characteristics of the steering wheel tie rod [27].
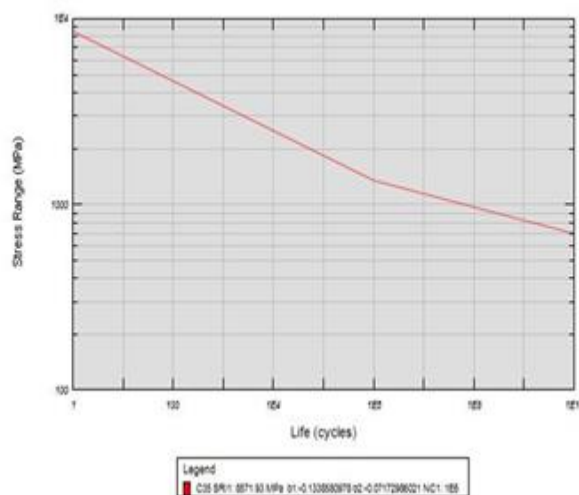
Fig. 14. S-N curve of the steering wheel tie rod

4.4. Plamgren-Miner Analysis

If a specimen is stressed at n_1 of N_1 cycles, the damage after n_1 cycles at σ_1 will be n_1/N_1 of the total damage, D, at failure. Similarly, for a second stress level test with lifetime N_2 the corresponding damage per cycle is D/N_2. Thus the total damage at failure is D= Dn_1/N_1 +Dn_2/N_2 where n_1 and n_2 are total number of cycles at σ_1 and σ_2 respectively. The Plamgren- Miner rule states that failures will occur if, n_1 /N_1 $_+n_2$ /N_2 $_+$ n_3 /N_3+........1 [28]. In this study the Plamgren-Miner rule is applied. Fatigue CAD analysis of steering wheel tie rod in terms of fatigue damage is given in Fig. 15. Fatigue damage is not occurred.

Fig. 15. Fatigue damage of steering wheel tie rod applying 200000 km MP data

5. Result

Resulting from the questionnaire, the automotive usage of Turkish customer for a LCV is defined in Table 1.

Table 1. Turkish customer usage of LCV-Passenger [13]

City Usage	50 %
Intercity	24 %
Highway	20 %
Mountain/Hill	6 %

When the derived data are analogue to one of the European countries, the most important difference is found in the amount of city usage, which is 50% in Turkey.[12,13]**.** These load spectra have been verified in terms of a fatigue damage analysis according to the Palmgren-Miner damage rule. From the MP test in Turkey 900 daN like the maximum axial force load is reached. Fig.16 shows 2D graphics of steering wheel tie rod data of mission profile 200.000 km.
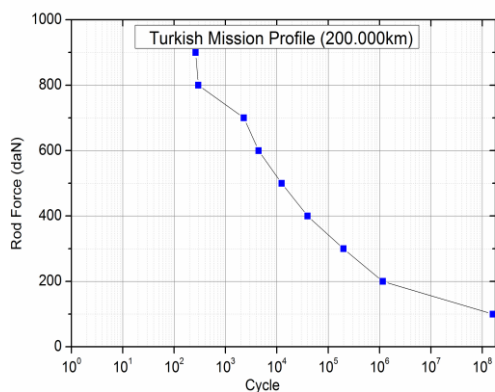
Fig.16. Steering wheel tie rod data of mission profile 200.000 km

6. Conclusion

In this study, Turkish customer usage profile was developed based on a questionnaire handed out to Turkish light commercial vehicle users [13]**.** A comparison of LCV usage between a European country and Turkey was presented. It discovered that the Turkish customers use this type of vehicle for city driving twice as much as typical users in a European country [12, 13].

After processing, classifying and normalizing different signals fatigue chcarcteristics of Turkey's roads (mission Profile) for 200.000 km in normal dirving condision were determined mathematicallyfor this kind of vehicle [14, 15]**.**

It is determined that the lineer analysis method that is used in virtuel analysis of the structure gave more precise result.

Based on this analysis, critical force and stress ranges have been defined and recorded in a database for future reference during development projects.

Tetra and hexagon type 3D elements have been used in FEA models of steering wheel tie rod. Tetra type elements were found to give more precise results in terms of frequent and geometrical aspect for this kind of component.

It has been observed that S/N fatigue method was more appropriate according to steering wheel tie rod's critical data amplitude which is lower than Wöhler line.

It has been verified that there was no fatigue damage occurred on the steering wheel tie rod after applying the Turkish customer profile (MP_200000 km).

It has been observed that computer aided analysis can be used as an alternative for laboratory tests because the results that were obtained from both methods were quite similar

Acknowledgements

References

[1] J. P. Heyes, X. Lin, A. Buczynski, and M. Brown: Application of biaxial plasticity and damage modeling for the life prediction and testing of automotive components, Proc. of the 5th International Conference on Biaxial/Multiracial Fatigue and Fracture, Cracow, Poland 1997

[2] V. Grubisic, Determination of load spectra for design and testing. International Journal of Vehicle Design, 1994. 15(1-2): pp. 8-26.

[3] Case Study - Complete Customer Usage Profiling Example

[4] N.W. Bishop and F. Sherratt, Finite element based fatigue calculations. USA (2000): NAFEMS. DOI:10.1111/j.1460-2695.1990.tb00604.x

[5] NCode International Inc.&MSC Software Corporation : User manuel MSC Corporation ,Los Angles, USA(1998)

[6] V.Grubisic, Criteria and methodology for lightweight design of vehicle components. 1986: Fraunhofer-Inst. für Betriebsfestigkeit.

[7] K.Ahlin, J. Granlund, and F. Lindstrom, Comparing road profiles with vehicle perceived roughness. International Journal of Vehicle Design, 2004. 36(2-3): p. 270-286.

[8] M.Fantacchiotti. and M. Vianello. Gradual improvement to the vehicle reliability up to the target value. in 4th International Conference ATA, Firenze. 1994.

[9] P.Paul, et al., Techniques for Accelerated Design Validation of Tractor Chassis. 2001, SAE Technical Paper ,01 pp.1-50

[10] F. D'Aprile, et al., Structural characterization of a vehicle on a rig test versus different road profiles: analysis of experimental results. ATA-TORINO-, 2001. 54(7/8): p. 251-261

[11] C.Marchesani. F. Parmigiani, and M. Vianello (1979) Integrated method to define the mission profile of a passenger car 'FIAT Auto S.p.A., Study Report (in Italian)

[12] V. Pizzari, Ricerca del profilo di Missione vetture segment B Turchia,. 1998: Turkish Ciklo Relazione Prot. No. 1 -1998, D.T.S.V. Affidabilita' e Terreni Prova Laboratorio Misure (in Italian), Arese.

[13] A.S.Sener, Fatigue life determination of the leaf spring on the light commercial vehicle according to Turkish Mission Profile (in Turkish). 2003, Yildiz Technical University.

[14] A.S.Sener, Finite Element Based Vehicle Component Fatigue Life Assessment According to a Customer Usage Profile. Materials Testing, 2014. 56(3): p. 198-207.Magnetism, 3rd ed., vol. 2. Oxford: Clarendon Press, 1892, pp.68-73. (Book)

[15] A.S.Sener, Fatigue life assessment of the driving shaft of a LCV by FEA using customer correlation data Materials Testing, 2016. 58(4): p. 325-332, DOI.10.3139/120.110861H.

[16] A.Falah, M. Alfares, and A. Elkholy, Failure investigation of a tie rod end of an automobile steering system. Engineering Failure Analysis, 2007. 14 (5): p. 895-902.

[17] M.A.Patil, D. Chavan, and M.K.U.S. Ghorpade, FEA of Tie Rod of Steering System of Car. International Journal of Application or Innovation Engineering and Management, 2013. 2(5): p. 222-227.

[18] J.Kim, J. et al., Structural design of an outer tie rod for a passenger car. International Journal of Automotive Technology, 2011. 12(3): p. 375-381.

[19] M.K.Pehlivan and M.Ozsoy, Computer aided structural analysis of rot head. Bilecik Şeyh Edebali Universitesi Fen Bilimleri Dergisi, 2014. 1(1): p. 45-51

[20] Regulation on Warranty application basis (in Turkish)

2003.

[21] M.Gobbi and G. Mastinu, Expected fatigue damage of road vehicles due to road excitation. Vehicle System Dynamics, 1998. 29(S1): p. 778-788.

[22] MSC. Software GmbH nSoft volumes 5.2 User Manuel. 1999.

[23] ASTM Standard E 1049-85, Philadelphia, USA. 1997.

[24] N.Bishop et al., 'Analytical Fatigue Life Assessment of Vibration Induced Fatigue Damage '. MSC World Users Conference, Universal City, CA, 1995.

[25] SolidWorks. 2011.

[26] ANSYS. 2012.

[27] The Ncode Book of Fatigue Theory, Ncode Technical Reference Book V4.3. Document rel 1.0, MSC Corporation. 2000.

[28] M.A.Miner, Cumulative damage in fatigue. Journal of applied mechanics, 1945. 12(3): p. 159-164.

Improvement of Density, Viscosity and Cold Flow Properties of Palm Oil Biodiesel by Alcohol Addition

Erinc Uludamar*, Vedat Karaman**‡, Safak Yildizhan***, Hasan Serin***

*Department of Mechanical Engineering, Cukurova University, 01330, Adana, Turkey.

**Department of Automotive Engineering, Istanbul Gelisim University, 34315, Istanbul, Turkey.

***Department of Automotive Engineering, Cukurova University, 01330, Adana, Turkey.

(euludamar@cu.edu.tr, vkaraman@gelisim.edu.tr, yildizhans@cu.edu.tr, hserin@cu.edu.tr)

‡Corresponding Author; Vedat Karaman, Department of Automotive Engineering, Gelisim University, 34315, Istanbul, Turkey, Tel: +90 212 422 70 00, Fax:+90 212 422 74 01, vkaraman@gelisim.edu.tr

Abstract-Alternative fuel researches has gained very importance due to depletion threads of fossil fuels, strictly narrowing emission regulations and high cost of petroleum. Biodiesel one of the most favorite alternative fuels since it is renewable and cleaner energy source. Many vegetable oils and animal fats are used for biodiesel production as raw material. Palm oil is an edible vegetable oil derived from the mesocarp (reddish pulp) of the fruit of the oil palms which is produced widely in some regions and used as raw material for many industrial sectors. Palm oil can be used as feedstock for biodiesel production but it has some drawbacks such as high viscosity and bad cold flow properties. In this study, some fuel properties of biodiesel produced from palm oil and its blends with various alcohols such as isopropyl alcohol, ethanol, and methanol were investigated. The study showed that the inadequate fuel properties of palm oil biodiesel such as viscosity and cold flow properties can be improved with various alcohol addition with the POME-5% methanol (CH_3OH).

Keywords: Biodiesel, False Flax Oil, Camelina Sativa, Transesterification, Fuel

1. Introduction

The diesel engines are the dominant tool of the field of commercial transportation and agricultural engine usage because of operational simplicity and fuel economy. Diesel engines have lower fuel consumption compared to petrol engines and higher torque production of diesel engines makes more favorable than gasoline engines[1]. Diesel fuel which is the main fuel of compression ignition engines are petroleum based fossil fuels. Depletion of fossil fuels, high cost and environmental concerns are significant problems and many researchers are studying on these particular subjects.

Alternative fuel researches are getting attention by many researchers. The one of the mostly studied alternative fuels are biodiesels which are produced with transesterification reaction of oil fats with alcohol in the presence of a catalyst. Biodiesel fuel can be produced from vegetable oils and animal fats. The main reason of too much interest on biodiesel fuel is the advantage of being a renewable energy source. Furthermore, being a cleaner energy source due to its extra oxygen content in the chemical composition which enhances the combustion and also sulfur-free structure make biodiesel more eco-friendly. Many researchers investigated various feedstocks for biodiesel production particularly waste materials and non-edible vegetable oils or animal fats [2-12]. On the other hand, biodiesel fuel has some drawbacks such as higher oxides of nitrogen (NOx), lower calorific value, and inadequate fuel properties of some feedstocks for direct usage in diesel engines. Especially, some fuel properties such as density, viscosity and cold flow properties which directly affects the performance of engine and fuel injection system are main problems occur with some feedstocks. In literature there are many studies which investigate the various fuel additives to biodiesels for improving the fuel properties [13-17].

Palm oil is an edible vegetable oil derived from the mesocarp (reddish pulp) of the fruit of the oil palms, primarily the African oil palm Elaeis guineensis [18] and to a lesser extent from the American oil palm Elaeis oleifera and the maripa palm Attalea maripa. Biodiesel production from palm oil has been investigated by many researchers . The main drawback of palm oil is being in solid phase in the room temperature which causes inadequate cold flow properties. These important drawbacks were investigated by many researchers to improve the fuel properties with some fuel additives [19-22].

In this study, biodiesel produced from palm oil were mixed with various alcohols in order to improve density, viscosity and cold flow properties.

2. Experimental

The experimental study was conducted in Petroleum Research and Automotive Engineering Laboratories of the Department of Automotive Engineering at Çukurova University. Palm oil was used as raw material for biodiesel production. The samples of palm oil were supplied from a local oil company, Adana, Turkey.

Palm oil is a edible vegetable oil derived from the mesocarp and common cooking ingredient in the tropical belt of Africa, Southeast Asia and parts of Brazil. It is used in the commercial food industry in some regions due to its low cost [23].

Palm oil methyl ester (POME) was produced by using the transesterification method. In this reaction, methyl alcohol and was used as reactant and catalyst in the reaction was sodium hydroxide (NaOH). The chemicals (methanol and sodium hydroxide) which were used during the experiments were purchased from Merck and methanol was purified prior to use. Before transesterification reaction the palm oil which is in the solid phase was heated and liquefied. In order to obtain best production condition, transesterification reaction was carried out in a spherical glass reactor equipped with reflux condenser, stirrer and thermometer. In the reaction, molar ratio of alcohol to oil was 6:1. The reaction were performed with , methanol 20 wt %, sodium hydroxide 0.5 wt %, temperature 65 °C, time 90 minutes. Methanol and sodium hydroxide were mixed in order to obtain sodium methoxide. Then, sodium methoxide and palm oil were mixed in the reactor. The mixture was heated up to 65 °C and kept at this temperature for 90 minutes by stirring. After the reaction period, the crude methyl ester was waited at separating funnel for 8 hours. And then, crude glycerin was separated from methyl ester. Finally, the crude methyl ester was washed by warm water until the washed water became clear and dried at 105 °C for 1 hour. Finally washed and dried methyl ester was passed through a filter. At the end of the transesterification reaction 98% conversion of oil was obtained.

In the study, 3 different alcohols were blended with palm oil biodiesel in order to improve some important fuel properties. Alcohols used in the experiments were isopropyl alcohol (2-propanol, C_3H_8O), ethanol (C_2H_5OH) and methanol (CH_3OH). Each alcohol was blended with palm oil 3% and 5% by volume of blend. The blends and the name of test samples were given in Table 1. Some fuel properties alcohols used in this study such as purity, density, melting point, dynamic viscosity, molar mass, and water content were given in Table 2. Table 3 shows the instruments used in this study for fuel property measurements.

Table 1. Experimental fuels

Fuel Name	Composition	Test Fuel Number
Palm oil methyl ester (POME)	100% POME	1
POME + Isopropyl Alcohol (C_3H_8O)	97% POME + 3% C_3H_8O	2
POME + Isopropyl Alcohol (C_3H_8O)	95% POME + 5% C_3H_8O	3
POME + Ethanol (C_2H_5OH)	97% POME + 3% C_2H_5OH	4
POME + Ethanol (C_2H_5OH)	95% POME + 5% C_2H_5OH	5
POME + Methanol (CH_3OH)	97% POME + 3% CH_3OH	6
POME + Methanol (CH_3OH)	95% POME + 5% CH_3OH	7

Table 2. Fuel properties of alcohols

Specification	Unit	Isopropyl Alcohol (C_3H_8O)	Ethanol (C_2H_5OH)	Methanol (CH_3OH)
Purity (GC)	%	>=99,5	>=99.0	>=99,8
Density (20 °C)	gr/cm^3	0,785-0,790	0,791-0,793	0,791-0,793
Melting Point	°C	-89	-116	-97,6
Viscosity Dynamical (20 °C)	m.Pa.s	2,20	1,2	0,545
Molar Mass	gr/mol	60,1	32,04	32,04
Water	(K.F.)	<=0,5	<=0,5	<=0,1

Table 3. Fuel properties and measurement devices

Property	Device	Accuracy
Density	Kyoto Electronics DA-130	±0.001 g/cm^3
Viscosity	TANAKA AKV-202 Auto Kinematic Viscosity	-
Pour/Cloud Point	Tanaka MPC-102L Pour/Cloud Point Tester	-

3. Results and Discussion

3.1. Oil Properties

In this study, properties of palm oil were measured before oil samples transesterified. Table 4 shows the fuel properties of crude palm oil.

Table 4. Fuel properties of crude palm oil

Fuel Property	Crude Palm Oil
Density (gr/cm^3)	0,912
Viscosity (mm^2/s)	38,62
Pour Point (^{o}C)	16,8
Cloud Point (^{o}C)	19

As it is shown in the table, palm oil has high viscosity and improper cold flow properties. Since it can cause fuel injection damage it is not recommended to use directly in the engine. Firstly it should be transesterified and blended with diesel fuel or with other additives.

3.2. Experimental Fuel Properties

In this study, POME and its blends with various alcohols were investigated in order to improve some fuel properties of POME. Table 3 shows the fuel measurement results of experimental fuels.

Table 5. Fuel properties of experimental fuels

Fuel Property	1	2	3
Density (gr/cm^3)	0,877	0,871	0,869
Kinematic Viscosity (mm^2/s)	4,529	4,099	3,929
Pour Point (^{o}C)	7	6	5,6
Cloud Point (^{o}C)	13	12,4	11,8

According to EN 14214 biodiesel standard the standard values for density, kinematic viscosity are 0,860-0,900 gr/cm^3 and 3,5-5,0 mm^2/s ,respectively.

The fuel measurement experiments showed that blending the POME with various alcohols resulted with some important improvements. Density, viscosity, pour point, and cloud point values of palm oil were reduced significantly after transesterification reaction.

Density values of alcohols are lower than POME, thus blending POME with alcohols caused a decrement in density values. Viscosity is a measure of resistance to flow of a liquid due to internal friction of one part of a fluid moving over another, affects the atomization of a fuel upon injection into the combustion chamber and thereby, ultimately, the formation of engine deposits. The general rule is; the higher the viscosity, the greater the tendency of the fuel to cause such problem [20]. Viscosity of crude palm oil was 38,62 cST which is too high. After transesterification reaction viscosity value of POME was 4,529 cST which meets the European and ASTM standards. Blending POME with alcohols further decreased the viscosity values. This improvement makes fuel blend more suitable for fuel injection systems and enhances combustion of fuel.

Pour point is the indicator of the lowest temperature which a fluid can flow. The crude palm oil samples were in the phase of solid-liquid mixture phase. Pour point of palm oil samples was 16,8 ^{o}C which is not suitable for direct usage. Pour point of POME was 7 ^{o}C which is better in comparison with crude palm oil but, still this property is not recommended for low temperature regions.. Alcohol additions to POME improved the pour point values and POME-alcohol blends. Increasing alcohol ratio further decreased the pour point values.

Cloud point of a fuel indicates the temperature below which wax in diesel or biowax in biodiesels form a cloudy appearance. Cloud point of a fuel indicates the tendency of a fuel to plug the filters at cold operating conditions. Cloud point of crude palm oil was 19 ^{o}C. As it is mentioned with pour point this property is not suitable for direct use. The cloud point of the POME was 13 ^{o}C. Even though, being a better value in comparison with crude palm oil, it is a very high temperature and may cause problems in filters. Blending POME with alcohols improved cloud point values. Increasing alcohol ratio in the blend further improved cloud point values. Pour point and cloud point of a fuel determines the fuel characteristics under cold working situations.

Thus in previous years, numerous studies on the use of technologies and different methods to evaluate optimal conditions of biodiesel production technically have been carried out.[2-5] In this study it was found a similar results that obtained in the previous studies.

The alcohol additions to POME improved fuel properties which investigated in this study. Since the blend ratios of alcohols were small (3% and 5% by volume) the fuel properties of fuels were not tremendously different. Analyses revealed that the most improvement of density, viscosity and cold flow properties were obtained with the POME-5% methanol (CH$_3$OH).

4. Conclusions

- Biodiesel produced from crude palm oil samples via transesterification reaction.

- The study showed that direct usage of palm oil in engines as fuel is not acceptable due to high density and viscosity and inadequate cold flow properties.

- The density and viscosity values were improved significantly after transesterification reaction.

- Analyses revealed that, cold flow properties of palm oil biodiesel are not acceptable for some cold regions since these values are higher compared to standard

fuels used in market and contingency of causing fuel injection system failures.

- Blending POME with alcohols improved cold flow properties of test fuels. Increasing alcohol ratio in the blend further improved these values.

- According to study, it not recommended to use crude palm oil or palm oil methyl ester directly in the engine. Direct usage may cause fuel injection system failures.

- Palm oil properties were improved by adding alcohol and it make a more utilizable.

References

[1] Ramadhas A.S., Muraleedharan C. and Jayaraj S., "Performance and Emission Evaluation of a Diesel Engine Fueled with Methyl Esters of Rubber Seed Oil", Renewable Energy, vol. 30, pp. 1789-1800, 2005.

[2] Ozcanli M., Serin H., Aydin K. and Serin S., "Ricinus Communis (Castor Oil) methyl ester as a natural additive for biodiesel fuel", Energy Education Science and Technology Part A: Energy Science and Research vol. 27(2), pp. 331-336, 2011.

[3] Serin H., M. Ozcanli, M.K. Gokce., G. Tuccar. Biodiesel Production From Tea Seed (Camellia Sinensis) Oil and its Blends With Diesel Fuel" International Journal of Green Energy, vol.10:4,pp. 370-377,2013.

[4] Juan C., Acevedoa C., Hernándeza J.A., Valdés C.F. and Kumar S., "Analysis of operating costs for producing biodiesel from palm oil at pilot-scale in Colombia", Bioresource Technology, vol.188, pp.117–123, 2015.

[5] Anwar F., Rashid U., Ashraf M. and Nadeem M., "Okra (Hibiscus esculentus) seed oil for biodiesel production", Applied Energy, vol.87, pp.779-785, 2010.

[6] Balusamy T. and Marappan R., "Effect of injection time and injection pressure on ci engine fuelled with methyl ester of thevetia peruviana seed oil", International Journal of Green Energy, vol.7, pp.397-409, 2010.

[7] Saribiyik O.Y., Ozcanli M., Serin H., Serin S. and Aydin K., "Biodiesel production from ricinus communis oil and its blends with soybean biodiesel. Strojniški vestnik", Journal of Mechanical Engineering, vol. 56, pp.811-816, 2010.

[8] Altun S.. "Fuel properties of biodiesels produced from different feed stocks", Energy Educ. Sci. Technol. Part A vol.26, pp.165-174, 2011.

[9] Caynak S., Gürü M., Biçer A., Keskin A. and Içingür Y., "Biodiesel production from pomace oil and improvement of its properties with synthetic manganese additive", Fuel vol.88, pp.534-538, 2009.

[10] Canakci M. and Van Gerpen J.H., "Compression of engine performance and emission for petroleum diesel fuel, yellow grease biodiesel, and soybean oil biodiesel", Trans. ASAE, vol.46, pp.937–44, 2003.

[11] Usta N., "Use of tobacco seed oil methyl ester in a turbocharged indirect injection diesel engine", Biomass and Bioenergy, vol.28, pp.77-86, 2005.

[12] Hamamci C., Saydut A., Tonbul Y., Kaya C. and Kafadar A.B., "Biodiesel production via transesterification from safflower (Carthamus tinctorius L.) seed oil", Energy Sources, Part A, vol.33, pp.512–520, 2011.

[13] Jianxin L.L., Zhi W. and Jianhua X., "Combustion and emission characteristics of diesel engine fueled with diesel/biodiesel/pentanol fuel blends", Fuel, vol.15 pp. 211-218, 2015.

[14] Karabektas M. and Hosoz M., "Performance and emission characteristics of a diesel engine using isobutanol–diesel fuel blends", Renewable Energy, vol.34, pp.1554-1559, 2009.

[15] Yilmaz N. and Vigil F.M., "Potential use of a blend of diesel, biodiesel, alcohols and vegetable oil in compression ignition engines", Fuel, vol. 124, pp. 168–172, 2014.

[16] Yasin M.H.M., Yusaf T., Mamat R. and Yusop A.F., "Characterization of a diesel engine operating with a small proportion of methanol as a fuel additive in biodiesel blend", Applied Energy, vol.114, pp. 865–873, 2014.

[17] Yasin M.H.M., Mamat R., Yusop A.F., Rahim R., Aziz A. and Shah L.A.," Fuel Physical Characteristics of Biodiesel Blend Fuels with Alcohol as Additives, Procedia", Engineering, vol.53, pp.701-706, 2013.

[18] Reeves J.B. and Weihrauch J.L., "Consumer and Food Economics Institute (1979). Composition of foods: fats and oils", Agriculture Handbook 8-4. Washington, D.C.: U.S. Dept. of Agriculture, Science and Education Administration. p. 4. OCLC 5301713.

[19] Poon, L.Y., Hashim, H., Mat, R., and Mustaffa, A.A.," Flash point prediction of tailor-made green diesel blends containing B5 palm oil biodiesel and alcohol" Fuel, vol.175, pp.287-293 2016.

[20] Puneet V., Sharma M.P. and Gaurav D., "Impact of alcohol on biodiesel production and properties", Renewable and Sustainable Energy Reviews, vol.56, pp. 319–333, 2016.

[21] Lv P., Cheng Y., Yang L., Yuan Z., Li. H. and Luo W., "Improving the low temperature flow properties of palm oil biodiesel: Addition of cold flow improver", Fuel Processing Technology, vol.110 pp. 61-64, 2013.

[22] "Palm Oil Continues to Dominate Global Consumption in 2006/07" (PDF) (Press release). United States Department of Agriculture. June 2006. Retrieved 22 September 2009.

[23] Gerpen J.V., Shanks R.P., Clements D. and Knothe G., "Biodiesel Analytic Methods, National Renewable Energy Laboratory", Colorado, 2004.

Study on Machining Parameters for Thrust Force and Torque in Milling AA7039 Composites Reinforced with Al₂O₃/B₄C/SiC Particles

Sener Karabulut[‡]

Department of Mechanical Program, Hacettepe University, 06935 Ankara, Turkey.

(senerkarabulut@hacettepe.edu.tr)

[‡] Corresponding Author; Department of Mechanical Program, Hacettepe University, 06935 Ankara, Turkey, Tel: +90 312 267 30 20, Fax: +90 312 267 33 38, senerkarabulut@hacettepe.edu.tr

Abstract-Metal matrix composites are used in many industrial fields such as automobile, military and aerospace applications due to their superior mechanical properties. In the present study, three aluminum 7039 metal matrix composite (MMCs) samples reinforced with 10 wt.% particulates of aluminum oxide (Al_2O_3), 10 wt.% boron carbide (B_4C), and 10 wt.% silicon carbide (SiC) were successfully fabricated using a powder metallurgy and hot extrusion method. The influences of cutting parameters on the thrust cutting force and torque during milling of the three MMCs were investigated under dry machining conditions. The milling tests were performed based on the Taguchi orthogonal -array design of experiments, L_{27} (3^4) for different machining parameters such as cutting speed, feed and depth of cut. The effect of reinforcement contents on cutting force and torque were specified by utilizing analysis of variance (ANOVA). Mathematical models have been generated for the thrust force and torque through regression method. The results indicated that the minimal thrust force and torque were obtained in the machining of the Al_2O_3 reinforced specimen. The cutting force was directly influenced by the cutting feed and the axial cutting depth was the most effective machining parameter affecting milling torque in the machining of three composite specimens. The experimental results were modeled using regression analysis and artificial neural networks (ANN) to predict the thrust force and torque. The thrust force and torque were predicted with a mean squared error equal to 5.85% and 5.12% respectively using ANN models.

Keywords: AA7039, Al_2O_3/B_4C/SiC, thrust force, torque, milling.

1. Introduction

In recent years, Aluminum based MMCs are being attractive materials in a variety of engineering applications such as automobile products, aerospace parts and armor because of their excellent mechanical and thermal properties. The different types of reinforcement ceramic particles are used to improve the mechanical properties of the aluminum alloys. Many researchers are preferred the Al_2O_3, B_4C and SiC particles as reinforcement element for their superior mechanical properties. On the other hand, the implementations of MMCs are restricted in a very specific industry due to high fabrication cost and their poor machinability [1-3]. Milling is one of the most common machining process for the desired form and size by removing material in industry. Milling operations are carried out to produce 3 dimensional complex shapes products for aerospace, automotive parts, mold and die at high quality using advanced high speed machining technologies. Despite the improving machining technologies, machining software, CNC, CAD/CAM and cutting tool performances, the milling operations are still limited due to the high cutting forces and machining stabilities [4]. The determination of optimum machining parameters, proper cutting tool material and geometry for ideal cutting forces must be considered to meet the increasing productivity demands and reliable machining. Determination of the amplitude and frequency of the cutting force and torque are the most important key parameter in machining process in order to design of mechanical structure of machine tool, machine tool components, bearings, jigs, spindle and feed drive mechanisms, power consumption, tool life and productivity based on physical constraints [5]. Many researchers have been studied on metal cutting with different points of view for over hundred years and developed a several theories for cutting forces. One of the most popular theory was established by Merchant based on the minimum power consumption. The relationships among the forces

acting on the chip during orthogonal cutting and machining parameters were formulated by Merchant. According to the Merchant's theory, the cutting speed is always constant, the tool cutting edge remains sharp during the cutting process and there is no built-up edge (BUE) constitution on the cutting insert [6]. Lee and Shaffer analyzed the process of orthogonal machining and they were theorized that the workpiece material on the cutting tool behaved as an ideal plastic metal and the chip was separated from the workpiece at the shear plane [7]. Several researchers are also investigated the cutting forces during machining MMCs. Kannan et al. [8] machined the MMCs orthogonally under different machining conditions to determine the effect of varying particulate size and volume fraction of Al_2O_3 particles on the plastic deformation behavior of matrix and correlation with cutting forces. They reported that the particle size and volume fraction were affected the deformation properties and cutting forces were indicated a correlation with the plastic deformation of MMCs. Ozcatalbas [9] investigated the influence of different amounts of Al_4C_3 reinforcements, depending on mechanical alloying on cutting forces, chip formation and surface roughness. High volume fraction of Al_4C_3 in the structure reduced the BUE formation resulted in lower cutting forces and shortened the chip contact length. Palanikumar and Muniaraj [10] performed an experimental study to determine the effect of drilling parameter on thrust force in machining Al6061 based MMCs. The experimental result showed the feed rate was the most significant machining parameter on the thrust force in drilling of hybrid MMCs. Many researchers have been reported to the BUE creation during machining of MMCs at lower machining speeds. Hence, the cutting force at lower cutting speed is lower compared with the higher machining speed. The feed rate and depth of cut have also significant effect on cutting forces. High cutting forces were observed in machining of MMCs due to the creation of voids around the reinforcement ceramic particles in the matrix structure [11-14]. The artificial neural networks are used in many different applications of MMCs including prediction of surface roughness, cutting force and cutting tool wear. The use of ANNs provides an easy methodology to solve the problems and has become increasingly popular in machining studies due to the ability to learn limited number of experimental results. Das et al. [15] studied on the machinability of Al–4.5%Cu/TiC MMCs and an ANN model was generated to estimate the cutting force in the milling of MMCs. experimental results indicated that cutting forces are comparatively higher in milling Al–4.5Cu–SiC composites as compared to those for Al–4.5Cu–TiC composites. The predicted values have shown a good correlation with the measured experimental values with the minimum error. Karabulut and Güllü [16] studied the machinability of the compacted graphite cast iron under different cutting conditions. Authors were investigated the influence of the entering angle on the cutting forces and prediction models for cutting forces were developed using artificial neural networks (ANN). The cutting forces were reduced with the increasing entering angles at all cutting conditions and the predicted cutting forces based on the ANN model had a good correlation with the measured data. Hiremath et al. [17] studied the influence of the reinforcement particle size on

cutting forces in machining of MMCs. They reported that the cutting forces were reduced with increase in cutting speed feed rate and cutting depth. Hayajneh et al. [18] investigated the drilling behavior of aluminum based alumina/graphite hybrid metal matrix composite and investigated the machining parameters on the cutting force and torque. The effect of cutting parameters and volume fraction of the reinforced particles on the thrust force and torque were modeled using ANN. The prediction results were indicated to be in a very good correlation with the experimental results

The purpose of this study is to determine the effect of B_4C, Al_2O_3, and SiC reinforcement particles on the thrust force and torque under different machining parameters. Machining performance of the composites during milling was evaluated to remove a unit volume of metal with respect to cutting forces and torque. The influence of reinforcement elements and milling parameters for the thrust force and torque were determined. The microstructure of specimens and cutting tool surfaces were analyzed using optical microscopy and scanning electron microscopy (SEM). The results were analyzed by analysis of variance and prediction models for optimal milling parameters were specified.

2. Experimental Methods and Analyses

2.1. Workpiece Material

The milling experiments were performed on three different aluminum 7039 based composite materials. Experimental samples reinforced with 10 wt.% B_4C, 10 wt.% Al_2O_3, and 10 wt.% SiC were fabricated by a powder metallurgy (PM) and hot extrusion method (HEM). Aluminum 7039, B_4C, Al_2O_3 and SiC powders were separately mixed and blended for 60 min in a three-dimensional Turbula mixer to achieve a uniform particle distribution in matrix structure. After that, the mixed compositions were cold compacted at 300 MPa and sintered at 550°C for 1 h, thereby increasing hardness and strength. In the next step composites were extruded using a pre-heated extrusion mold to achieve a high degree of densification in the resulted product. After the extrusion process, the experimental specimens were solution heat-treated at 470°C for 2 h and then quenched in water at room temperature. Finally, the specimens were aged at 120 °C for 2 h in a furnace. Chemical compositions and microstructures of the specimens were determined using a JEOL JSM-6060LV scanning electron microscopy (SEM). Hardness tests were performed at different regions utilizing a EMCO-TEST Duravision 200 Vickers hardness testing machine. Chemical composition of aluminum 7039 and the average hardness values of the specimens are presented in Table 1 and Table 2, respectively.

Table 1. Chemical compositions of aluminum 7039

Chemical composition (wt.%)								
Al	Mg	Zn	Cu	Si	Mn	Ti	Fe	Cr
89.91	4.17	4.39	0.53	0.45	0.2	0.19	0.12	0.02

Table 2. Hardness of composite specimens (Hv)

10 wt.% Al_2O_3	10 wt.% B_4C	10 wt.% SiC
142	129	101

2.2. Machining Experiments

The milling tests were performed on a three-axis CNC milling machine using uncoated carbide inserts under dry machining environment. A single Walter LNGX130708R-L88, WK10 grade carbide insert was mounted on the ISO code F4041.B16.040.Z03.13 tool holder and a fresh cutting tool was used for every cutting force experiment. In literature, several researchers were recommended polycrystalline diamond (PCD) inserts because of their extremely hardness, wear resistance, abrasion and fracture resistance in machining of MMCs. On the other hand, PCDs are fairly low portion among the cutting tool materials due to the machining costs. Hence, carbide cutting inserts were used instead of PCDs in milling experiments [2]. The cutting parameters were chosen based on the cutting-tool-manufacturer recommendations, previous studies and preliminary experiments. The experimental cutting factors and their levels used in tests are depicted in Table 3. The torque and thrust force components in feed (Fy), tangential (Fx) and radial (Fz) directions generated during the milling tests were measured by utilizing a Kistler 9257B 3-component dynamometer and Kistler 5070A amplifier Experimental setup and the directions of the cutting forces are illustrated in Fig.1 (a). All the measured cutting force signals were saved to a computer and evaluated with the help of Dynoware software at the end of the tests.

The cutting forces applied the workpiece to remove the chip by cutting insert can be separated into two categories as friction force and normal force to friction. The resultant force oriented at the friction angle β can be obtained vectorial. There are also two cutting force components, shear force Fs and normal force to shear Fn, acting on the removing chip. The resultant force, F_r, and normal force, F_n, were computed with the equations $F_n = \sqrt{F_y^2 + F_z^2}$ and, $F_r = \sqrt{F_n^2 + F_x^2}$ where F_y is the force in the feed direction, F_x is the force in the x direction and F_z is the radial force. The cutting forces and thrust force are also depicted in Fig.1 (b).

The down–milling method was employed in the experiments due to the direction of cutter rotation and cutting feed is same. In down milling method, the cutting tool are begun with the maximum chip thickness and reaching zero at the end of the cut. Therefore, the cutting forces are in tendency to pull the specimen into the cutter and holding the insert in the machining. The experiments were conducted based on the Taguchi orthogonal-array design of experiments, $L_{27}\,(3^4)$ to reduce the total number of tests. time, cost and to measure data uniformly from within the range of the determined studying area.
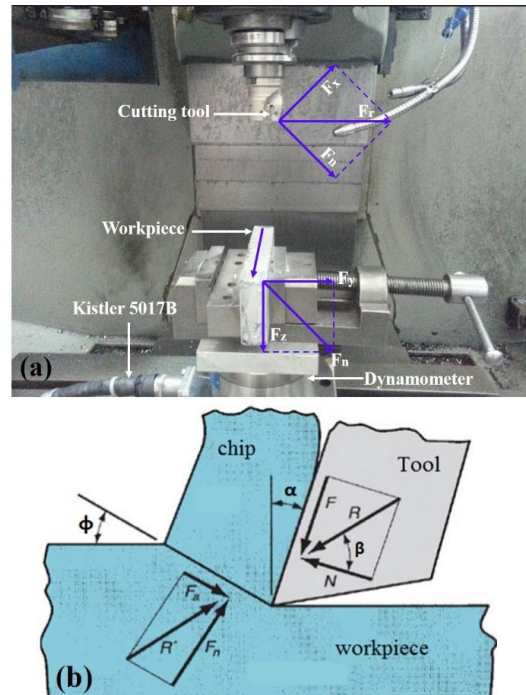
Fig.1 Experimental milling setup for cutting force and torque (a) measurement, (b) forces acting on the chip in orthogonal cutting

3. Experimental Results and Discussion

In the present study, three AA7039 based reinforced with 10 wt.% B_4C, 10 wt.% Al_2O_3, and 10 wt.% SiC composites were successfully fabricated and studied the microstructural properties to determine the particle distribution in matrix. The optical image of surface texture of these composites and the particle distribution in matrix structure are depicted in Fig.2 (a), (b) and (c). As shown these figures, homogenous particle distributions were observed within the matrix structure as a result of the hot-extrusion fabrication route and the blending system. The milling experiments were performed for aluminum 7039 based MMCs and the influence of machining variables on cutting trust forces and cutting torques are presented in Figs. 3 and 4, respectively.

Table 3. The experimental milling parameters and the Taguchi $L_{27}\,(3^4)$ test levels

Factor	Notation	Unit	Level 1	Level 2	Level 3
A–Material	M	pieces	10 wt.% Al_2O_3	10 wt.% B_4C	10 wt.% SiC
B–Cutting speed	Vc	m/min	290	375	488
C–Cutting feed	f_z	mm/tooth	0.10	0.13	0.17
D–Axial cutting depth	a_p	mm	0.8	1.0	1.3
Cutting width	a_e	mm	24		
Tool holder diameter	D_c	mm	40		
Number of cutting edge	Z_n	pieces	1		
Workpiece dimension		mm^3	$90 \times 50 \times 20$		
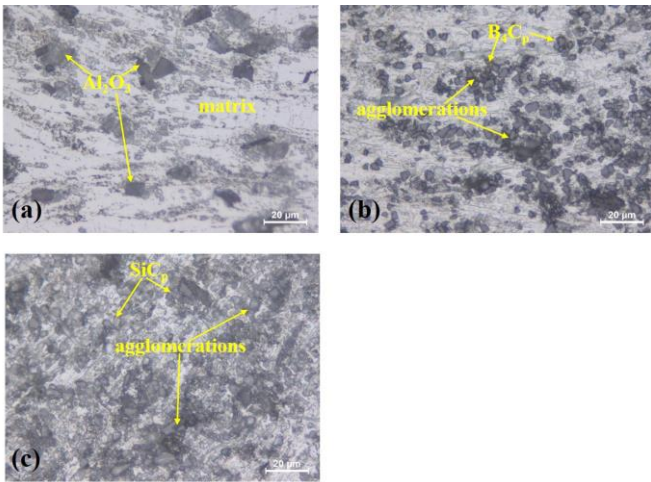
Fig. 2 Microstructures of (a) AA7039/Al$_2$O$_3$, (b) AA7039/ B$_4$C (b), and (c) AA7039/SiC.

As shown in three dimensional response surface graphs, increasing the feed rate and cutting depth results an increase in thrust force in the machining of all specimens. The thrust force was greatly affected with an increase in cutting feed due to the more chip was removed. The rise in axial depth of cut was also caused an increase in thrust force because the axial depth of cut was affected the width of the contact area in the table feed direction. This led to an increase in the load at high cutting depth influencing the cutting insert. Fig. 3 shows the influence of machining parameters on the thrust force. From the figures, it can be concluded that the thrust force is higher at lower cutting speed and decreased with the increase of cutting speed. The lower values of the thrust force are due to the reducing interface friction between cutting insert and workpiece in high cutting speeds. The machining speed effects the strength of the workpiece in the plastic deformation area through increasing cutting temperatures and strain rate at a higher cutting speeds. As a result, this causes plastic deformation of workpiece and required cutting force for machining are decreased. Fig.4 depicts the influence of cutting variables on the torque during machining of AA7039 based MMCs. The power and torque requirements in milling process are also a significant criterion for a stable machining performance. The spindle speeds for milling of metal matrix composites containing harder ceramic particles such as Al$_2$O$_3$, B$_4$C, and SiC have a great importance on the availability of adequate power and torque. That is why the effect of milling parameters on the torque was investigated in the milling of composite specimens. From the Fig.4 and mean effect graph in Fig.6, the torques were increased with the increasing axial cutting depth while cutting speed was observed to have insignificant effect on the result of torques in the milling of all composite specimens. The torque values are increased with the amount of removed metal due to the friction force at the cutting edge and chip interface regardless of the workpiece materials. In this study, the torque increased for a cutting feed of 0.17 mm/tooth while remaining almost constant for cutting feed of 0.1 mm/tooth and 0.13 mm/tooth in the milling of composite specimens. The results depicted that the torque was not affected effectively by increasing feed rate. The cutting feed showed a less negative effect on the torque value due to reducing in contact time between the cutting tool and workpiece.

The minimal mean cutting force and torque values are achieved in the milling of AA7309 reinforced with 10 wt.% Al$_2$O$_3$ composites among the studied composites. However, the highest cutting force and torque results are measured in the milling of AA7309 reinforced with 10 wt.% SiC composites. Increasing thrust force and torque can be attributed to the particle distribution in the matrix structure and BUE creation on the insert. A uniform particle distribution was obtained in Al$_2$O$_3$ reinforced composites with 7.1 μm particle size. Although the mixing time was the same, the particle distribution of B$_4$C with 3.1 μm particle size and SiC with 4.8 μm particle size was not sufficiently homogenous. Small B$_4$C and SiC particles caused to more agglomeration of the particles and hence, some agglomerated particles are observed in the matrix structure [1]. BUE creation was also seen at all machining parameters in the milling of AA7039/B$_4$C and AA7039/SiC composites (Fig.5). These agglomerated particles and BUE formation are negatively affected the cutting tool performance, thrust force and torque.
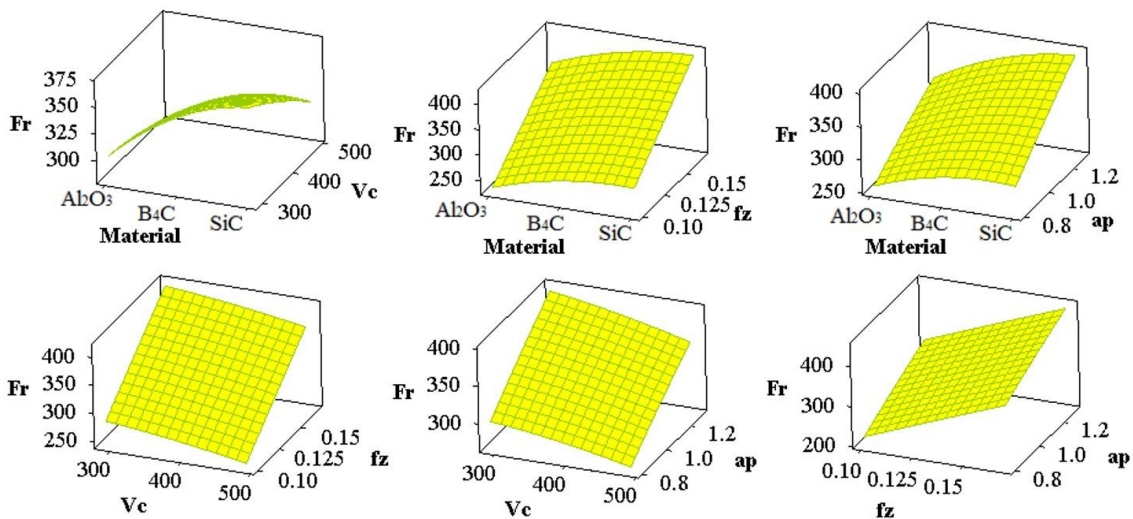
Fig. 3. The effect of the milling parameters on thrust forces in the milling of AA7039 based MMCs
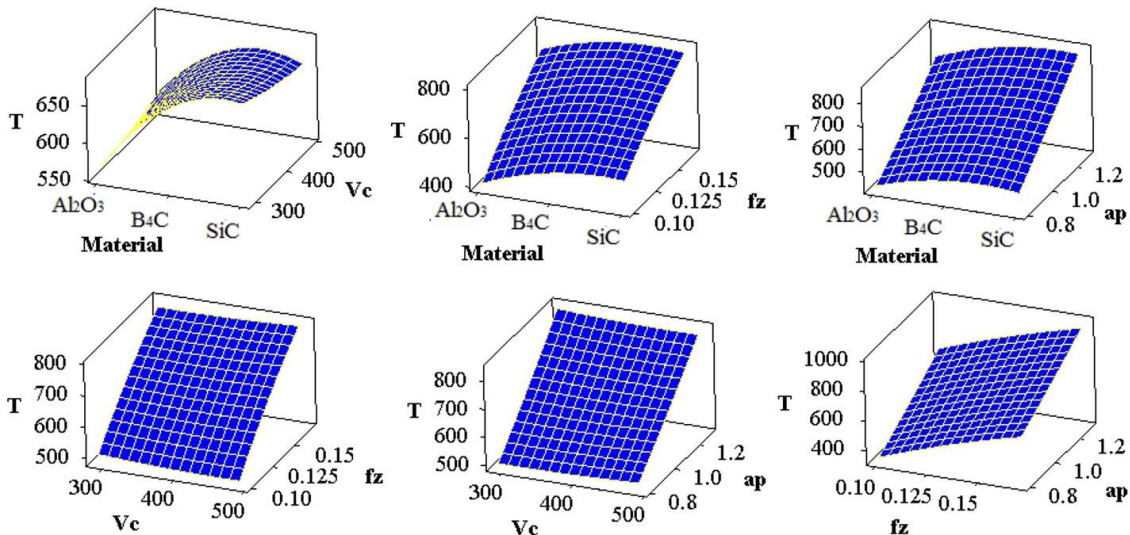
Fig. 4. The effect of the milling parameters on torque in the milling of AA7039 based MMCs
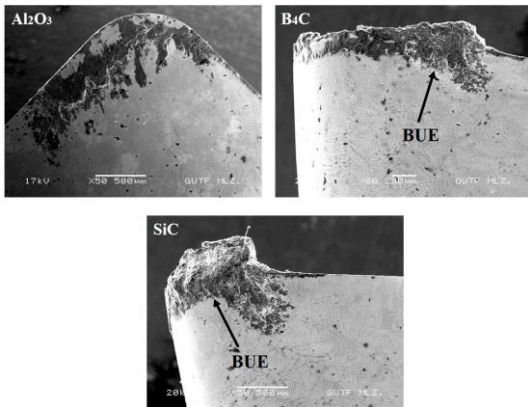
Fig. 5. SEM micrographs of cutting edge used in milling AA7039 based MMCs

Fig. 6. Effect of cutting parameters on average thrust force
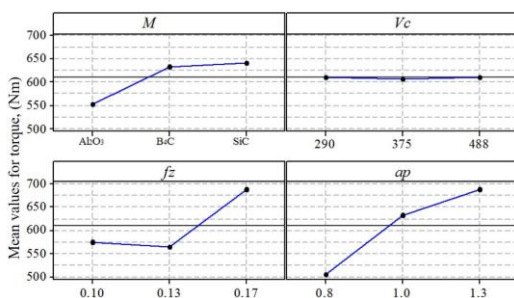
Fig. 7. Effect of cutting parameters on average torque

3.1. Analysis of Variance (ANOVA)

Statistical method of linear regression and ANOVA was used to study the relationship among the machining parameters and to analyze which factors most affecting thrust force and torques at the 95% confidence level. The significant coefficients of cutting parameters on the thrust forces and torques are given in Tables 4. The percentage of contributing column shows that the cutting feed and depth of cut have a significant influence on the trust force. From the mean effect plot and ANOVA results, the feed rate and cutting depth affected the thrust force 42.67%% and 31.98% respectively, for all composite specimens. The most significant cutting parameters for torque in the milling of three specimens was the axial cutting depth with the percentage contribution of 72.57 %. The ANOVA results and mean effect graphs showed that the machining speed has insignificant effect on the cutting force and torque for all experimental specimens and can be neglected. As shown in Figs. 6 and 7, the minimal thrust forces and requirement of lower torque can be achieved by decreasing feed rates and cutting depth and increasing machining speed. Thrust force and torque in milling three metal matrix composites are given below:

$$F_r = -106.577 + 25.0195 \times M - 0.1759 \times V_c + 1922.45 \times f_z + 178.45 \times a_p$$

$$(1)$$

$$T = -672.776 + 44.965 \times M - 0.00684 \times V_c + 4025.52 \times f_z + 637.156 \times a_p$$

$$(2)$$

The adequacy of the linear regression models are confirmed by using the coefficient of correlation, R^2. The coefficient of correlation values of the equations derived from the regression models for cutting force and torque were computed as 94.59% and 93.87% respectively. R^2 values are indicated that the models are adequate at the 95% confidence level.

Table 4. Analysis of Variance for thrust forces

Source	DF	SS	SS	F	P	Rate (%)
Thrust force						
M	1	11267.6	11267.6	54.537	0.0000002	13.40%
Vc	1	5497.8	5497.8	26.610	0.0000359	6.54%
fz	1	35882.2	60776.6	294.169	0.0000000	42.67%
a_p	1	26891.6	26891.6	130.160	0.0000000	31.98%
Error	22	4545.3	206.6			5.41%
Total	26	84084.5				
Torque						
M	1	36395	36395	27.638	0.000028	7.70%
Vc	1	8	8	0.006	0.937448	0.00%
fz	1	64216	266484	202.367	0.000000	13.59%
a_p	1	342823	342823	260.338	0.000000	72.57%
Error	22	28970	1317			6.13%
Total	26	472412				

3.2. Artificial Neural Networks for Thrust Force and Torque.

The experimental results were modelled to predict the cutting force and torque value during milling of AA7039 based MMCs using a multilayer ANN model with feed forward back propagation algorithm. Based on Fig.8, the multilayer feedforward training network with the input, output and hidden layers was applied. The designed neural network expects all input and output values to be between 0 to 1 or -1 to 1. Hence, in the first step of the network training, the input and output parameters were normalized in (-1,1) using the following equation (3).

$$N_i = \frac{m_i - m_{min}}{m_{max} - m_{min}} \tag{3}$$

where

m_i is the input/output data, m_{min} is the minimum possible value of the input parameters

m_{max} is the maximum possible value of the input parameters data.

This calculation is done automatically in Pythia software. The type of composite specimens, machining speed, cutting feed and depth of cut were defined as input neurons and the output neurons are thrust force and torque. The network was trained with 21 test data and subsequently confirmed with the 7 experimental data. Three different metal matrix composites specimen were machined in the present experimental study to specify the influence of reinforcement particles on the cutting force and torque. Therefore, the samples are coded minimum 1 and maximum 3 for the artificial network training. The minimum and maximum input parameters used in the experiments for normalization are presented in Table 5. The Pythia software uses the Fermi function as the transfer function using equation (4).

$$N_{(i)} = \frac{1}{1 + e^{-4(E_i - 0.5)}} \tag{4}$$

Table 5. Limiting values of the ANN software

Inputs	Minimum	Maximum
Material M	1	3
Cutting speed V_c	290	488
Feed rate f_z	0.1	0.17
Axial depth of cut a_p	0.8	1.3

The network parameters are processed to optimize the network output values in order to predict fit data. After the training and reproduction phase, the ANN structure was determined with three layers and twelve neurons as show in Fig. 8.
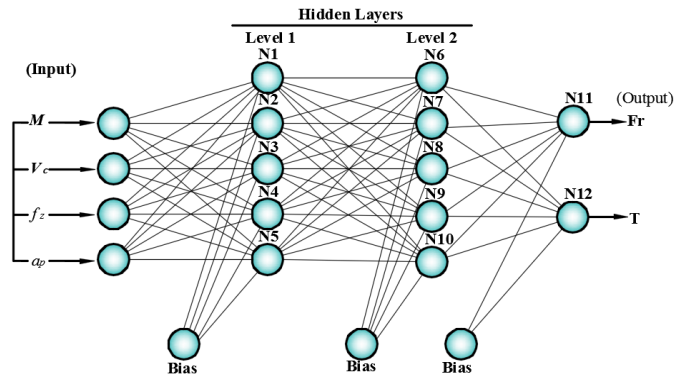
Fig.8 ANN in the Levenberg–Marquardt algorithm structure for the thrust force and torque

Each network input data is connected to every neuron in the first level and the output of each neuron is connected to every neuron in the next level. The calculated weights are presented in Table 6.

The activities of the $N_1 - N_5$ are calculated as;

$$E_i = w_{1i} * M + w_{2i} * V_c + w_{3i} * f_z + w_{4i} * a_p \tag{5}$$

Where,

E_i is the activities of the neurons,

i is the number of inputs,

w_i is the neurons weights

The outputs of N_1-N_5 are calculated as

$$N_{(i)} = \frac{1}{1 + e^{-4(E_i - 0.5)}} \tag{6}$$

$$E_i = w_{1i} * N_1 + w_{2i} * N_2 + w_{3i} * N_3 + w_{4i} * N_4 + w_{5i} * N_5 \tag{7}$$

Table 6. Weight values used in Equation 6

i	weights for thrust force			
	w_{1i}	w_{2i}	w_{3i}	w_{4i}
1.1	−0.641615	0.964341	−0.674801	−0.710380
1.2	0.453339	1.064664	−0.923088	−0.975535
1.3	−0.018847	0.724369	0.595416	−2.019125
1.4	0.565030	0.720068	0.131456	−0.125667
1.5	0.347206	0.898850	0.569796	−1.219484
i	weights for torque			
	w_{1i}	w_{2i}	w_{3i}	w_{4i}
1.1	−0.613107	0.798307	−0.587410	−1.104612
1.2	0.738065	1.316772	−1.965709	−1.741744
1.3	0.486763	−0.146797	−0.236760	−1.546769
1.4	0.542935	0.484263	0.424082	−0.118507
1.5	0.448045	0.245691	0.602117	−1.659422

Similarly, the activities of the N6 to N10 are computed using equation (8). The computed weights are presented in Table 7. The network is processed from left to right and the outputs of N_1–N_5 are the inputs for the computation of N_6 to N_{10}.

Table 7. Weight values used in Equation 7

| i	weights for thrust force				
	w_{1i}	w_{2i}	w_{3i}	w_{4i}	w_{5i}
2.6	1.308292	0.254031	−0.155567	−0.707301	0.345201
2.7	1.325259	−0.207788	0.591904	1.635325	−2.048602
2.8	−0.621627	−1.382413	−1.911599	1.964388	−1.074672
2.9	0.327757	−0.060671	0.689212	−1.811071	0.842268
2.10	−1.389981	−0.551511	−0.153293	0.385712	0.757761
i	weights for torque				
	w_{1i}	w_{2i}	w_{3i}	w_{4i}	w_{5i}
2.6	3.559735	0.010124	0.224909	−0.088282	−0.439165
2.7	0.164152	−0.502624	−0.512776	0.068015	−1.182625
2.8	−1.451413	−1.694781	−1.549240	0.321606	−1.007977
2.9	0.424412	−0.019804	0.978870	−0.938918	1.386686
2.10	−1.634803	−0.140478	−0.178953	0.698680	0.625789

The analytical models were generated with the weight values in Tables 7 and 8 so as to predict the cutting force and torque. The following equations (8 and 9) were derived using the weight values of the neurons in the ANN network structure with the given milling parameters. These prediction models can be used for the prediction of the thrust force and torque in the milling of AA7039 based MMCs using the uncoated carbide inserts.

$$N_{11(Fr)} = \frac{1}{1+e^{-4(-0.103036*N_6-1.978958*N_7+2.307554*N_8-0.226579*N_9+0.974846*N_{10}-0.5)}}$$
(8)
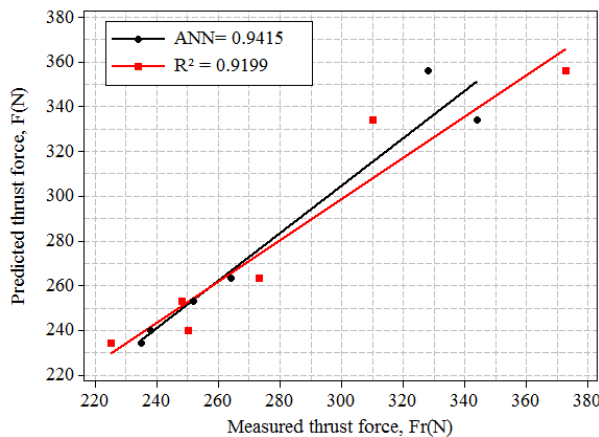
$$N_{12(T)} = \frac{1}{1+e^{-4(-2.443297*N_6+1.453050*N_7+3.432468*N_8-0.466388*N_9+0.918279*N_{10}-0.5)}}$$
(9)

ANN and regression equations were confirmed by performing the confirmation experiments. the verification experiments were conducted at random intermediate values of cutting parameters, and the comparison of the validation test results and estimated values were depicted in Fig.9. Prediction accuracy of the ANN model equations for Fr and T were computed as 94.15% and 94.88% respectively. R^2 values of the equations derived from the regression model for Fr and T were calculated as 91.9% and 92.2% respectively. The confirmation experiment results showed that the ANN model has been successfully employed to the machining variables of milling AA 7039 based composites. Figs. 9 depict the estimated values obtained from regression and ANN models and confirmation test results. ANN models have shown a good agreement between the estimated and experimental results and the developed equations were also successful at predicting the cutting force and torque in the milling of AA7039 based MMCs.
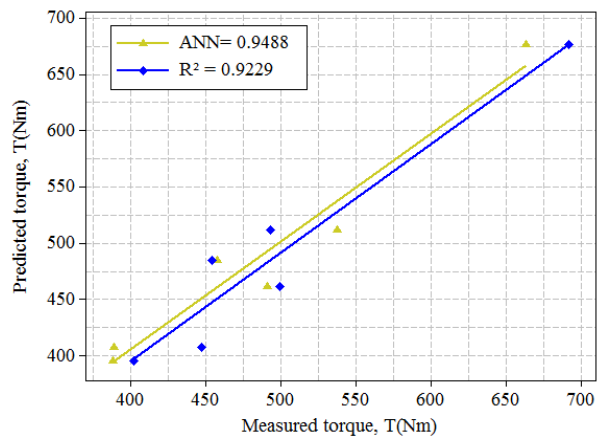
Fig. 9. Confirmation test results of ANN and regression model for experimental outputs

4. Conclusion

This study investigated the influences of the B_4C, Al_2O_3 and SiC reinforcement particles in the AA7039 matrix and cutting parameters on thrust force and torque in the milling process. Mathematical models of thrust force and torque were generated using an ANN and regression analysis. The test results were also analyzed using ANOVA. The experimental results can be summarized as follow:

- Three AA7039 composite specimens reinforced with 10 wt.% B_4C, 10 wt.% Al_2O_3, and 10 wt.% SiC were successfully fabricated through a powder metallurgy and hot extrusion route. The reinforced particles are generally uniformly distributed in the matrix but some agglomerations were observed in AA7039 reinforced with SiC and B_4C.

- The lower thrust force and requirement of torque were achieved during milling of AA7039 reinforced Al_2O_3 composite specimens. Well distributed Al_2O_3 particles in the matrix remarkably decreased the BUE creation, cutting force and torque.

- The optimal machining parameters for cutting force and torque were determined at the lowest cutting feed, depth of cut and the highest machining speed for all composite specimens.

- The cutting feed was the most effective machining parameters for thrust force with a percentage contribution of 42.67%% and followed by the axial cutting depth with the percentage contribution of 31.98%.

- The most effective machining parameters for torque was the axial cutting depth with the percentage contribution of 72.57 % during milling of experimental specimens.

- From the ANOVA results and mean effect plots, the cutting speed was not presented to have a significant

correlation on the thrust force and torque in the milling of composites.

- The generated ANN models indicated a good agreement with determination coefficients for thrust force and torque $R^2 = 94.15\%$ and 94.88%, respectively.

These results depicted that ANNs can be used successfully for the estimation of thrust force and torque in the milling of AA7039 based metal matrix composites.

Acknowledgments

References

[1] Ş. Karabulut, U. Gökmen and H. Çinici, "Study on the mechanical and drilling properties of AA7039 composites reinforced with $Al_2O_3/B_4C/SiC$ particles", Compos. Part. B, vol. 93, pp. 43-55, May 2016.

[2] K. Umanath, K. Palanikumar and ST. Selvamani, "Composites: Part B Analysis of dry sliding wear behaviour of $Al6061/SiC/Al_2O_3$ hybrid metal matrix composites", Compos Part B, vol. 53, pp. 159–68, October 2013.

[3] Ş. Karabulut, "Optimization of surface roughness and cutting force during AA7039/ Al_2O_3 metal matrix composites milling using neural networks and Taguchi method" Measurement, vol. 66, pp. 139-149, April 2015.

[4] E. Budak, "Analytical models for high performance milling. Part I: Cutting forces, structural deformations and tolerance integrity", Int. J. Mach. Tools Manuf, vol. 46, no. 12, pp. 1478-1488, October 2006.

[5] H. Saglam, S. Yaldiz and F. Unsacar, "The effect of tool geometry and cutting speed on main cutting force and tool tip temperature", Mater. Des., vol. 28, no. 1, pp. 101-111, 2007.

[6] M.E. Merchant, "Basic mechanics of the metal cutting process", ASME J. Appl. Mech, vol. 66, pp. 168–175, 1944.

[7] E.H. Lee and B.W. Shaffer, "The theory of plasticity applied to a problem of machining", ASME Trans. J. Appl. Mech., vol. 18, pp. 405–413, 1951.

[8] S. Kannan, H.A. Kishawy and I. Deiab, "Cutting forces and TEM analysis of the generated surface during machining metal matrix composites", J. Mater. Process. Technol, vol. 209, no. 5, pp. 2260-2269, 2009.

[9] Y. Ozcatalbas, "Investigation of the machinability behaviour of Al_4C_3 reinforced Al-based composite produced by mechanical alloying technique", Compos. Sci. Technol., vol. 63, no. 1, pp. 53-61, 2003.

[10] K. Palanikumar and A. Muniaraj, "Experimental investigation and analysis of thrust force in drilling cast hybrid metal matrix (Al–15%SiC–4%graphite) composites", Measurement, vol. 53, pp. 240–250, 2014.

[11] J.T. Lin, D. Bhattacharyya and C. Lane, "Machinability of a silicon carbide reinforced aluminium metal matrix composite", Wear, vol. 181, pp. 883–888, 1995.

[12] A. Manna, B. Bhattacharayya, "A study on machinability of Al=SiC-MMC" J. Mater. Process. Technol, vol. 140, no. 1, pp. 711–716, 2003.

[13] M. El-Gallab and M. Sklad, "Machining of Al/SiC particulate metal matrix composites: part II: workpiece surface integrity", J. Mater. Process. Technol, vol. 83, no. 1, pp. 277–285, 1998.

[14] Ş. Karabulut, H. Çinici and H. Karakoç, "Experimental Investigation and Optimization of Cutting Force and Tool Wear in Milling Al7075 and Open-Cell SiC Foam Composite", AJSE–Engineering., vol. 41, pp. 1797-1812, 2016.

[15] B. Das, S. Roy, R.N. Rai and S.C. Saha, "Study on machinability of in situ Al–4.5%Cu–TiC metal matrix composite-surface finish, cutting force prediction using ANN", CIRP J. Manuf. Sci. Technol., vol 12, pp. 67–78, 2016.

[16] Ş. Karabulut, A. Güllü, "Farklı yanaşma açıları ile vermiküler grafitli dökme demirin frezelenmesinde kesme kuvvetlerinin araştırılması ve analitik modellenmesi", Gazi Üniv. Müh. Mim. Fak. Der., vol. 28 1, pp. 135-143, 2013.

[17] V. Hiremath, P. Badiger, V. Auradi, S.T. Dundur and S.A. Kori, "Influence of particle size on Cutting Forces and Surface Roughness in Machining of B_4Cp-6061 Aluminium Matrix Composites", In IOP Conference Series: Materials Science and Engineering, vol. 114, pp. 012041, February 2016.

[18] M.T. Hayajneh, A.M. Hassan and A.T. Mayyas, "Artificial neural network modeling of the drilling process of self-lubricated aluminum/alumina/graphite hybrid composites synthesized by powder metallurgy technique", J. Alloys Compd., vol. 478, no. 1, pp. 559-565, 2009.

New Solidification Materials in Nuclear Waste Management

Neslihan Yanikomer*‡, Sinan Asal**, Sevilay Haciyakupoglu**, Sema Akyil Erenturk**

*Department of Mechanical Engineering, Faculty of Engineering and Architecture, Istanbul Gelisim University, 34315 Avcilar, Istanbul, Turkey.

**Energy Institute, Istanbul Technical University, 34469 Maslak, Istanbul, Turkey.

(nyanikomer@gelisim.edu.tr, asal@itu.edu.tr, haciyakup1@itu.edu.tr, erenturk@itu.edu.tr)

‡Corresponding Author; Neslihan Yanikomer, Department of Mechanical Engineering, Faculty of Engineering and Architecture, Istanbul Gelisim University, 34315 Avcilar, Istanbul, Turkey, Tel: +90 5445989846, nyanikomer@gelisim.edu.tr

Abstract-One of the major worldwide environmental issue is the long-term storage or disposal of nuclear waste. Research in solidification materials for long-term storage of high-level nuclear wastes in nuclear industry has started as an imperative need. During the last decade, new solidification materials have been developed for immobilization of actinides and fission products for geological disposal. The materials used for immobilization generally have relatively complex compositions. The structure of these materials investigates using diffraction and spectroscopic methods. Most of the interest has focused on their chemical durabilities and capacity of waste loading. Their physical and chemical properties should not be degraded by α-decay event irradiation from the incorporated actinides. The development of new materials either for storage or for disposal for a long time is still required. In this article, recent developments in the use of solidification materials for the immobilization of high level of nuclear wastes have been reviewed. The comparison of properties of solidification materials is summarized with several applications in connection with experience and technological needs in literature.

Keywords: Nuclear energy, nuclear waste, solidification materials, immobilization, long-term storage.

1. Introduction

The environmental impact of energy generation can be evaluated on several ways that includes evaluation of type and amount of contaminant produced per unit energy generated by the source, contaminant distribution in atmosphere and environment, effects on occupants and public's health, amount and toxicity of waste and long term effects on environment and ecological systems [1, 2].

Nuclear energy has been used since 1950s in the world. Progress in energy has increased the demand of nuclear power plants and also made it a current issue against global warming in the world. Nuclear industry uses the highest technologies of the world and develops rapidly as a high-tech sector. Even a very good pollution controls, nuclear power plants still generates waste materials. Nuclear industry is accepted one of the rare industries considering its special attention to waste management. Nuclear industry prepares regulations in accordance with laws and monitors the implementation by independent organizations [1, 2].

Ionizing radiations from radioactive materials are utilized for diagnose and treatment in medical sector. Radioisotopes are producing in nuclear plants continuously to supply the needs of research, industry and medical sectors. Radioactive sources or materials are managed as radioactive waste; therefore, they are isolated carefully for every usage.

After one-year operation of a 1000 MW light water reactor, the obtained spent fuel without reprocessing is approximately 30 tonnes consisting of 95.6% uranium, 1% plutonium, 0.1% transuranium isotopes (plutonium, neptunium etc.) and 3.3% fission products (cesium, strontium, iodine etc.). After separating uranium and plutonium for reuse, the percentage of fission products in reprocessed spent fuel (proximately 1 ton) is 93.3%. Fission products loss 98% of their radioactivities within 200 years. For this reason, storage of fission products in radioactive waste by solidification is very important. There are many radionuclides as fission products in the waste. Cesium and strontium are the most important radionuclides in fission products. Despite ^{137}Cs has 30.2 and ^{134}Cs 2.1 years of physical half-life, their biological and whole body half-life

are almost 40 days. Thereby, it seems that in terms of radiological point of view, ^{137}Cs is the most important radionuclide produced in a nuclear process. ^{90}Sr radionuclide has long physical ($t_{1/2}$: 28.60 years) and biological half-life and dispersion of ^{90}Sr to the environment causes damages to human body by incorporation into bones and teeth due to its high energetic beta particles (E_β: 546 keV) [3-8].

Immobilization of high level radioactive waste by a way that will not harm to human and environment is an important subject. Despite scientific authorities do not accept as a problem to nuclear wastes requiring a new immobilization technology, public perception for nuclear wastes is seriously problem to threat life and environment comparison with other industrial wastes [1, 3, 9].

The development of nuclear power industry brings back the responsibility to address the issue of nuclear wastes in stable solid forms for interim storage or disposition in geologic repositories. The solidification of nuclear wastes has been an active and booming research area for over 50 years. The aim of this review is to contribute literature by providing an overview including important developments and methods about immobilization of high-level radioactive waste with the help of researches executed so far and to make some interpretations and recommendations for the optimization and selection of solidification materials for the applications.

2. Storage by Solidification of Nuclear Wastes

High level nuclear waste have buried to deep underground repositories in specifically chosen geological formations. Further studies on nuclear waste storage are continuing in the world. Geological and environmental factors like groundwater movement, structure of rock, erosion, flood, earthquake, volcanic activities, natural resources and population etc. are important factors regarding disposal site selection [10-14].

Considering that the only mechanism to leak radioactivity from underground repositories to biosphere is groundwater movement, repositories constructed in geological formations have to select far from groundwater. It is clarified that geological formations like granite, basalt, salt and tuff have proper specifications for a waste repository. Considering fossil fuel-fired power plants, nuclear power plants produce less waste and own better protection procedures for the wastes. The nuclear wastes are stored in heavy concrete containers that are placed in deep boreholes or caverns excavated deep underground and monitored continuously. Some waste packages are shown in Figure 1. The containers have ability to retain radionuclides over ~100000 years in fact the nuclear wastes become safe in 300-500 years [10-14].

Immobilisation of radioactive wastes in relatively inert solid matrices before storage is advantageous for safety and economic reasons. Practically the most common method is pouring concrete around waste in containers. Liquid wastes are occasionally used as part of concrete mixture but the durability of final product is relatively weak. The long-term trend of radionuclides moves upward to the surface of the

solid material. Cementation and vitrification techniques are the most preferable methods for solidification of nuclear wastes [10-13].

Fig. 1. Waste packages in use: a) drum, b) metal box, c) concrete cylinder d) concrete container [13]

Depending on the classification of nuclear waste, different solidification material uses for immobilization of radioactive waste. Figure 2 shows immobilization techniques related to radioactivity levels in waste [13].
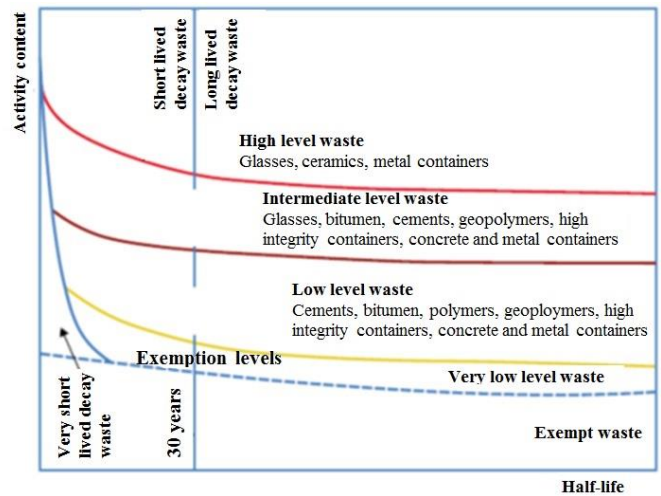
Fig. 2. Typical materials used for nuclear waste conditioning (reproduced from [13])

Selection of a solidification form depends on the physical and chemical nature of the radioactive waste and the acceptance criteria for the storage and disposal facilities. The key considerations on selecting an immobilising material are [12]:

Chemical durability is one of the most important properties in waste forms. Chemical durability of waste forms can be determined with several methods. The leach rate in g m^{-2} d^{-1} is given by;

$$L = \frac{A_i}{\left(A_0 \times S \times t\right)} \tag{1}$$

where A_i is the amount of the interested element in solution after the durability test, A_o is the amount of the interested element in the sample; S is the sample surface area of the waste form; and t is the duration of the experiment [12].

Waste loading capacity is to accommodate a significant amount of waste in the host matrix to minimise volume for storage, transportation and disposal.

Radiation stability is to have a high tolerance to radiation effects from the decay of radioactive elements [12].

2.1. Cement Waste Forms

Cementation is the most practical and economical method for immobilization of nuclear wastes. The cement is prepared by mixing the waste and cement composition in ratio 1:1. Cement and cement compositions are intensively used in immobilisation of low level radioactive wastes and in special cases in immobilisation of medium level wastes. Cementation technique has some advantages like low cost, convenience of process, higher-level elimination than the other techniques and products of acceptable quality. Cement compositions with proper additives have been developed to improve structure of host matrix for waste immobilization. Disadvantages of cementation technique are weak mechanical durability of solidified waste products and high corrosion risk for long-term disposal in environmental conditions [15, 22].

2.2. Vitrified Waste Forms

Vitrification technique is one of the immobilization methods for high level radioactive waste. In this process, radioactive waste is converted to solid glass blocks for long-term storage and waste volume is reduced to 1/3 of its original volume. The desired vitrified waste form is durable for thousands of year, poorly soluble in water, relatively cheap and easily workable and has appropriate mechanical properties [5, 12].

Borosilicate glasses have been commonly used for vitrification of high level wastes. Generally, it is thought that complex borosilicate glasses are relevant for long term immobilisation of radioactive waste products. It is more correct to say that borosilicate glass is the most suitable type of glass under current conditions, nevertheless, these glasses are not ideal for immobilisation because of several reasons [16]. One of the limitations of this type glass is the phase separation usually at microscopic scale. Phase separation on microscopic scale do not have an impact on the transparency and therefore invisible to the naked eye. Phase separation phenomenon in borosilicate glasses is often observed using scanning electron microscope (SEM) or small angle X-ray scattering (SAXS). This fact actually plays an important role in the glass production and its outstanding features [5, 16].

The reason for high chemical stability of borosilicate glasses is the diversity of highly decomposed silica and second phase. Main of second phase is alkaline borate which has weak chemical durability. In this way, it is obtained a glass having chemical durability close to that of pure silica. However, these two phases may be nested in some compositions. In this case, leaching of alkali metal and boron ions form host glass matrix is very easy. Therefore, the microstructure of different composition of borosilicate glasses needs to examined in sensitive applications such as the storage of nuclear waste in detail [5, 16].

Pure B_2O_3 glass consists of three $[BO_3]$ groups containing boroxol rings and $[BO_3]$ bridges combining them. $[BO_3]$ group reacts with water easily; therefore, chemical durability of pure boron glass decreases. When alkaline oxides add to boron glasses, $[BO_3]$ groups turn into $[BO_4]$ groups and strengthen the glass lattice. Chemical durability of these glasses is higher than borosilicate glasses because of more stable $[BO_4]$ groups. Addition of alkaline oxides over 30-40% mole to host glass causes to enter of oxygen into the structure and chemical durability of the glass decreases again. Though alkaline oxide-borate glasses have relatively high chemical stability, they are insufficient for any structural applications alone. However, addition of some oxides such as Al_2O_3 or PbO provides usability of the boron glasses in some applications [5].

Addition of PbO in suitable amounts to boron glass transforms $[BO_3]$ groups to $[BO_4]$ and the chemical stability increases for the host glass structure [18, 19]. Addition of P_2O_5 in low ratio significantly increases chemical stability in some boron glasses. Chemical durability of $SrTiO_3$ alumina borate glasses with the addition of 9% mole P_2O_5 has increased up to 100 times at 90°C. Fourier Transform Infrared Spectroscopy (FTIR) and Raman spectroscopy analysis has showed that increase in chemical durability was related to decrease in $[BO_3]$ groups and increase in $[BO_4]$ groups [20].

In another study, lead borate and lead bismuth borate glass have been compared for gamma radiation shielding applications. The mass attenuation coefficients of containing 20-70% additive glass have been investigated and obtained better radiation shielding properties comparing to barite concrete [21].

3. The Development of New Materials for the Removal of Radioactive Waste

The main immobilization techniques that can be applied commercially for low-level and high-level radioactive waste are cementation and vitrification, respectively. Even though vitrification enables substantial reduction of waste volume and works successful for waste safety, the method is highly complex and has high cost for initial investment. Current immobilization methods has some limitations, however they provide sufficient security. According to the new approaches, there is a need for creation of new waste forms, which can make for safety of nuclear waste management scenarios using geochemical stable materials.

Thermodynamically stable minerals may retain radionuclides in their structures because of their high isomorphic capacity. Different matrices such as glass, ceramic and glass–ceramic have been studied [24]. Ceramic waste forms can be used as immobilization matrices due to their analogous minerals durability in the long-term performance of geological conditions. Many natural

analogues are potential ceramic structures for high-level radioactive waste. These are monazite (Ce,La,Nd,Th)PO_4, zirconium, zirconium silicate ($ZrSiO_4$), zirconolite ($CaZr_xTi_{(3-x)}O_7$ where $0.8<x<1.35$), apatite ($M_{e10}(XO_4)6Y_2$, where M_e presents divalent cations, e.g: Ca^{2+}, Pb^{2+}, Ba^{2+}; XO_4 presents trivalent anions, e.g: PO_4, VO_4, SiO_4 and Y presents monovalent anions, e.g: F^-, Cl^-, OH^-, Br^- and hollandite ($A_2B_8O_{16}$) [16].

3.1. Glass Composite Materials (GCM)

Glass composite materials (GCM) are classified as completely amorphous glass waste forms and/or completely crystalline ceramic waste forms and can be produced in various ways. Such composite materials inherit both non-crystalline (glassy) and crystalline components. Depending on the intended application, the main component may be a crystalline phase, which plays a role as a binding agent in a glassy phase or alternatively glassy phase which is a particles of crystalline phase dispersed in the glass matrix. GCM can be used to immobilize long-lived radionuclides in the durable crystalline phase. The short-lived radionuclides are held in a less durable glassy phase. High tendency to crystallizing is common for glass-waste form. Recently, GCM are in great demand. This case is clearly seen in more difficult waste or improving acceptable durability of material [12, 25].

3.2. Ceramic Materials

Glass as a solidification material has some disadvantages for volatile radionuclides such as Tc, I, Cs etc. in HLW at the glass melting temperatures and solubility in glass matrix including some important radionuclides, such as actinides with long half-life.

Crystalline ceramic materials with a higher waste loading capacity than the glasses have advantageous for specific wastes. Ceramic waste forms including mineral analogues provide long-term durability for the nuclear wastes like a geological barrier. In addition, the use of hot press technology to ceramics prevents volatile losses in nuclear wastes. Radionuclides incorporate easily into crystalline phases in the ceramic structures and these crystalline phases allow high loadings of specific radionuclides [12, 23].

Ceramic structure has different coordination types for charge balance with radionuclide substitutions due to the complex composition of ceramic matrix. Specific crystalline phases are produced as a host for the different radionuclides in multiphase ceramic waste forms. Zirconolite, monazite, apatite, or sodium zirconium phosphate is single-phase ceramics to incorporate nearly all of the radionuclides into a single structure.

Several researchers have investigated in detail the use of ceramic materials for the immobilization of actinides in nuclear wastes [26-32]. Table 1 shows the leaching rate and waste loading capacity of some ceramic forms for different radionuclides. Most widely studied ceramics as waste form are titanate-based ceramics such as hollandite, perovskite or zirconolite [27, 32]. Synthetic mineral compositions such as

monazite (Ce,Y,La,Th)PO_4, apatite (Ca_5PO_4)$_3$(F,Cl,OH) etc. has been developed for disposal of high-level nuclear wastes due to their lower dissolution rate compared with borosilicate glass [26]. In recent, the candidate crystalline waste forms for the geological disposal of nuclear wastes are phosphate ceramics, which have a high stability, a high waste loading, a refractory nature and easy method of synthetic and their resistant to radiation damage [28-30].

3.3. Glass-Ceramic Materials

Glass-ceramics are produced by melting viscous glass materials and due to their high absorption capacities they are potential immobilisation materials for radioactive waste. Glass-ceramics are polycrystalline materials produced by controlled crystallization of amorphous glasses [12, 35]. A glass ceramic is a fine-grained mixture of glass and ceramic phases ideally derived from a homogeneous glass through a devitrification and can combine for immobilization of HLW with durable residual glass and ceramic phases [36]. Glass ceramics, which the formation of the desired phase by controlled crystallization is facilitated, gains improved mechanical and chemical properties comparing to main glass material.

Several crystal materials comprising silicate, glass ceramic, titanate ($CaTiOSiO_4$), zirconolite and zirconium dioxide (ZrO_2) were tested for sorption of long-lived actinides. Waste loading (50-70%) is successfully applied in zirconolite and perovskite with high durability [25]. In particular, glass ceramics are ideal for producing ferroelectric ceramics. In addition, durability under high temperature, pressure and extreme environmental conditions make them attractive for many applications [37]. Despite difficulties in the preparation of glass ceramics due to low temperature sintering properties and fragility, $BaTiO_3$ and $PbTiO_3$ ceramics are being studied for many years considering their ferroelectric, piezoelectric and pyroelectric properties [38].

Physical properties of silicate-based glass-ceramics have found similar to that of commercial glass-ceramics and largely better than traditional natural stones. The elastic modulus and Vickers hardness have obtained as 70.2 GPa and 6.35 GPa, compared to 86 GPa and 5.88 GPa for commercial neoparies glass ceramics or 82 GPa and 4.22 GPa for natural stone marble or 60 GPa and 5.59 for granite, respectively [9].

An important advantage of glass-ceramic materials compared to ceramic materials for immobilization of nuclear wastes is their better chemical durabilities. Table 2 shows the leaching rates of a glass-ceramic for different radionuclides.

Radiation stability on glass-ceramic forms has been investigated on glass-ceramics by researchers. The results indicate that radiation tolerance of these materials by irradiation with ions of various masses and energies of the damage created by the different sources of radiation is good for β-particles and γ-rays, but susceptible to amorphization under recoil nuclei effects [12, 39].

Table 1. Leaching rate and waste loading capacity of some ceramic forms for different radionuclides

Ceramic materials	Radionuclides	Leaching rate ($gm^{-2}d^{-1}$)	References
Zirconolite-based Titanate	Pu	10^{-5}	[32]
Zirconolite-based Titanate	U	10^{-3}	[32]
Zirconium phosphate	Sr	5	[33]
Titanate	U	7	[27]
Phosphate	Th	-	[28]
Phosphate	Th	10^{-5}	[30]
Phosphate	U	10^{-4}	[30]
Ceramicrete	Cs	3.04×10^{-5}	[34]
Zirconium phosphate	Sr	$<10^{-6}$	[29]

Table 2. Leaching rates of a glass-ceramic forms for different radionuclides

Ceramic materials	Radionuclides	Leaching rate ($g\,cm^{-2}\,d^{-1}$)	References
Ca doped $CePO_4$ monazite	Cs	2.1×10^{-8}	[24]
Ca doped $CePO_4$ monazite	U	2.4×10^{-7}	[24]
Ca doped $CePO_4$ monazite	Sr	1.1×10^{-6}	[24]

4. Conclusion

Glass forms are recognized to be more technologically and ecologically feasible as compared to cement forms. Different glass compositions are used for immobilization of various radionuclides in HLW. Glass forms are not a suitable matrix due to its thermodynamic instability and its insufficient chemical durability and radiation resistance. From this point of view, the new solidification forms are considered as an alternative to glass forms.

Therefore, ceramic, glass-ceramic and composite forms as an alternative solidification form to glass forms can be used as host matrix for the immobilization of high-level radioactive wastes for long-term disposal in geologic storage. Chemical durability and physical properties of these forms are the most important parameters to immobilize the radionuclides in host matrix.

Chemical durability plays a vital role for the solidification materials to describe the mobility of the radionuclides from host matrix to eco-system. Chemical durability should be very high for the solidification materials for safety disposal of the waste form. Although the low cost of the immobilization process of the nuclear wastes is the most desirable property to choose the proper material for solidification, chemical durability and waste capacity of the solidification material should be stand in the forefront in the last decision.

Although many applications have released to immobilize of radionuclides in ceramic forms for understanding of chemical and physical durabilities and radiation-solid interaction in ceramics, these type researches for glass-ceramics are insufficient in detail to predict the effects of these parameters on host matrix for different radionuclides.

All solidification materials used for immobilization of nuclear wastes have different properties depending on their chemical compositions. Glass technology is well known process for thousands of years and has an advantage to produce with different compositions of raw materials.

Comparison with the glass materials, ceramics are traditional and well defined inorganic materials. However, their mechanical properties are lower than the glass likewise their low cost. Alternatively, glass-ceramics are a type of glass undergo controlled crystallisation. The mechanical properties and loaded waste capacities of glass-ceramics are superior to those of the parent glass. Usage of correct material for immobilization of nuclear waste depends on type of nuclear waste, availability of raw materials, feasibility and economic potential of the country

The development of host forms for nuclear waste management in repository conditions will require a fundamental understanding of effects of corrosion in different media, radiation-host matrix interaction, effect of time and temperature on micro and macro structural evaluation of the host and wasted forms. Therefore, different host matrix for radioactive wastes from nuclear industry should be systematically studied over the widest range of conditions using new compositions and techniques.

References

[1] M. Benedict, T.H. Pigford and H.W. Levi, "Nuclear Chemical Engineering", McGraw-Hill Book Company, Second Edition, 1981, USA.

[2] F. Cattant, D. Crusset and D. Feron, "Corrosion Issues in Nuclear Industry Today", Materials Today, 11(10) (2008) 32-37.

[3] L. Cecille, "New Separation Chemistry Techniques for Radioactive Waste and other Specific Applications", Elsevier Applied Science, 1991, London and New York.

[4] J.H. Saling and A.W. Fentiman, "Radioactive Waste Management", Second Edition, Taylor&Francis, 2002, NewYork, London.

[5] J.E. Shelby, "Introduction to Glass Science and Technology", Second Edition, New York State College of Ceramics at Alfred University School of Engineering,

Alfred, NY, USA, The Royal Society of Chemistry, 2005.

[6] K. Raj, K.K. Prasad and N.K. Bansal, "Radioactive Waste Management Practise in India", Nuclear Engineering and Design, 236: p.914-930, 2006.

[7] International Atomic Energy Agency (IAEA), "Nuclear Energy Series, Policies and Strategies for Radioactive Waste Management, No: NW-G-1.1, International Atomic Energy Agency, Vienna, 2009a.

[8] International Atomic Energy Agency (IAEA), "Safety Standards Series, Predisposal Management of Radioactive Waste", No: G SR Part 5, International Atomic Energy Agency, Vienna, 2009b.

[9] E. Bernardo, M. Varrasso, F. Cadamuro and S. Hreglich, "Vitrification of Wastes and Preparation of Chemically Stable Sintered Glass-Ceramic Products", Journal of Non-Crystalline Solids, 352: p. 4017–4023, 2006.

[10] European Commission, "Geological Disposal of Radioactive Wastes Produced by Nuclear Power, Community Research", Editor: Neil Chapman, Belgium, 2004.

[11] F. Cattant, D. Crusset and D. Féron, "Corrosion issues in nuclear industry today", Materials Today, 11(10): p.32-37, 2008.

[12] C.M. Jantzen, W.E. Lee and M.I. Ojovan, "Radioactive Waste (RAW) Conditioning, Immobilization, and Encapsulation Processes and Technologies: Overview and Advances, Radioactive Waste Management and Contaminated Site Clean-up", p.171-272, 2013.

[13] M. I. Ojovan and William E. Lee, "An Introduction to Nuclear Waste Immobilisation", 2nd Edition, Elsevier, 2014.

[14] C. Bayliss and K. Langley, "Nuclear Decommissioning, Waste Management, and Environmental Site Remediation", First Edition, Elsevier, pp.330, 2003.

[15] L. Junfeng, W. Jianlong, "Advances in cement solidification technology for waste radioactive ion exchange resins: A review", Journal of Hazardous Materials B, 135: p. 443–448, 2006.

[16] C. Erdogan, M. Bengisu, S. Akyil Erenturk, "Chemical Durability and Structural Analysis of $PbO–B_2O_3$ Glasses and Testing for Simulated Radioactive Wastes", Journal of Nuclear Materials, 445: p. 154–164, 2014.

[17] W. Vogel, "Chemistry of Glass", American Ceramic Society, Columbus, Ohio, 1985.

[18] Y. Cheng, H. Xiao and W. Guo, "Structure and Crystallization Kinetics of $PbO-B_2O_3$ Glasses", Ceramic International, 33: p. 1341-1347, 2007.

[19] Y. Saddeek, "Structural and Acoustical Studies of Lead Sodium Borate Glasses", Journal of Alloys and Compounds, 467(1): p. 14-21, 2008.

[20] M. Bengisu, R.K. Brow, E. Yilmaz, A. Mogus-Milankovic and S.T. Reis, "Aluminoborate and Aluminoborosilicate Glasses with High Chemical Durability and the Effect of P_2O_5 Additions on the Properties", Journal of Non-Crystalline Solids, 352: p. 3668–3676, 2006.

[21] N. Singh, K.J. Singh, K. Singh and H. Singh, "Comparative Study of Lead Borate and Bismuth Lead Borate Glass Systems as Gamma Radiation Shielding Materials", Nuclear Instruments and Methods in Physic Researches B, 225: p.305-309, 2004.

[22] M.I. Ojovan and W.E. Lee, "An Introduction to Nuclear Waste Immobilisation", 2nd Edition, Elsevier Insight, 376: 2013.

[23] S.V. Stefanovsky, S.V. Yudintsev, R. Giere and G.R. Lumpkin, "Nuclear waste forms", in Energy, Waste, and the Environment: A Geochemical Perspective, R. Giere, P. Stille (eds), Geological Society, London, Special Publications, 236: p.37-63, 2004.

[24] R. Asuvathraman, K. Joseph, R. Raja Madhavan, R. Sudha, R. Krishna Prabhu and K.V. Govindan Kutty, "A versatile monazite–IPG glass–ceramic waste form with simulated HLW: Synthesis and characterization", Journal of the European Ceramic Society, 35: p.4233–4239, 2015.

[25] W.E. Lee, M.I. Ojovan, M.C. Stennett and N.C. Hyatt, "Immobilisation of Radioactive Waste in Glasses, Glass Composite Materials and Ceramics", Advances in Applied Ceramics, 105(1): p. 3-12, 2006.

[26] L. Bois, M.J. Guittet, F. Carrot, P. Trocellier and M. Gautier-Soyer, "Preliminary Results on the Leaching Process of Phosphate Ceramics, Potential Hosts for Actinide Immobilization", Journal of Nuclear Materials, 297: p.129-137, 2001.

[27] M.L. Carter, H. Li, Y. Zhang, E.R. Vance and D.R.G. Mitchell, "Titanate Ceramics for Immobilisation of Uranium-Rich Radioactive Wastes arising from ^{99}Mo Production", Journal of Nuclear Materials, 384: p.322–326, 2009.

[28] E. Du Fou de Kerdaniel, N. Clavier, N. Dacheux, O. Terra and R. Podor, "Actinide Solubility-Controlling Phases during the Dissolution of Phosphate Ceramics", Journal of Nuclear Materials, 362: p.451–458, 2007.

[29] S. Nakayama and K. Itoh, "Immobilization of Strontium by Crystalline Zirconium Phosphate", Journal of the European Ceramic Society, 23: p.1047–1052, 2003.

[30] O. Terra, N. Dacheux, F. Audubert and R. Podor, "Immobilization of Tetravalent Actinides in Phosphate Ceramics", Journal of Nuclear Materials, 352: p.224–232, 2006.

[31] W.J. Weber, R.C. Ewing, C.R.A. Catlow, T. Diaz de la Rubia, L.W. Hobbs, C. Kinoshita, Hj. Matzke, A.T. Motta, M. Nastasi, E.K.H. Salje, E.R. Vance and S.J. Zinkle, "Radiation Effects in Crystalline Ceramics for

the Immobilization of High-Level Nuclear Waste and Plutonium", Journal of Materials Research, 13(6): p.1434-1484, 1998.

[32] Y. Zhang, M.W.A. Stewart, H. Li, M.L. Carter, E.R. Vance and S. Moricca, "Zirconolite-rich Titanate Ceramics for Immobilisation of Actinides–Waste Form/HIP can Interactions and Chemical Durability", Journal of Nuclear Materials, 395: p. 69–74, 2009.

[33] V. Pet'kov, E. Asabina, V. Loshkarev and M. Sukhanov, "Systematic investigation of the strontium zirconium phosphate ceramic form for nuclear waste immobilization", Journal of Nuclear Materials, 471: p.122-128, 2016.

[34] A.S. Wagh, S.Y. Sayenko, V.A. Shkuropatenko, R.V. Tarasov, M.P. Dykiy, Y.O. Svitlychniy, V.D. Virych and E.A. Ulybkin, "Experimental Study on Cesium Immobilization in Struvite Structures", Journal of Hazardous Materials, 302: p.241–249, 2016.

[35] M. Kim and J. Heo, "Calcium-Borosilicate Glass-Ceramics Wasteforms to Immobilize Rare-Earth Oxide Wastes from Pyro-Processing", Journal of Nuclear Materials, 467: p. 224-228, 2015.

[36] W.J. Weber, A. Navrotsky, S. Stefanovsky, E.R. Vance and E. Vernaz, "Materials Science of High-Level Nuclear Waste Immobilization", MRS Bulletin, Volume 34: p.46-53, 2009.

[37] S. Jakkula and V. Deshpande, "Effect of MgO Addition on the Properties of PbO–TiO$_2$–B$_2$O$_3$ Glass and Glass–Ceramics", Ceramics International, 39: p.15–18, 2013.

[38] S. Golezardi, V.K. Marghussian, A. Beitollahi and S.M. Mirkazemi, "Crystallization Behavior, Microstructure and Dielectric Properties of Lead Titanate Glass Ceramics in the Presence of Bi$_2$O$_3$ as a Nucleating Agent", Journal of the European Ceramic Society, 30: p.1453–1460, 2010.

[39] M. Tang, A. Kossoy, G. Jarvinen, J. Crum, L. Turo, B. Riley, K. Brinkman, K. Fox, J. Amoroso, and J. Marra, "Radiation Stability Test on Multiphase Glass Ceramic and Crystalline Ceramic Waste Forms", Nuclear Instruments and Methods in Physics Research B, 326: p.293–297, 2014.

INTERNATIONAL JOURNAL OF ENGINEERING TECHNOLOGIES-IJET

Guide for Authors

The *International Journal of Engineering Technologies* **(IJET)** seeks to promote and disseminate knowledge of the various topics of engineering technologies. The journal aims to present to the international community important results of work in the fields of engineering such as imagining, researching, planning, creating, testing, improving, implementing, using and asking. The journal also aims to help researchers, scientists, manufacturers, institutions, world agencies, societies, etc. to keep up with new developments in theory and applications and to provide alternative engineering solutions to current.

The *International Journal of Engineering Technologies* is a quarterly published journal and operates an online submission and peer review system allowing authors to submit articles online and track their progress via its web interface. The journal aims for a publication speed of **60 days** from submission until final publication.

The coverage of IJET includes the following engineering areas, but not limited to:

All filed of engineering such as;

Chemical engineering

- Biomolecular engineering

- Materials engineering

- Molecular engineering

- Process engineering

Civil engineering

- Environmental engineering

- Geotechnical engineering

- Structural engineering

- Transport engineering

- Water resources engineering

Electrical engineering

- Computer engineering

- Electronic engineering

- Optical engineering

- Power engineering

Mechanical engineering

- Acoustical engineering

- Manufacturing engineering

- Thermal engineering

- Vehicle engineering

Systems (interdisciplinary) engineering

- Aerospace engineering

- Agricultural engineering

- Applied engineering

- Biological engineering

- Building services engineering

- Energy engineering

- Railway engineering

- Industrial engineering

- Mechatronics

- Military engineering

- Nano engineering

- Nuclear engineering

- Petroleum engineering

Types of Articles submitted should be original research papers, not previously published, in one of the following categories,

- Applicational and design studies.

- Technology development,

– Comparative case studies.

– Reviews of special topics.

– Reviews of work in progress and facilities development.

– Survey articles.

– Guest editorials for special issues.

Ethic Responsibilities

The publication of an article in peer-reviewed *"International Journal of Engineering Technologies"* is an essential building block in the development of a coherent and respected network of knowledge. It is a direct reflection of the quality of the work. Peer-reviewed articles support and embody the scientific method. It is therefore important to agree upon standards of expected ethical behavior for all parties involved in the act of publishing: the author, the journal editor, the peer reviewer, the publisher and the society of society-owned or sponsored journals.

All authors are requested to disclose any actual or potential conflict of interest including any financial, personal or other relationships with other people or organizations within three years of beginning the submitted work that could inappropriately influence, or be perceived to influence, their work.

Submission of an article implies that the work described has not been published previously that it is not under consideration for publication elsewhere. The submission should be approved by all authors and tacitly or explicitly by the responsible authorities where the work was carried out, and that, if accepted, it will not be published elsewhere in the same form, in English or in any other language, including electronically without the written consent of the copyright-holder.

Upon acceptance of an article, authors will be asked to complete a "Copyright Form". Acceptance of the agreement will ensure the widest possible dissemination of information. An e-mail will be sent to the corresponding author confirming receipt of the manuscript together with a "Copyright Form" form or a link to the online version of this agreement.

Author Rights

As a journal author, you retain rights for a large number of author uses, including use by your employing institute or company. These rights are retained and permitted without the need to obtain specific permission from *IJET*. These include:

- ❖ The right to make copies (print or electronic) of the journal article for your own personal use, including for your own classroom teaching use;

- ❖ The right to make copies and distribute copies (including via e-mail) of the journal article to research colleagues, for personal use by such colleagues for scholarly purposes;

- ❖ The right to post a pre-print version of the journal article on internet web sites including electronic pre-print servers, and to retain indefinitely such version on such servers or sites for scholarly purposes

- ❖ the right to post a revised personal version of the text of the final journal article on your personal or institutional web site or server for scholarly purposes

- ❖ The right to use the journal article or any part thereof in a printed compilation of your works, such as collected writings or lecture notes.

Article Style

Authors must strictly follow the guide for authors, or their articles may be rejected without review. Editors reserve the right to adjust the style to certain standards of uniformity. Follow Title, Authors, Affiliations, Abstract, Keywords, Introduction, Materials and Methods, Theory/Calculation, Conclusions, Acknowledgements, References order when typing articles. The corresponding author should be identified with an asterisk and footnote. Collate acknowledgements in a separate section at the end of the article and do not include them on the title page, as a footnote to the title or otherwise.

Abstract and Keywords:

Enter an abstract of up to 250 words for all articles. This is a concise summary of the whole paper, not just the conclusions, and is understandable without reference to the rest of the paper. It should contain no citation to other published work. Include up to six keywords that describe your paper for indexing purposes.

Abbreviations and Acronyms:

Define abbreviations and acronyms the first time they are used in the text, even if they have been defined in the abstract. Abbreviations such as IEEE, SI, MKS, CGS, sc, dc, and rms do not have to be defined. Do not use abbreviations in the title unless they are unavoidable.

Text Layout for Peer Review:

Use single column layout, double spacing and wide (3 cm) margins on white paper at the peer review stage. Ensure that each new paragraph is clearly indicated. Present tables and figure legends in the text where they are related and cited. Number all pages consecutively; use 12 pt font size and standard fonts; Times New Roman, Helvetica, or Courier is preferred.

Research Papers should not exceed 12 printed pages in two-column publishing format, including figures and tables.

Technical Notes and *Letters* should not exceed 2,000 words.

Reviews should not exceed 20 printed pages in two-column publishing format, including figures and tables.

Equations:

Number equations consecutively with equation numbers in parentheses flush with the right margin, as in (1). To make equations more compact, you may use the solidus (/), the exp function, or appropriate exponents. Italicize Roman symbols for quantities and variables, but not Greek symbols. Use an dash (–) rather than a hyphen for a minus sign. Use parentheses to avoid ambiguities in denominators. Punctuate equations with commas or periods when they are part of a sentence, as in

$$C = a + b \hspace{10cm} (1)$$

Symbols in your equation should be defined before the equation appears or immediately following. Use "Eq. (1)" or "equation (1)," while citing.

Figures and Tables:

All illustrations must be supplied at the correct resolution:

   * Black and white and colour photos - 300 dpi

   * Graphs, drawings, etc - 800 dpi preferred; 600 dpi minimum

   * Combinations of photos and drawings (black and white and color) - 500 dpi

In addition to using figures in the text, upload each figure as a separate file in either .tiff or .eps format during submission, with the figure number.

Table captions should be written in the same format as figure captions; for example, "Table 1. Appearance styles.". Tables should be referenced in the text unabbreviated as "Table 1."

References:

Please ensure that every reference cited in the text is also present in the reference list (and viceversa). Any references cited in the abstract must be given in full. Unpublished results and personal communications are not recommended in the reference list, but may be mentioned in the text. Citation of a reference as "in press" implies that the item has been accepted for publication. Number citations consecutively in square brackets [1]. Punctuation follows the bracket [2]. Refer simply to the reference number, as in [3]. Use "Ref. [3]" or Reference [3]" at the beginning of a sentence: "Reference [3] was …". Give all authors' names; use "et al." if there are six authors or more. For papers published in translated journals, first give the English citation, then the original foreign-language citation.

Books

[1]   J. Clerk Maxwell*, A Treatise on Electricity and Magnetism,* 3rd ed., vol. 2. Oxford:Clarendon Press, 1892, pp.68-73.

Journals

[2]   Y. Yorozu, M. Hirano, K. Oka, and Y. Tagawa, "Electron spectroscopy studies on magneto-optical media and plastic substrate interface", *IEEE Transl. J. Magn. Japan*, vol. 2, pp. 740-741, August 1987.

Conferences

[3]   Çolak I., Kabalci E., Bayindir R., and Sagiroglu S, "The design and analysis of a 5-level cascaded voltage source inverter with low THD", *2nd PowerEng Conference*, Lisbon, pp. 575-580, 18-20 March 2009.

Reports

[4]   IEEE Standard 519-1992, Recommended practices and requirements for harmonic control in electrical power systems, *The Institute of Electrical and Electronics Engineers*, 1993.

Text Layout for Accepted Papers:

A4 page margins should be margins: top = 24 mm, bottom = 24 mm, side = 15 mm. Main text should be given in two column. The column width is 87mm (3.425 in). The space between the two columns is 6 mm (0.236 in). Paragraph indentation is 3.5 mm (0.137 in). Follow the type sizes specified in Table. Position figures and tables at the tops and bottoms of columns. Avoid placing them in the middle of columns. Large figures and tables may span across both columns. Figure captions should be centred below the figures; table captions should be centred above. Avoid placing figures and tables before their first mention in the text. Use the abbreviation "Fig. 1," even at the beginning of a sentence.

Type size (pts.)	Appearance		
	Regular	**Bold**	*Italic*
10	Authors' affiliations, Section titles, references, tables, table names, first letters in table captions,figure captions, footnotes, text subscripts, and superscripts	**Abstract**	
12	Main text, equations, Authors' names, [a]		*Subheading (1.1.)*
24	Paper title		

Submission checklist:

It is hoped that this list will be useful during the final checking of an article prior to sending it to the journal's Editor for review. Please consult this Guide for Authors for further details of any item. Ensure that the following items are present:

❖ One Author designated as corresponding Author:

• E-mail address

• Full postal address

• Telephone and fax numbers

❖ All necessary files have been uploaded

• Keywords: a minimum of 4

• All figure captions (supplied in a separate document)

• All tables (including title, description, footnotes, supplied in a separate document)

❖ Further considerations

• Manuscript has been "spellchecked" and "grammar-checked"

• References are in the correct format for this journal

• All references mentioned in the Reference list are cited in the text, and vice versa

• Permission has been obtained for use of copyrighted material from other sources (including the Web)

• Color figures are clearly marked as being intended for color reproduction on the Web (free of charge) and in print or to be reproduced in color on the Web (free of charge) and in black-and-white in print.

Article Template Containing Author Guidelines for Peer-Review

First Author*, Second Author**‡, Third Author***

*Department of First Author, Faculty of First Author, Affiliation of First Author, Postal address

**Department of Second Author, Faculty of First Author, Affiliation of First Author, Postal address

***Department of Third Author, Faculty of First Author, Affiliation of First Author, Postal address

(First Author Mail Address, Second Author Mail Address, Third Author Mail Address)

‡Corresponding Author; Second Author, Postal address, Tel: +90 312 123 4567, Fax: +90 312 123 4567,corresponding@affl.edu

Abstract- Enter an abstract of up to 250 words for all articles. This is a concise summary of the whole paper, not just the conclusions, and is understandable without reference to the rest of the paper. It should contain no citation to other published work. Include up to six keywords that describe your paper for indexing purposes. Define abbreviations and acronyms the first time they are used in the text, even if they have been defined in the abstract. Abbreviations such as IEEE, SI, MKS, CGS, sc, dc, and rms do not have to be defined. Do not use abbreviations in the title unless they are unavoidable.

Keywords- Keyword1; keyword2; keyword3; keyword4; keyword5.

2. Introduction

Authors should any word processing software that is capable to make corrections on misspelled words and grammar structure according to American or Native English. Authors may get help by from word

processor by making appeared the paragraph marks and other hidden formatting symbols. This sample article is prepared to assist authors preparing their articles to IJET.

Indent level of paragraphs should be 0.63 cm (0.24 in) in the text of article. Use single column layout, double-spacing and wide (3 cm) margins on white paper at the peer review stage. Ensure that each new paragraph is clearly indicated. Present tables and figure legends in the text where they are related and cited. Number all pages consecutively; use 12 pt font size and standard fonts; Times New Roman, Helvetica, or Courier is preferred. Indicate references by number(s) in square brackets in line with the text. The actual authors can be referred to, but the reference number(s) must always be given. Example: "..... as demonstrated [3, 6]. Barnaby and Jones [8] obtained a different result ...."

IJET accepts submissions in three styles that are defined as Research Papers, Technical Notes and Letter, and Review paper. The requirements of paper are as listed below:

➢ Research Papers should not exceed 12 printed pages in two-column publishing format, including figures and tables.

➢ Technical Notes and Letters should not exceed 2,000 words.

➢ Reviews should not exceed 20 printed pages in two-column publishing format, including figures and tables.

Authors are requested write equations using either any mathematical equation object inserted to word processor or using independent equation software. Symbols in your equation should be defined before the equation appears or immediately following. Use "Eq. (1)" or "equation (1)," while citing. Number equations consecutively with equation numbers in parentheses flush with the right margin, as in Eq. (1). To make equations more compact, you may use the solidus (/), the exp function, or appropriate exponents. Italicize Roman symbols for quantities and variables, but not Greek symbols. Use an dash (–) rather than a hyphen for a minus sign. Use parentheses to avoid ambiguities in denominators. Punctuate equations with commas or periods when they are part of a sentence, as in

$$C = a + b \tag{1}$$

Section titles should be written in bold style while sub section titles are italic.

3. Figures and Tables

3.1. *Figure Properties*

All illustrations must be supplied at the correct resolution:

➢ Black and white and colour photos - 300 dpi

➢ Graphs, drawings, etc - 800 dpi preferred; 600 dpi minimum

➢ Combinations of photos and drawings (black and white and colour) - 500 dpi

In addition to using figures in the text, Authors are requested to upload each figure as a separate file in either .tiff or .eps format during submission, with the figure number as Fig.1., Fig.2a and so on. Figures are cited as "Fig.1" in sentences or as "Figure 1" at the beginning of sentence and paragraphs. Explanations related to figures should be given before figure. Figures and tables should be located at the top or bottom side of paper as done in accepted article format.

Figure 1. Engineering technologies.

Table captions should be written in the same format as figure captions; for example, "Table 1. Appearance styles.". Tables should be referenced in the text unabbreviated as "Table 1."

Table 1. Appearance properties of accepted manuscripts

Type size (pts.)	Appearance		
	Regular	**Bold**	*Italic*
10	Authors' affiliations, Abstract, keywords, references, tables, table names, figure captions, footnotes, text subscripts, and superscripts	**Abstract**	
12	Main text, equations, Authors' names, Section titles		*Subheading (1.1.)*
24	Paper title		

4. Submission Process

The *International Journal of Engineering Technologies* operates an online submission and peer review system that allows authors to submit articles online and track their progress via a web interface. Articles that are prepared referring to this template should be controlled according to submission checklist given in "Guide f Authors". Editor handles submitted articles to IJET primarily in order to control in terms of compatibility to aims and scope of Journal.

Articles passed this control are checked for grammatical and template structures. If article passes this control too, then reviewers are assigned to article and Editor gives a reference number to paper. Authors registered to online submission system can track all these phases.

Editor also informs authors about processes of submitted article by e-mail. Each author may also apply to Editor via online submission system to review papers related to their study areas. Peer review is a critical element of publication, and one of the major cornerstones of the scientific process. Peer Review serves two key functions:

➢ Acts as a filter: Ensures research is properly verified before being published

➢ Improves the quality of the research

5. Conclusion

The conclusion section should emphasize the main contribution of the article to literature. Authors may also explain why the work is important, what are the novelties or possible applications and extensions. Do not replicate the abstract or sentences given in main text as the conclusion.

Acknowledgements

Authors may acknowledge to any person, institution or department that supported to any part of study.

References

[1] J. Clerk Maxwell, *A Treatise on Electricity and Magnetism*, 3rd ed., vol. 2. Oxford:Clarendon Press, 1892, pp.68-73. (Book)

[2] H. Poor, *An Introduction to Signal Detection and Estimation*, New York: Springer-Verlag, 1985, ch. 4. (Book Chapter)

[3] Y. Yorozu, M. Hirano, K. Oka, and Y. Tagawa, "Electron spectroscopy studies on magneto-optical media and plastic substrate interface", *IEEE Transl. J. Magn. Japan*, vol. 2, pp. 740-741, August 1987. (Article)

[4] E. Kabalcı, E. Irmak, I. Çolak, "Design of an AC-DC-AC converter for wind turbines", *International Journal of Energy Research*, Wiley Interscience, DOI: 10.1002/er.1770, Vol. 36, No. 2, pp. 169-175. (Article)

[5] I. Çolak, E. Kabalci, R. Bayindir R., and S. Sagiroglu, "The design and analysis of a 5-level cascaded voltage source inverter with low THD", *2nd PowerEng Conference*, Lisbon, pp. 575-580, 18-20 March 2009. (Conference Paper)

[6] IEEE Standard 519-1992, Recommended practices and requirements for harmonic control in electrical power systems, *The Institute of Electrical and Electronics Engineers*, 1993. (Standards and Reports)

Article Template Containing Author Guidelines for Accepted Papers

First Author*, Second Author**‡, Third Author***

*Department of First Author, Faculty of First Author, Affiliation of First Author, Postal address

**Department of Second Author, Faculty of First Author, Affiliation of First Author, Postal address

***Department of Third Author, Faculty of First Author, Affiliation of First Author, Postal address

(First Author Mail Address, Second Author Mail Address, Third Author Mail Address)

‡ Corresponding Author; Second Author, Postal address, Tel: +90 312 123 4567,

Fax: +90 312 123 4567,corresponding@affl.edu

Abstract- Enter an abstract of up to 250 words for all articles. This is a concise summary of the whole paper, not just the conclusions, and is understandable without reference to the rest of the paper. It should contain no citation to other published work. Include up to six keywords that describe your paper for indexing purposes. Define abbreviations and acronyms the first time they are used in the text, even if they have been defined in the abstract. Abbreviations such as IEEE, SI, MKS, CGS, sc, dc, and rms do not have to be defined. Do not use abbreviations in the title unless they are unavoidable.

Keywords Keyword1, keyword2, keyword3, keyword4, keyword5.

1. Introduction

Authors should any word processing software that is capable to make corrections on misspelled words and grammar structure according to American or Native English. Authors may get help by from word processor by making appeared the paragraph marks and other hidden formatting symbols. This sample article is prepared to assist authors preparing their articles to IJET.

Indent level of paragraphs should be 0.63 cm (0.24 in) in the text of article. Use single column layout, double-spacing and wide (3 cm) margins on white paper at the peer review stage. Ensure that each new paragraph is clearly indicated. Present tables and figure legends in the text where they are related and cited. Number all pages consecutively; use 12 pt font size and standard fonts; Times New Roman, Helvetica, or Courier is preferred. Indicate references by number(s) in square brackets in line with the text. The actual authors can be referred to, but the reference number(s) must always be given. Example: "..... as demonstrated [3,6]. Barnaby and Jones [8] obtained a different result ...."

IJET accepts submissions in three styles that are defined as Research Papers, Technical Notes and Letter, and Review paper. The requirements of paper are as listed below:

➢ Research Papers should not exceed 12 printed pages in two-column publishing format, including figures and tables.

➢ Technical Notes and Letters should not exceed 2,000 words.

➢ Reviews should not exceed 20 printed pages in two-column publishing format, including figures and tables.

Authors are requested write equations using either any mathematical equation object inserted to word processor or using independent equation software. Symbols in your equation should be defined before the equation appears or immediately following. Use "Eq. (1)" or "equation (1)," while citing. Number equations consecutively with equation numbers in parentheses flush with the right margin, as in Eq. (1). To make equations more compact, you may use the solidus (/), the exp function, or appropriate exponents. Italicize Roman symbols for quantities and variables, but not Greek symbols. Use an dash (-) rather than a hyphen for a minus sign. Use parentheses to avoid ambiguities in denominators. Punctuate equations with commas or periods when they are part of a sentence, as in

$$C = a + b \tag{1}$$

Section titles should be written in bold style while sub section titles are italic.

6. Figures and Tables

6.1. Figure Properties

All illustrations must be supplied at the correct resolution:

➢ Black and white and colour photos - 300 dpi

➢ Graphs, drawings, etc - 800 dpi preferred; 600 dpi minimum

➢ Combinations of photos and drawings (black and white and colour) - 500 dpi

In addition to using figures in the text, Authors are requested to upload each figure as a separate file in either .tiff or .eps format during submission, with the figure number as Fig.1., Fig.2a and so on. Figures are cited as "Fig.1" in sentences or as "Figure 1" at the beginning of sentence and paragraphs. Explanations related to figures should be given before figure.

Fig. 1. Engineering technologies.

Figures and tables should be located at the top or bottom side of paper as done in accepted article format. Table captions should be written in the same format as figure captions; for example, "Table 1. Appearance styles.". Tables should be referenced in the text unabbreviated as "Table 1."

Table 1. Appearance properties of accepted manuscripts

Type size (pts.)	Appearance		
	Regular	**Bold**	*Italic*
10	Main text, section titles, authors' affiliations, abstract, keywords, references, tables, table names, figure captions, equations, footnotes, text subscripts, and superscripts	**Abstract-**	*Subheading (1.1.)*
12	Authors' names,		
24	Paper title		

6.2. Text Layout for Accepted Papers

A4 page margins should be margins: top = 24 mm, bottom = 24 mm, side = 15 mm. The column width is 87mm (3.425 in). The space between the two columns is 6 mm (0.236 in). Paragraph indentation is 3.5 mm (0.137 in). Follow the type sizes specified in Table. Position figures and tables at the tops and bottoms of columns. Avoid placing them in the middle of columns. Large figures and tables may span across both columns. Figure captions should be centred below the figures; table captions should be centred above. Avoid placing figures and tables before their first mention in the text. Use the abbreviation "Fig. 1," even at the beginning of a sentence.

7. Submission Process

The International Journal of Engineering Technologies operates an online submission and peer review system that allows authors to submit articles online and track their progress via a web interface. Articles that are prepared referring to this template should be controlled according to submission checklist given in "Guide f Authors". Editor handles submitted articles to IJET primarily in order to control in terms of compatibility to aims and scope of Journal. Articles passed this control are checked for grammatical and template structures. If article passes this control too, then reviewers are assigned to article and Editor gives a reference number to paper. Authors registered to online submission system can track all these phases. Editor also informs authors about processes of submitted article by e-mail. Each author may also apply to Editor via online submission system to review papers related to their study areas. Peer review is a critical element of publication, and one of the major cornerstones of the scientific process. Peer Review serves two key functions:

➢ Acts as a filter: Ensures research is properly verified before being published

➢ Improves the quality of the research

8. Conclusion

The conclusion section should emphasize the main contribution of the article to literature. Authors may also explain why the work is important, what are the novelties or possible applications and extensions. Do not replicate the abstract or sentences given in main text as the conclusion.

Acknowledgements

References

[7] J. Clerk Maxwell, A Treatise on Electricity and Magnetism, 3rd ed., vol. 2. Oxford:Clarendon Press, 1892, pp.68-73. (Book)

[8] H. Poor, An Introduction to Signal Detection and Estimation, New York: Springer-Verlag, 1985, ch. 4. (Book Chapter)

[9] Y. Yorozu, M. Hirano, K. Oka, and Y. Tagawa, "Electron spectroscopy studies on magneto-optical media and plastic substrate interface", IEEE Transl. J. Magn. Japan, vol. 2, pp. 740-741, August 1987. (Article)

[10]   E. Kabalcı, E. Irmak, I. Çolak, "Design of an AC-DC-AC converter for wind turbines", International Journal of Energy Research, Wiley Interscience, DOI: 10.1002/er.1770, Vol. 36, No. 2, pp. 169-175. (Article)

[11]   I. Çolak, E. Kabalci, R. Bayindir R., and S. Sagiroglu, "The design and analysis of a 5-level cascaded voltage source inverter with low THD", 2nd PowerEng Conference, Lisbon, pp. 575-580, 18-20 March 2009. (Conference Paper)

[12]   IEEE Standard 519-1992, Recommended practices and requirements for harmonic control in electrical power systems, The Institute of Electrical and Electronics Engineers, 1993. (Standards and Reports)

INTERNATIONAL JOURNAL OF ENGINEERING TECHNOLOGIES (IJET)
COPYRIGHT AND CONSENT FORM

This form is used for article accepted to be published by the IJET. Please read the form carefully and keep a copy for your files.

TITLE OF ARTICLE (hereinafter, "The Article"):

………..……………………………………….....................………………………………………………

………..………………………………………….....................………………………………………………

………..………………………………………………………..…………………………………………

LIST OF AUTHORS:

………..………………………………………………....…..…………………………………………………

………..…………………………………………......................…………………………………………………

………..…………………………………………………………………………………..……………

CORRESPONDING AUTHOR'S ("The Author") NAME, ADDRESS, INSTITUTE AND EMAIL:

………..………………………………………………..…………………………………………………

………..………………………………………….....................…………………………………………………

………..…………………………………………………………………..…………………………….……

COPYRIGHT TRANSFER

The undersigned hereby transfers the copyright of the submitted article to International Journal of Engineering Technologies (the "IJET"). The Author declares that the contribution and work is original, and he/she is authorized by all authors and/or grant-funding agency to sign the copyright form. Author hereby assigns all including but not limited to the rights to publish, distribute, reprints, translates, electronic and published derivates in various arrangements or any other versions in full or abridged forms to IJET. IJET holds the copyright of Article in its own name.

Author(s) retain all rights to use author copy in his/her educational activities, own websites, institutional and/or funder's web sites by providing full citation to final version published in IJET. The full citation is provided including Authors list, title of the article, volume and issue number, and page number or using a link to the article in IJET web site. Author(s) have the right to transmit, print and share the first submitted copies with colleagues. Author(s) can use the final published article for his/her own professional positions, career or qualifications by citing to the IJET publication.

Once the copyright form is signed, any changes about the author names or order of the authors listed above are not accepted by IJET.

   Authorized/Corresponding Author   **Date/ Signature**